STRUCTURE AND STRATIGRAPHY OF THE BOGAL INVERSION ZONE, ANZA BASIN, KENYA:

IMPLICATIONS FOR THE PETROLEUM SYSTEM

UNIVERSITY OF NAIROBI

DEPARTMENT OF GEOLOGY

ANGENGO JANICE HELIANA

I56/86726/2016

A DISSERTATION SUBMITTED IN PARTIAL FULFILMENT OF THE REQUIREMENTS FOR THE DEGREE OF MASTER OF SCIENCE IN GEOLOGY

(PETROLEUM GEOLOGY)

2020

DECLARATION

I declare that this is my original work and has not been submitted elsewhere for a degree in any other university or publication. Where other people's work has been used, this has been acknowledged and referenced in accordance to the University of Nairobi's requirements.

Signed ..... **Date:** 27/11/2020

JANICE HELIANA ANGENGO
UNIVERSITY OF NAIROBI, DEPARTMENT OF GEOLOGY
I56/86726/2016
Janiceheliana@gmail.com

This dissertation has been submitted for examination with my knowledge as the university supervisor.

Signed..... **Date**……

DR. DANIEL DENNIS WAGA
UNIVERSITY OF NAIROBI, DEPARTMENT OF GEOLOGY
wagaden@uonbi.ac.ke

This dissertation has been submitted for examination with my knowledge as the university supervisor.

Signed..... **Date**……

PROF. DANIEL OLAGO
UNIVERSITY OF NAIROBI, DEPARTMENT OF GEOLOGY
dolago@uonbi.ac.ke

To my family. For their patience,

understanding and support.

ABSTRACT

The Anza basin is part of the larger Central African Rift System (CARS) that traverses the African continent from the west to the east. Inversion tectonics occurred in the various sub-basins of the CARS, including the Anza rift during the Late Cretaceous to Early Tertiary. Inversion affects the petroleum system in various ways. It can affect the petroleum system positively by creating new structural and stratigraphic traps or negatively through the re-migration of hydrocarbons, erosion of reservoirs and seals and the redistribution of source rocks and reservoirs. The aim of the study is to apply an integrated structural-stratigraphic and geochemical concept in the evaluation of the hydrocarbon potential of the Bogal play and to establish the consequence of inversion tectonics on the petroleum system of this area. The interpretation of 2D seismic and borehole data from the Bogal-1 well was applied in the analysis of the stratigraphy, structural geometry and the petroleum system elements within the Bogal play. Time-Temperature Indexes (TTI) analysis was used to determine the maturity of the Cretaceous source rocks, and to estimate the timing of hydrocarbon expulsion. The stratigraphy of Bogal-1 well is composed of thick Cretaceous and thinner layers of Tertiary and Quaternary sediments. An angular unconformity separates the Neogene and the Paleogene sediments, forming a potential stratigraphic trap for hydrocarbons. The Upper Cretaceous sediments contain reservoir-quality sandstones and thick mudstone layers that could possibly form the sealing rocks of the Bogal play. The thick Lower Cretaceous sediments contain mudstones that form the potential source rocks of this area. A 100m thick diabase sill penetrates the Lower Cretaceous sediments. It is believed to be of Tertiary origin. Seismic data reveals that the Bogal structural zone is composed of inversion anticlines with wavelengths of approximately 16 Km. The inversion phase occurred after initial extensional forces were replaced by compressional stress. The presence of positive, negative and hybrid flower structures form viable structural traps for hydrocarbons. Fault restoration of the Cretaceous sediments estimates a shortening of approximately 1,714.6m. TTI analysis of the Cretaceous sediments gives a value of 6.04 for the Upper Cretaceous sediments, implying that they are located at the onset of the early oil window, and are therefore immature. The Lower Cretaceous sediments obtain a TTI value of 457.2, suggesting maturation within the wet gas zone. The maturation and expulsion might have occurred in the Oligocene, approximately 27 Ma, probably at the same time as the inversion. The timing of inversion and hydrocarbon expulsion is therefore considered sufficient for petroleum entrapment. More wells should be drilled in this area to examine the trap potential of the lateral angular unconformity that extends throughout this area.

ACKNOWLEDGEMENTS

I would like to thank TOTAL Kenya for awarding me the scholarship to pursue a Master's degree in Petroleum Geology. I also wish to thank the National Oil Corporation of Kenya (NOCK) for providing the data used in this this study.

I extend my sincere gratitude to the Chairman of the Department of Geology, Dr Daniel W. Ichangi, for his patience, encouragement and guidance while writing this dissertation.

I am very grateful to my supervisors, Dr Daniel Dennis Waga and Professor Daniel Olago for their invaluable advice.

TABLE OF CONTENTS

ABSTRACT iii

ABBREVIATIONS xiii

CHAPTER 1: INTRODUCTION 1

1.1 BACKGROUND INFORMATION 1

1.2 PROBLEM STATEMENT 3

1.3 AIM AND OBJECTIVES 4

1.4 JUSTIFICATION AND SIGNIFICANCE 5

1.4.1 Justification 5

1.4.2 Significance 5

CHAPTER 2: LITERATURE REVIEW 6

2.1 REGIONAL SETTING 6

2.2 STRUCTURAL SETTING 10

2.3 STRATIGRAPHY OF THE ANZA BASIN 12

2.4 PETROLEUM SYSTEM OF THE ANZA BASIN 15

2.5 INVERSION STRUCTURES 16

2.5.1 Definition 16

2.5.2 Occurrence 18

2.5.3 Geometric Characteristics 19

2.5.4 Significance of inversion structures to the petroleum system 23

2.5.5 Inversion in the CARS 24

2.6 GAPS IN LITERATURE 25

2.7 SUMMARY 25

CHAPTER 3: MATERIALS AND METHODS 27

3.1 THE STUDY AREA 27
3.1.1 Location 27
3.1.2 Physiography and Drainage 28
3.1.3 Climate 29
3.1.4 Vegetation 29
3.1.5 Land Use and Land Resources 31
3.1.6 Geology 31
3.1.7 Structure 33
3.2 GENERAL WORKFLOW 35
3.3 STRATIGRAPHIC ANALYSIS 36
3.3.1 Dataset and Software 36
3.3.2 Petroleum System Elements Identification 37
3.3.3 Well to Seismic Tie 37
3.4 STRUCTURAL ANALYSIS 39
3.4.1 Dataset and Software 39
3.4.2 Structural Geometry Analysis 39
3.4.3 Fault Restoration 39
3.5 BURIAL HISTORY ANALYSIS 41
3.5.1 Dataset 41
3.5.2 TTI Analysis 41
CHAPTER 4: RESULTS AND DISCUSSIONS 46
4.1 STRATIGRAPHY AND PETROLEUM SYSTEM ELEMENTS 46
4.1.1 Lower Cretaceous Sediments (2563.5m - 5085m) 46
4.1.2 Upper Cretaceous Sediments (1071m-2563m) 50

4.1.3 Quaternary and Tertiary Sediments 53
4.1.4 Seismic Stratigraphy 56
4.2 STRUCTURAL ANALYSIS 59
4.2.1 Structural Restoration 75
4.3 BURIAL HISTORY 78
4.4 DISCUSSION 84
CHAPTER 5: CONCLUSIONS AND RECOMMENDATIONS 90
5.1 CONCLUSIONS 90
5.2 RECOMMENDATIONS 91
REFERENCES 92
APPENDIX 1: Vertical seismic profile (VSP) for Bogal-1 well 98
APPENDIX 2: Time-Depth chart for Bogal-1 well 99
APPENDIX 3: Temperature gradient for Bogal-1 well 100
APPENDIX 4: Exploration blocks and wells in Kenya 101

LIST OF FIGURES

Figure 1.1: Hydrocarbon discoveries and exploration licences in Eastern Africa (modified from GEO ExPro, 2014) 1

Figure 2.1: The Central African Rift System, after Fairhead (1988). 6

Figure 2.2: The separation of Africa and Madagascar at a triple junction. The image shows the paleoposition of Madagascar adjacent to the Somali and Mombasa coastline. VLCC-Very Large Crude Carrier Fracture Zone, ARS-Auxiliary Rescue and Salvage Fracture Zone. (Phethean et al., 2016)..... 9

Figure 2.3: Sedimentary basins of Kenya, after Nyaberi and Rop (2014). 10

Figure 2.4: Gravity map of the Anza basin showing the major faults and sub-basins (Morley et al., 1999) 11

Figure 2.5: Stratigraphy of the Anza basin (Winn et al., 1993) 14

Figure 2.6: Illustration showing the inversion of a half basin. From (Buiter and Pfiffner, 2003) 16

Figure 2.7: Extensional deformation before inversion. After Cooper and Warren (2010) 17

Figure 2.8: Inversion structure after compression. After Cooper and Warren (2010) 17

Figure 2.9: The two modes of structural inversion: mode I (a), where the post-rift is thinner than the syn-rift, and mode II, where the opposite occurs (Tari et al., 2020) 19

Figure 2.10: An extension of Bally, 1984's model of inversion as cited by Tari et al., (2020)..... 20

Figure 2.11: Sandbox experiment showing extension phase with normal faults (Gomes et al., 2010) .. 21

Figure 2.12: Sandbox experiment showing compressional phase during inversion. E1 - E3 are structures that formed during inversion and F1 -F3 are forethrusts while B1 is a backthrust (Gomes et al., 2010) 22

Figure 2.13: Illustration of the geometric characteristics of inversion structures, from Cooper and Warren (2010). The bold dashed lines represent the regional elevation. 22

Figure 2.14: Effect of inversion on the petroleum system elements (Cooper and Warren, 2010) 24

Figure 3.1: The study area: (A) Regional position of the Anza basin, relative to the Sudan rifts, after Bosworth (1992). The red dot shows the position of the Bogal play (B) Location of the Bogal-1 well in

Isiolo County, courtesy of Google Earth. (C) Digitized map of Block 9 in the Anza basin showing the five seismic lines used in the study and the position of Bogal-1 well 27

Figure 3.2: Topographic and drainage map of the Anza basin. The study area is enclosed by the seismic lines on the south-eastern part of Block 9. The topography in the study area is generally low, averaging around 190m above sea level. River Ewaso Nyiro and its tributaries extend widely in this area 28

Figure 3.3: Average temperature of 30^0 C (A) and rainfall of 400mm per annum (B) in Kenya (BGS, 2019). The black square indicates the study area. 29

Figure 3.4: Vegetation map of north-eastern Kenya, after Breugel et al. (2015). The study area, highlighted in red, is dominated by Acacia Commiphora bushland 30

Figure 3.5: Land use map of Isiolo County. Modified from: Survey of Kenya, map no. 500/3/83. The study area, highlighted with a blue square, is used as grazing land or rangeland..... 31

Figure 3.6: Geological map of the Anza basin. Volcanic sediments are present in the NW and Quaternary sediments in the SE. Digitized after Beicip (1987)..... 32

Figure 3.7: DTEM Satellite gravity map of the Anza Basin with the Bogal inversion located on the paleohigh.in the Yamicha Sag. Free air gravity data adopted from http://topex.ucsd.edu/cgi-bin/get_data.cgi after Sandwell and Smith (2009) and Sandwell et al., (2013, 2014)..... 33

Figure 3.8: The extent of inversion anticlines in central and southern Anza basin. The study area is enclosed with the five seismic lines marked in red. Bogal-1 well is at the centre. Modified from Morley et al. (1999). 34

Figure 3.9: General workflow 35

Figure 3.10: 2D seismic lines used in the study. Three lines have a trend that is parallel to the axis of the Anza basin (NW-SE), while two lines, trending NE-SW, cut across the basin. The red line indicates the position of Bogal-1 well. The data is displayed in Petroleum Experts Midland Valley Move software, 2017..... 36

Figure 3.11: Reflection of waves in a sedimentary sequence. The degree of reflection is a function of the acoustic impedance (Bjørlykke, 2010)..... 37

Figure 3.12: The process of creating a synthetic seismogram: The sonic log is multiplied by the density log to obtain an acoustic impedance log, which subsequently creates a reflection coefficient log using

equation 1 (A). The reflection coefficient is used to create a synthetic seismogram (B) (Bjørlykke, 2010) 38

Figure 3.13: Concept of trishear deformation in flower structures (Cristallini et al., 2004) 40

Figure 3.14: Simple shear (a) and Flexural slip (b) deformation styles applied in unfolding beds. Images from Midland Valley Move Knowledge Base (2017) 41

Figure 3.15: Construction of burial curves (Barker, 1996)..... 43

Figure 4.1: Synthetic seismogram for Bogal-1 well showing a correlation value of 0.7..... 56

Figure 4.2: Basemap of the seismic survey..... 59

Figure 4.3: Uninterpreted seismic section (A) and fault picks in line c08-9-11c (B). The inset picture shows the position of the seismic line..... 60

Figure 4.4: Interpreted faults and horizons in line c08-9-11c showing an inversion anticline on the south-western side and an inversion monocline on the north-eastern side. Inversion is more prominent on the Cretaceous sediments (Z=2). (Abbreviations: Q- Quaternary, N- Neogene, E-Paleogene) 61

Figure 4.5: Uninterpreted seismic section (A) and fault picks in line c08-9-21c (B) The inset picture shows the position of the seismic line..... 62

Figure 4.6: Interpreted faults and horizons in line c08-9-21c..... 63

Figure 4.7: Uninterpreted seismic section (A) and fault picks in line c08-9-30c showing a negative flower structure (B) 64

Figure 4.8: Interpreted faults and horizons in line c08-9-30c. (Q- Quaternary, N- Neogene, E-Paleogene) 65

Figure 4.9: Uninterpreted seismic section (A) and fault picks in line c08-9-24c (B)..... 66

Figure 4.10: Interpreted faults and horizons in line c08-9-24c..... 67

Figure 4.11: Uninterpreted seismic section (A) and fault picks in line c08-9-18c (B)..... 68

Figure 4.12: Interpreted faults and horizons in line c08-9-18c..... 69

Figure 4.13: Depth-converted illustrations of line c08-09-24c and c08-09-21c..... 70

Figure 4.14: Seismic stratigraphy and PSE of line c08-9-24c 71

Figure 4.15: Seismic stratigraphy and PSE of line c08-9-11c 71

Figure 4.16: Time Structure map for the sill horizon. 72

Figure 4.17: Time-Structure map for the Lower Cretaceous horizon 73

Figure 4.18: Time Structure map for the Upper Cretaceous horizon 74

Figure 4.19: Seismic line c08-9-11c before restoration. The arrows show the direction of movement . 75

Figure 4.20: Seismic line c08-9-11c after decompaction of the Quaternary post-inversion strata 76

Figure 4.21: Seismic line c08-9-11c after decompaction of the Neogene post-inversion strata 76

Figure 4.22: Seismic line c08-9-11c after restoration and decompaction of the Paleogene syn-inversion strata 77

Figure 4.23: Seismic line c08-9-11c after restoration of the Cretaceous horizons. The image shows the bed lengths before inversion tectonics occurred 77

Figure 4.24: Sedimentation rate for Bogal-1 well 79

Figure 4.25: Burial curve for Bogal-1 well 80

Figure 4.26: Superposition of the temperature grid on the burial curves 81

Figure 5.1: Recommended target areas (white circles) on the time structure maps in the Bogal area ... 91

LIST OF TABLES

Table 1-1: History of oil exploration in the Anza Basin summarized from NOCK (2019) 2

Table 2-1: Evolution of the Anza Basin. Summarized from Bosworth, 1992; Bosworth & Morley, 1994; Greene et al., 1991; Reeves et al., 1987; Schull, 1988; Dindi, 1992; Winn et al., 1993..... 26

Table 3-1: Formation tops for Bogal-1 well (CNOOC, 2010)..... 39

Table 3-2: Temperature factors for every 10 ^{0}C used in the Lopatin method (Barker, 1996)..... 42

Table 3-4: Formation ages and erosion history for sediments in Bogal-1 well based on Sewe (1995; Foster and Gleadow (1996) and the GSA geological timescale 44

Table 3-3: TTI- Vitrinite reflectance correlation and hydrocarbon type (Waples, 1985)..... 44

Table 3-5: Summary of the data and software used in this study 45

Table 4-1: A generalized lithological, palaeoenvironmental, tectonic sequence chart with corresponding petroleum system elements (PSE) of the Lower Cretaceous section..... 48

Table 4-2: A generalized lithological, palaeoenvironmental, tectonic sequence chart with corresponding petroleum system elements (PSE) of the Lower Cretaceous section (continuation) 49

Table 4-3: A generalized lithological, palaeoenvironmental, tectonic sequence chart with corresponding petroleum system elements (PSE) of the Upper Cretaceous section 52

Table 4-4: A generalized Lithological, palaeoenvironmental, tectonic sequence chart for the Quaternary and Tertiary section in SE Anza basin..... 55

Table 4-5: Length of the horizons before restoration 75

Table 4-6: Section analysis after fault restoration 77

Table 4-7: An estimation of the shortening factor of the Bogal inversion area..... 78

Table 4-8: TTI calculations for the Upper Cretaceous sediments 82

Table 4-9: TTI calculations for the Lower Cretaceous Sediments 83

Table 4-10: A comparison of the TTI values obtained from this study and those of Sewe (1995) and Waga and Mwachoni (2019).The numbers in brackets show the approximate time for the beginning of hydrocarbon expulsion..... 88

ABBREVIATIONS

AOC	Africa Oil Corporation
BBO	Billion Barrels of Oil
Bcf	Billion cubic feet
BGS	British Geological Survey
CARS	Central African Rift System
CASZ	Central African Shear Zone
CNOOC	China National Offshore Oil Corporation
EARS	East African Rift System
GR	Gamma Ray
Mdst	Mudstone
MMBO	Million Barrels of Oil
NOCK	National Oil Corporation of Kenya
PSE	Petroleum System Element
RES	Reservoir
SR	Source Rock
Sst	Sandstone
Tcf	Trillion cubic feet
TOC	Total Organic Carbon
TTI	Time Temperature Index
VSP	Vertical Seismic Profile

CHAPTER 1: INTRODUCTION

1.1 BACKGROUND INFORMATION

Several countries in the Eastern Africa region have recently announced the discovery of commercial amounts of hydrocarbons in the Tertiary and Cretaceous rifts. Sudan is the largest producer in the region with 5 billion barrels of oil in the Cretaceous rifts, while Uganda holds 1 billion barrels of oil reserves in the Tertiary rift (World Oil Review, 2019). Tanzania has discovered a total of 57 trillion cubic feet (Tcf) of natural gas in their onshore and offshore licences (EWURA, 2017), turning Eastern Africa into a developing petroleum province. Figure 1.1 below shows the hydrocarbon discoveries and exploration licences in the region.

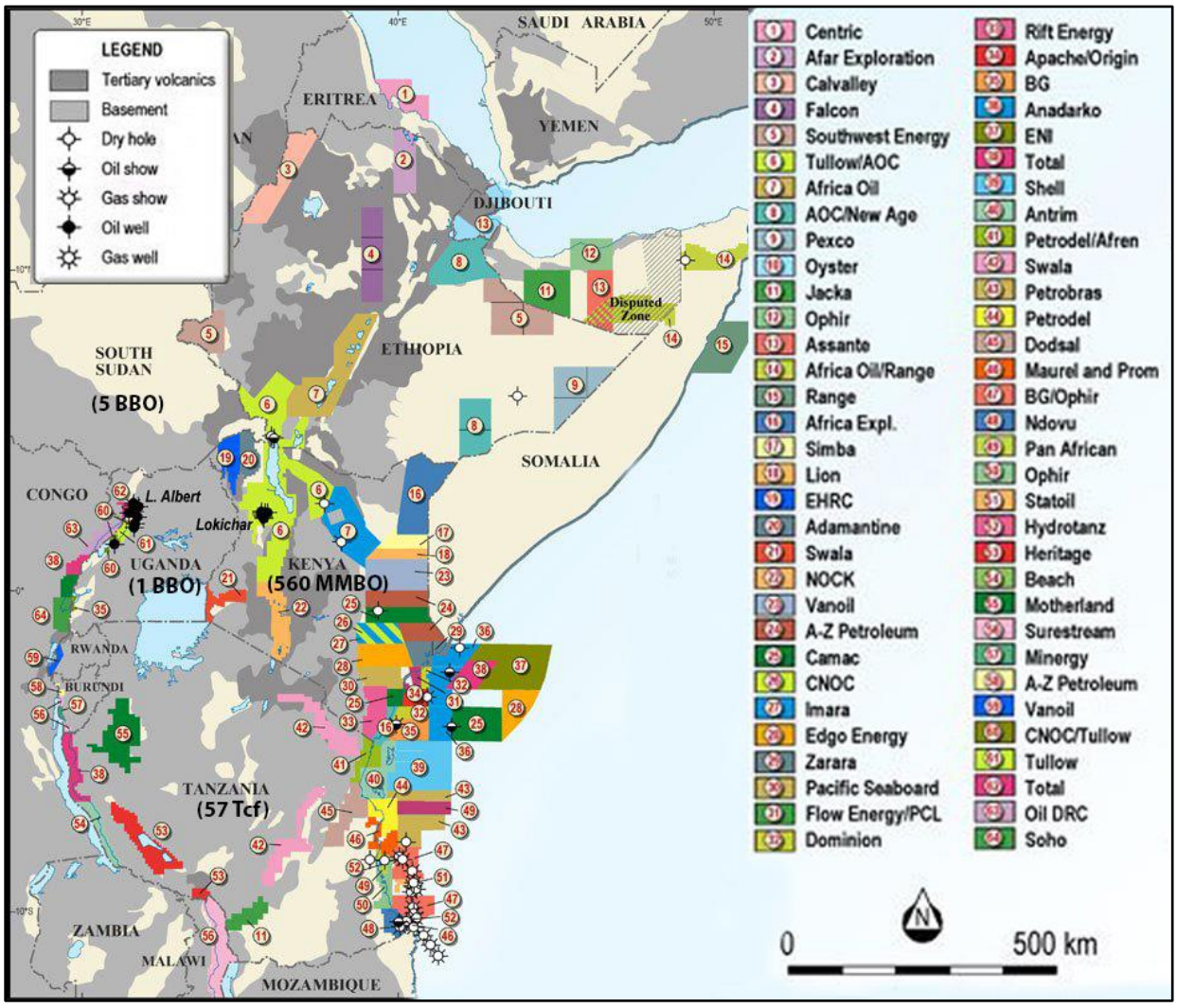

Figure 1.1: Hydrocarbon discoveries and exploration licences in Eastern Africa (modified from GEO ExPro, 2014)

The exploration of hydrocarbons in Kenya began in the 1950s and so far, commercial discoveries have only been found in the Tertiary Rift, where Tullow Oil discovered 560 million barrels of recoverable oil resources in the South Lokichar Basin (Tullow Oil, 2019). No hydrocarbons of commercial value have been discovered in the Anza or Lamu basins to this date, despite the evidence of a working petroleum system.

The southern Anza basin has the potential for harbouring commercial amounts of hydrocarbons. In 2009, CNOOC discovered gas in two pay zones in Bogal-1 well in the Anza basin, and in 2014, Africa Oil drilled Sala-1 well and discovered more gas in three zones. However, Sala-2 well, drilled up-dip from Sala-1, did not find any significant amounts of hydrocarbons. Table 1-1 below gives a history of oil exploration in the Anza basin. It highlights the stages of oil exploration since the 1960s.

Table 1-1: History of oil exploration in the Anza Basin summarized from NOCK (2019)

STAGE		**ACTIVITIES**
1.	*1960s – 1970s*	Exploration in the Anza basin began in the 1960s. It mainly focused on the south-eastern part of the basin, with the aim of finding oil on the edge of the passive continental margin. Seismic acquisition began in 1975, and in 1976, Anza-1 and Bahati-1wells were drilled by Chevron. They were both dry.
2.	*Mid and late 1980s*	Exploration focused on the northern part of Anza basin. This was inspired by the discovery of large oil reserves in Sudan. TOTAL drilled 3 wells in Block 9: Ndovu-1 (oil and gas shows), Duma-1 (gas shows), and Kaisut-1 (no oil or gas shows), while Amoco drilled Sirius-1, Bellatrix-1, Chalbi-3, Hothori-1 (all had oil and gas shows) and Endela-1(gas shows).
3.	*After 1900s*	Exploration was paused in Anza Basin. However, two productive wells: Eliye Springs-1 and Loperot-1 were drilled in the neighbouring Tertiary Rift.

4.	*2005- present*	Exploration resumed due to discoveries of offshore gas in Mozambique and Tanzania, and onshore oil discoveries in Uganda. CNOOC and its partners started exploration in Block 9. They acquired 2D seismic data in 2008, and later drilled Bogal-1 in 2009. Gas was discovered in Bogal-1 well. Paipai-1 well, which was drilled by Tullow in 2013, contained light hydrocarbon shows in a 55m sandstone interval. It was drilled up to a depth of 4255m with the aim of evaluating the large Cretaceous structure in the Anza basin. Sala-1 well, drilled by Africa Oil in 2014 discovered gas in three zones (1000m interval). However, the Sala-2 well, drilled up-dip from Sala-1, did not find any significant amounts of hydrocarbons.

From the table above, it is clear that the Anza Basin has a working petroleum system. However, its full economic potential is still unknown. This study focuses on the southern part of Block 9 in the Anza basin, where inversion tectonics has been identified (Morley *et al.*, 1999). A critical analysis of the structure, stratigraphy and burial history of the Bogal Play is conducted to determine the consequences of inversion on the petroleum system.

1.2 PROBLEM STATEMENT

The Anza basin is part of the larger Central African Rift System (CARS) that traverses the African continent in the north, west and east (Figure 2.1). Inversion tectonics took place in the various sub-basins of the CARS, including the Anza basin in Kenya. Several authors have studied the inversion structures of the other basins in the CARS and their effect on the petroleum system (Petters and Ekweozor, 1982; Genik, 1992; Warren, 2009), but little is known of the inversion structures in the Anza basin. Bosworth and Morley (1994)and Morley *et al.* (1999) acknowledged the presence of inversion anticlines in the south-eastern part of the Anza basin. However, they did not explain the consequence of this deformation on the source rock and reservoir distribution, trap systems and seal in this part of the Anza basin.

Inversion tectonics can affect the petroleum system in different ways, depending on the degree of deformation. Some positive effects of inversion include the creation of new anticlinal traps. Mild

inversion may retain the original fault traps created during extension e.g. in the Sudan rifts (Mohamed *et al.*, 2000). It may also create new stratigraphic traps that form through a change from reservoir facies to seal facies, or the formation of unconformities.

The negative effects of inversion include the re-migration of hydrocarbons towards non-sealing rocks and the redistribution of source rocks and reservoirs. If the degree of inversion is high, uplift created from tectonic inversion may lead to the erosion of seals and reservoirs. It may also expose hydrocarbons to lower temperatures and microbial activities that leads to biodegradation (Cooper and Warren, 2010).

This study seeks to describe the inversion tectonics that took place in the Bogal area and to determine the consequences it had on the petroleum system. This study will answer the following questions:

- What is the degree of inversion in the Bogal play, and what structures were created as a result?
- How were the source rock, reservoir, seal affected by the inversion?
- What is the potential for hydrocarbon fault entrapment?
- Was the timing of inversion suitable for the entrapment of hydrocarbons?

1.3 AIM AND OBJECTIVES

Aim:

To determine the magnitude and geometry of inversion tectonics in the Bogal play and to establish the consequence of the deformation on the petroleum system of this area.

To accomplish this, the following specific objectives were met:

1. To define the stratigraphy and the petroleum system elements within the Bogal Play through the analysis of seismic and lithostratigraphic data in order to establish the deformations that may have affected the petroleum system of the Bogal play.
2. To demonstrate the structural geometry of the Bogal Play based on 2D seismic data interpretation and fault restoration.
3. To determine the hydrocarbon potential of the area by generating burial history graphs of Bogal-1 well and calculating the TTI values.

1.4 JUSTIFICATION AND SIGNIFICANCE

1.4.1 Justification

An integrated analysis of the structural and stratigraphic components of the Bogal play offer more insights on the compressional dynamics of the Anza basin. Stratigraphic analysis examines the re-distribution of the petroleum system elements caused by inversion tectonics. Extreme deformation and re-distribution of the source rocks, reservoir and seal might destroy the hydrocarbon traps that may have formed during the extensional phase, while mild deformation will preserve them. This potential re-organization of the petroleum system depends on the degree of inversion, whether partial, mild or complete. Therefore, structural analysis and fault restoration is key in evaluating the amount of shortening and its impact on hydrocarbon accumulation.

Timing is a crucial factor in the entrapment and preservation of petroleum. The critical moment of hydrocarbon entrapment in inversion structures depends on the timing of hydrocarbon expulsion from the source rocks relative to the timing of inversion tectonics. Therefore, TTI analysis plays an important role in determining whether hydrocarbon entrapment within the Bogal Play will be successful.

1.4.2 Significance

Inversion structures in the Sudan rifts have proven to be good hydrocarbon prospects (Cooper and Warren, 2010). Mild inversion in Sudan preserved the original trap geometries and source-reservoir-seal distribution that formed during the extensional phase thereby preventing the re-migration of hydrocarbons or the erosion of seals. Inversion in Sudan also created new anticlinal traps that trapped significant amounts of oil e.g. in the Heglig field in Sudan (ElHassan *et al.*, 2017). Cretaceous to Tertiary inversion tectonics in the neighbouring oil-rich Sudan rifts can be related to Kenya due to the structural similarities between these basins. An examination of the inversion dynamics within the Bogal structure in the Anza basin checks for any similarities or differences between the Kenyan and Sudan rifts that can help in understanding the unsuccessful search for commercial amounts of hydrocarbons in Kenya. Information obtained from this study will contribute to the understanding of the viability of other inversion structures developed within the Anza basin.

CHAPTER 2: LITERATURE REVIEW

This chapter gives a review of the literature published by various authors in relation to the geology of the Anza Basin. It presents a synthesis of the previous works done on the geological and structural setting of the basin, its petroleum system and inversion tectonics.

2.1 REGIONAL SETTING

The Anza Basin is part of the Central African Shear zone (CASZ) that stretches 2000 Km from the Gulf of Guinea to Cameroon, Chad and The Central African Republic up to Sudan and Kenya. Figure 2.1 below shows the extent of the CASZ in Africa.

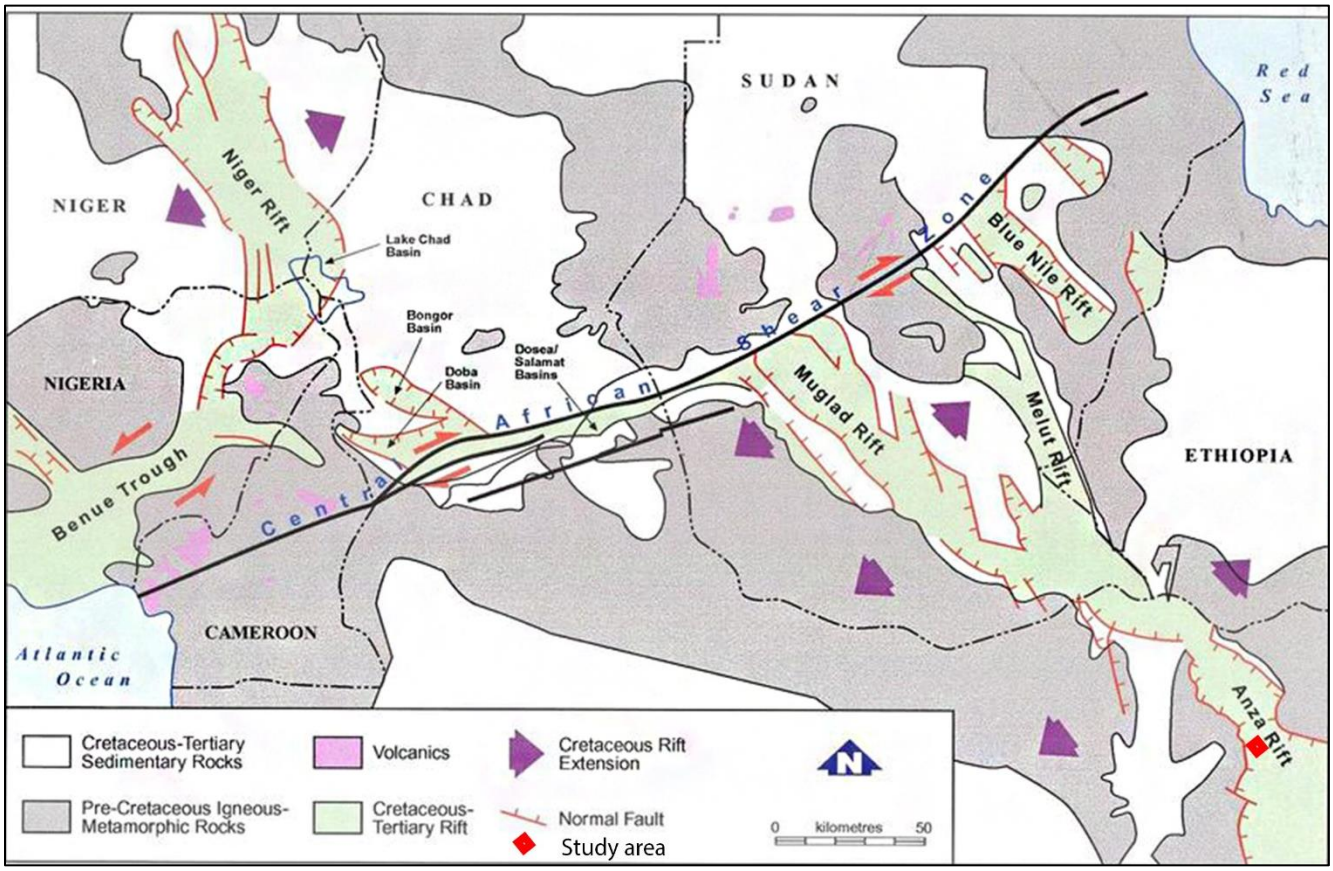

Figure 2.1: The Central African Rift System, after Fairhead (1988).

The CASZ formed as a result of global tectonic plate motions that led to the separation of Africa and South America in the Early Cretaceous. This caused widespread rifting and sedimentation that created basins within and adjacent to the shear zone. The dextral movement of the CASZ along

fracture zones, during the opening of the Atlantic, caused extension and a change in orientation from NE-SW to a NW-SE (Moulin *et al.*, 2010). Basins such as the Benue Trough, East Niger Basin, (Kome) Doba Basin and the Ngaoundere Rift developed within this shear zone while others such as the Muglad, Melut, Anza, Benue and East Niger basins developed adjacent to the shear zone as shown in Figure 2.1 (Fairhead, 1988). The CARS and Anza rift systems were connected during the Cretaceous by oblique-slip faults striking in an east-west direction (Ebinger and Ibrahim, 1994).

Reeves *et al.*, (1987) suggested that the Sudan rifts extend south-eastwards into Kenya to become the Anza Basin and the Lamu Embayment. This thought is upheld by Bosworth (1992), who studied the general geometry of the CARS in Sudan and Kenya in detail. He examined seismic reflection data in the Sudan rifts as well as those from the Anza basin in Kenya and concluded that both NW-SE-trending basins are related to each other in structure and tectonic development. This point echoes the work of (Schull, 1988), who describes the rifting phases of the Sudan rifts and draws similarities between them and the Anza Basin. Both basins are characterized by deep bounding faults filled with thick Cretaceous to Tertiary sediments. Rift initiation in the Anza rifts began as early as the Early Jurassic (Bosworth and Morley, 1994), while the Sudan rift may have initiated in the Late Jurassic to Early Cretaceous (Schull, 1988). Winn *et al.*, (1993) noted that the Sudan and Anza rifts have similar Cretaceous-Tertiary strata. Both rifts are filled with fluvial, alluvial and aeolian sediments. However, marine sediments that are developed in the Anza basin have not been encountered in the Sudan rifts.

Both the opening of the Atlantic during the Early Cretaceous and the separation of Madagascar and Africa in the Mid Jurassic contributed to the evolution of the Anza Basin and the Sudan rifts (Schull, 1988; Greene *et al.*, 1991; Bosworth, 1992). Reeves *et al.*, (1987), using aeromagnetic and gravity data, describe the Anza Basin as a failed arm of a triple junction that formed as a result of the separation of Africa and Madagascar during the Jurassic. Similar conclusions were made by Rabinowitz *et al.*, (1983), who, on the basis of paleomagnetic data, place the original position of Madagascar adjacent to the coast of Kenya and Somalia. The other two arms of the triple junction, according to their data, are the Kenyan coast and the Somali coast.

The Mombasa coastline is the first arm of the triple junction. It represents the initial rifting phase during the Late Carboniferous (Pennsylvanian), when the thick strata of the Karoo formation

accumulated. During the Permian, Triassic and Jurassic, continental sediments were deposited during rifting that was associated with minor marine transgression. Marine conditions began encroaching from the north, in the Somali coastline.

The second arm of the triple junction is the southern end of the basement exposed in northeast Kenya. It extends eastwards to the southern edge of the basement in Mogadishu. It became active during the Jurassic after the failure of a parallel rift, which is now the Mandera-Lugh Basin between Kenya and Somalia. Rifting in the Somali and Mombasa coastline developed into the Indian Ocean and the separation of Madagascar and Africa during the breakup of Gondwanaland. These coastlines show evidence of Jurassic marine conditions. Jurassic shallow water carbonates occur on the Matasade Horst and at Dogogicha as shown in the geological map of the Anza basin in figure 3.6.

The third arm is the failed Anza Rift. Marine transgression occurred in the trough during the Upper Jurassic. Regression then occurred during the Cretaceous, with marine conditions retreating southwards towards the Lamu Embayment. During the Tertiary, the Lamu embayment underwent large-scale subsidence, which led to an expansion of the delta of the triple junction into the entire coast of Kenya. Reeves *et al.*, (1987) point out the similarity of this triple junction to the Benue Trough of the Niger Delta as see in figure 2.1 above.

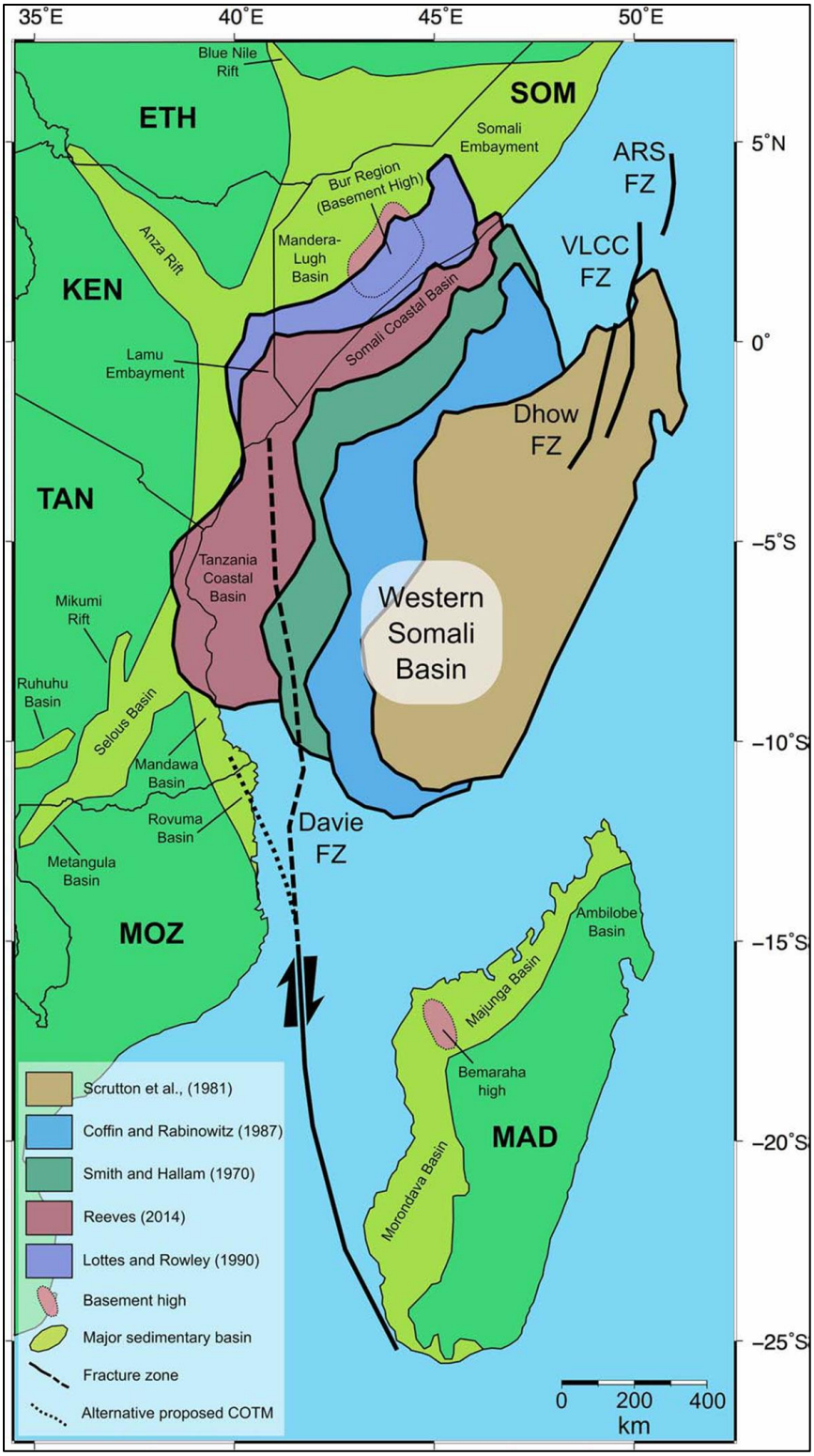

Figure 2.2: The separation of Africa and Madagascar at a triple junction. The image shows the paleoposition of Madagascar adjacent to the Somali and Mombasa coastline. VLCC-Very Large Crude Carrier Fracture Zone, ARS-Auxiliary Rescue and Salvage Fracture Zone. (Phethean *et al.*, 2016)

2.2 STRUCTURAL SETTING

The Anza rift is one of the four major sedimentary basins in Kenya. It neighbours the Lamu embayment to the south-east, the Mandera basin to the north-east and the Tertiary rift to the west (Figure 2.3). Anza basin generally trends in a NW-SE direction.

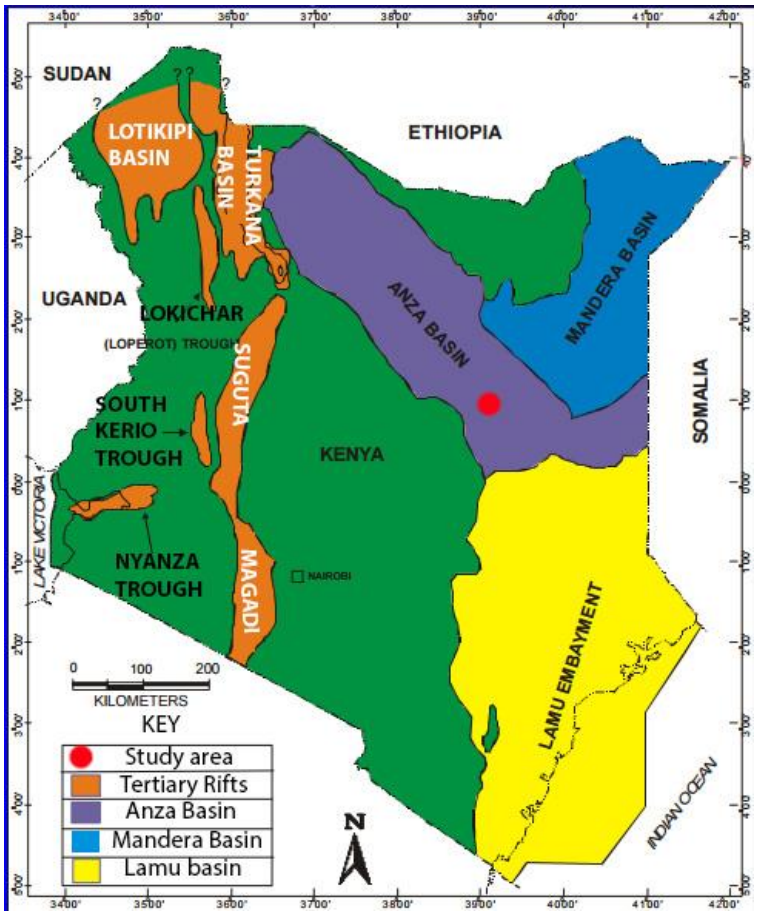

Figure 2.3: Sedimentary basins of Kenya, after Nyaberi and Rop (2014).

The Anza basin is the most extended basin of the CARS (Bosworth, 1992). The geometry of the basin has been examined using seismic data (Bosworth, 1992), gravity and magnetic data (Reeves *et al.*, 1987; Greene *et al.*, 1991; Dindi, 1994) and the results show that Anza basin consists of numerous sub basins, each with a different structural history. It is subdivided into two major parts: The Northern Basin, and the Southern Basin. The Matasade horst separates the main Anza basin from Kaisut sub-basin. The entire Anza rift is about 580 km long, 150 km wide, with a sediment thickness of 6-10 km. Dindi (1994) notes that the Anza basin has an alternating symmetry, with the northern basin dipping to the south-west, and the southern basin dipping to the north-east. He

recognizes three structural trends: the NW-SE main trend associated with the extension of the Anza rift, an ENE-WSW trend of structures such structures around Garissa and Mado Gashi that may have formed due to compressional stress that created uplifts. The third trend is in a N-S direction and is associated with the Kenyan Rift Valley. It is more pronounced in the western Anza than in the east.

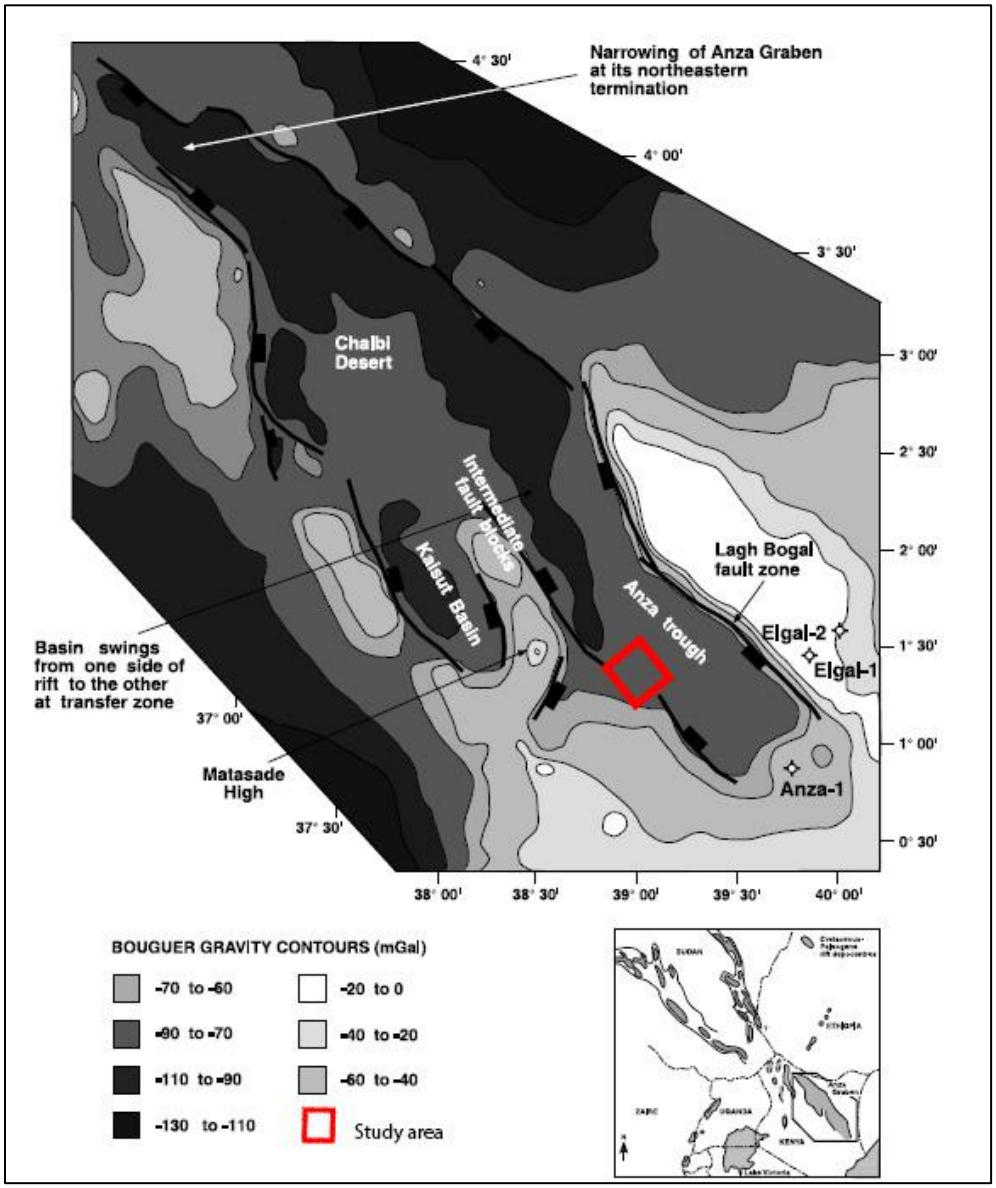

Figure 2.4: Gravity map of the Anza basin showing the major faults and sub-basins (Morley *et al.*, 1999)

2.3 STRATIGRAPHY OF THE ANZA BASIN

The stratigraphy of the Anza basin mainly consists of Jurassic, Cretaceous and Tertiary sediments that were deposited in lacustrine, deltaic, fluvial and flood basin environments (Winn *et al.*, 1993). No well section has encountered the crystalline basement yet. Wells in the Central and Southern Anza rift have only reached the Late Cretaceous sediments because the Upper Cretaceous and Tertiary sediments thicken towards the southeast of the basin (Bosworth and Morley, 1994).

Jurassic

The Jurassic sequence in Kenya predominantly consist of limestone with lessor sandstones, siltstones, mudstones and shales (Winn *et al.*, 1993). Jurassic strata have not yet been encountered by any well in the Anza basin. However, they appear as outcrops on the Matasade horst (figure 3.6).

Early Cretaceous

Early Cretaceous sediments have been encountered in the Sirius-1 well section. They consist of interbedded sandstone, limestone and shale. The sandstone is described as moderately sorted, fine to coarse grained and moderately mature with less than 10% of feldspar. The shale is reported to be medium-brown in colour, while the limestone is characterized as fine-grained with visible pellets (Winn *et al.*, 1993). This limestone and shale are likely to be of lacustrine origin while the sandstones may be of deltaic origin. Aptian-Albian sediments are absent from all wells in the Anza basin except for Chalbi-3 well. However, it is present as a marine section in Wal-Merer-1, located further south-east in the northern Lamu basin (Morley *et al.*, 1999).

Late Cretaceous:

Cenomanian: Thick Cenomanian sediments are present in central Anza. They comprise deep water, marine, brackish and lacustrine shales as indicated in Ndovu-1 well. This suggests a brief marine incursion occurred in central Anza during the Cenomanian. The Turonian-Santonian presented a break in tectonic extension (Morley *et al.*, 1999).

Santonian – Coniacian: They occur as light-medium grey shale, white-light grey sandstone and a little fine-grained limestone deposited in a lacustrine depositional environment.

Campanian- Maastrichtian: These sediments are thick in Sirius-1 Bellatrix-1, Ndovu-1 and Hothori-1 wells. They consist of poorly sorted, fine-grained, angular sands with thick layers of mudstones with subordinate sandstones. They are less mature than the Santonian-Coniacian sediments, implying that they may represent syn-rift deposits (Winn *et al.*, 1993).

Red beds consisting of oxidized shale, sandstone, conglomerate and mudstone occur in Sirius-1, Bellatrix-1, Ndovu and Hothori-1 wells. They were probably deposited in exposed flood basins, fluvial and fan environments. Coal beds were encountered in Bellatrix-1. The strata might have been deposited in a deltaic-lacustrine to deep water-lacustrine environment. Duma-1 well contained dinoflagellate microfossils that indicate a second marine incursion during the Late Cretaceous. Similar deep marine shales were encountered in the Ndovu-1 well section.

Tertiary - Quaternary

Tertiary sediments have been described as course fluvial clastics interbedded with overbank lacustrine sediments that increase in thickness towards the south-east (Bosworth and Morley, 1994).

Eocene-Oligocene: Eocene-Oligocene strata are represented by immature, poorly sorted, fine-course sandstone, green-brown shale that suggest syn-rift sedimentation (Winn *et al.*, 1993). They have been encountered in Bellatrix-1, Ndovu-1 and Hothori-1 well sections. The green- brown coloration of the shale units suggests low organic content with a moderately oxygenated depositional environment frequently observed in flood basins or lacustrine environments.

Miocene: Miocene-recent sandstone, conglomerate and basalt that are a few hundreds of metres thick, cover a large part of the basin. These unfaulted sediments form an unconformity above the older sediments (Morley *et al.*, 1999). These sediments are mature, well sorted and have a higher sand content. They may have been deposited in a braided stream depositional environment and constitute the post-rift sequence in the Anza basin. Winn *et al.*, (1993) suggested that they may have been deposited during a passive subsidence phase.

Pliocene-Holocene: Thick layers of basalt conceal most of the sediments in the western Anza basin as observed in Sirius-1, Bellatrix-1 and Ndovu-1 well sections. They are absent in the Southern Anza rift (figure 2.5).

Diabase intrusion

A diabase sill has been identified in the Sirius-1 well section (Winn *et al.*, 1993) and in seismic sections of the Kaisut basin (Bosworth and Morley, 1994). This sill is crystalline, lacks vesicles and commonly consists of plagioclase and pyroxene. It is believed to be of Tertiary age, although, this is not confirmed. The sill intrusion may have caused an increase in the maturity rate of the source rocks of the Anza basin.

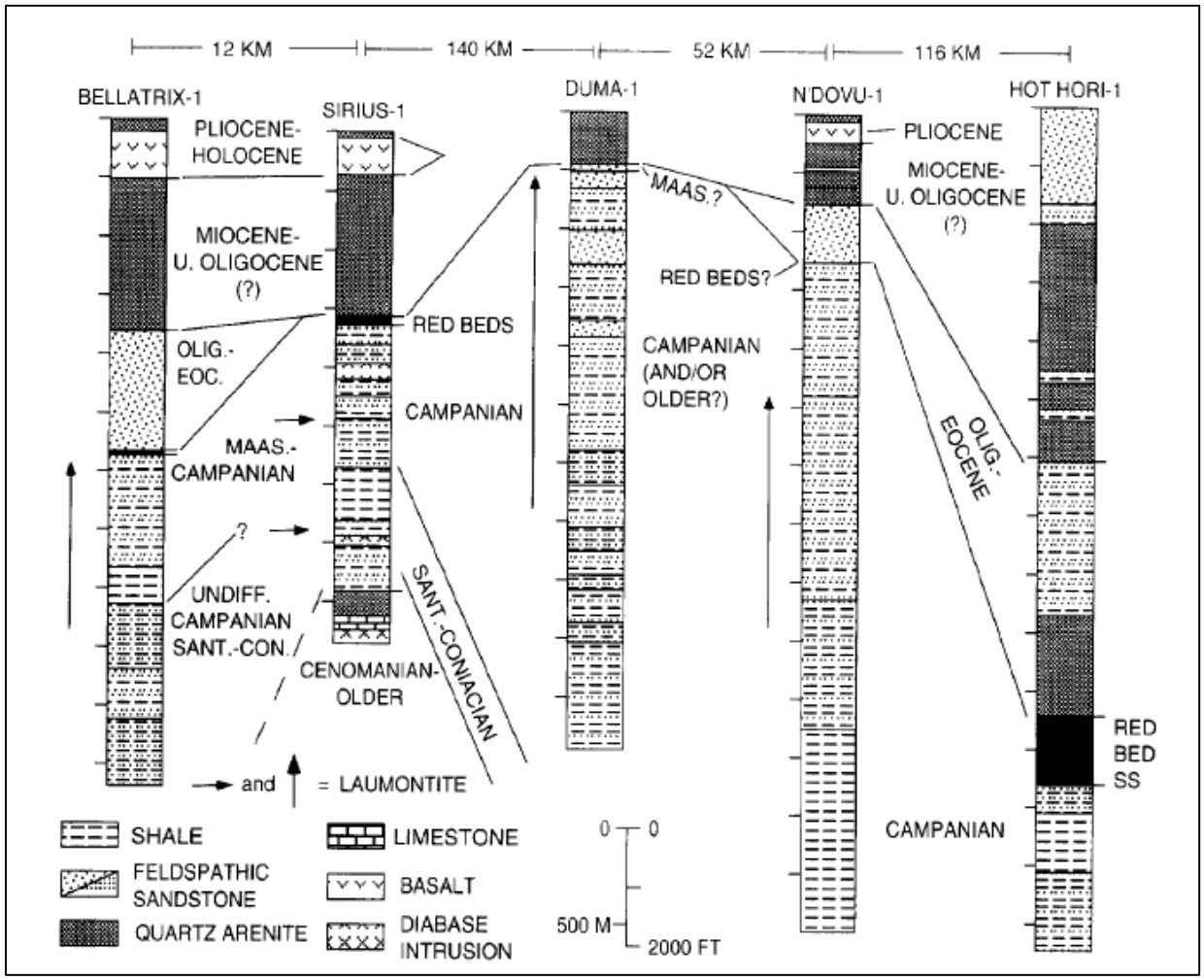

Figure 2.5: Stratigraphy of the Anza basin (Winn *et al.*, 1993)

2.4 PETROLEUM SYSTEM OF THE ANZA BASIN

Most of the wells drilled in Anza Trough have exhibited oil and gas shows that indicate the presence of a working petroleum system. They have given evidence of good source rocks, reservoirs and sealing rocks. Wells in the north and central part of the basin contain both oil and gas shows, while wells in the southern part mainly highlighted the presence of gas. Wells drilled in Block 9 have recorded both oil and gas shows. Ndovu-1 displayed strong oil and gas shows in the Late Cretaceous sandstones, while Duma-1 denoted weak oil and gas shows (Africa Oil Corp, 2008). Bogal-1 well contained gas in the Upper and Lower Cretaceous sediments (CNOOC, 2010). Africa Oil Corp announced the discovery of gas in the 3030m-deep Sala-1 well, located 51 Km NE of Bogal-1 (appendix 4). However, Sala-2 did not discover any commercial amounts of gas up dip from Sala-1. Commercial amounts of hydrocarbons were discovered in the Neocomian-Lower Albian sediments that make up the source, seal and reservoir rocks in the Sudan rift basins.

2.4.1.1 Source Rocks

Wells drilled in Anza Basin indicate the presence of source rocks in the Upper Cretaceous and Lower Cretaceous sediments. Sirius-1 well contained shales with TOC values of 3.4- 9% in the Lower Cretaceous sediments (Morley *et al.*, 1999). Thick oil- prone source rocks were also discovered in the Upper Cretaceous segment of this well. Bellatrix-1 well recorded TOC values ranging from 0.71 to 4.6. Bosworth and Morley (1994) suggest the possibility of an Aptian-Albian lacustrine source rocks being present in the undrilled parts of Anza rift, similar to the source rocks of the Sudan rifts. However, these have only been encountered by Chalbi-3 well (Morley *et al.*, 1999).

2.4.1.2 Reservoir Rocks

Good reservoir rocks with porosity values of about 30% and permeability of up to 223mD have been identified in the Anza basin. Sirius-1 well recorded porosity values that range between 19 and 32% in the Lower Cretaceous sediments while Bellatrix-1 well recorded porosities up to 20% (NOCK, 2005)**.** However**,** in Block 9, reservoir values are much lower, for instance, Lower Cretaceous sediments in Ndovu-1 recorded gas in the low permeability sediments with porosity values of 10%-12%. Duma-1 also recorded some gas shows in reservoirs of low porosities ranging from 6% to 13% (Africa Oil Corp, 2008).

2.4.1.3 Seal

Thick Upper Cretaceous shales form a regional seal in the Anza basin as indicated by Sirius-1 well. This seal is laterally limited in extent as observed in the Bellatrix structure in northern Anza. Duma-1 well in Block 9, drilled on an inverted anticline and Kaisut-1 well also illustrated the absence of a sealing rock (Africa Oil Corp, 2008). Unconformities present in the Anza basin could act as potential seals due to their lateral extent.

2.5 INVERSION STRUCTURES

2.5.1 Definition

The term inversion is used to describe basins that have undergone a reversal from subsidence to uplift. Inversion structures form when a previously extensional tectonic setting is subjected to compressional or transpressional forces (Bally, 1984). These forces may be due to changes in regional stress regime e.g. the collision of plates. The process of inversion involves basin formation through normal faulting, deposition of sediments and subsequent compression leading to uplift of the basin (Cooper *et al.*, 1989). Figure 2.6 illustrates the formation of an inversion structure. Figure 2.6(a) shows a half basin that formed due to normal faulting and sediment deposition during extension while 2.6 (b) and (c) illustrate compressional deformation that led to the formation of inversion anticlines.

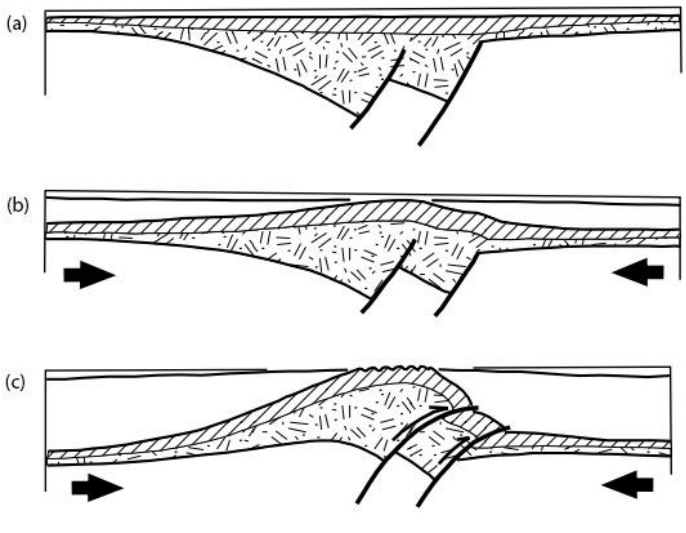

Figure 2.6: Illustration showing the inversion of a half basin. From (Buiter and Pfiffner, 2003)

Cooper *et al.* (1989) describe inversion structures in terms of regional elevation whereby the term 'regional' refers to the original structural elevation of the horizon before any deformation. Extensional deformation will lower the structural elevation of the marker horizon below the regional elevation (figure 2.7), while compressional deformation will raise the elevation of the marker horizon above the regional elevation (Figure 2.8).

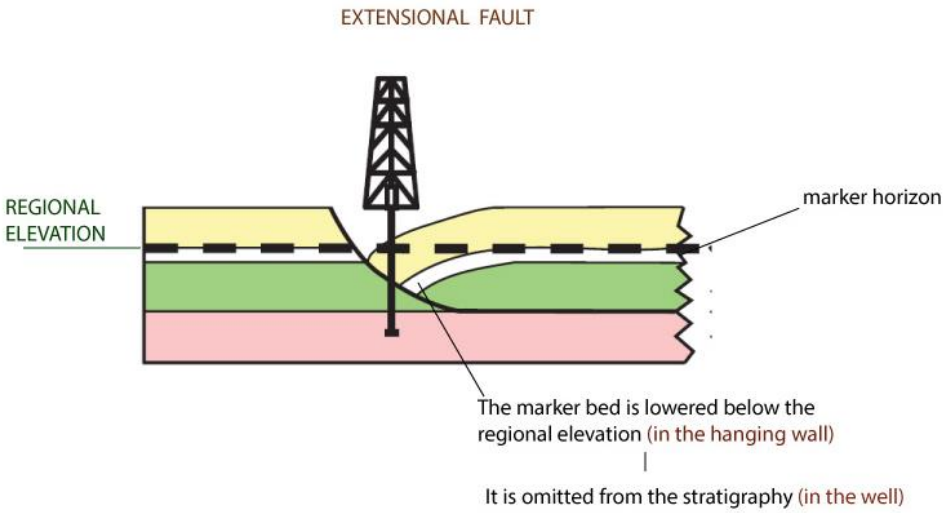

Figure 2.7: Extensional deformation before inversion. After Cooper and Warren (2010)

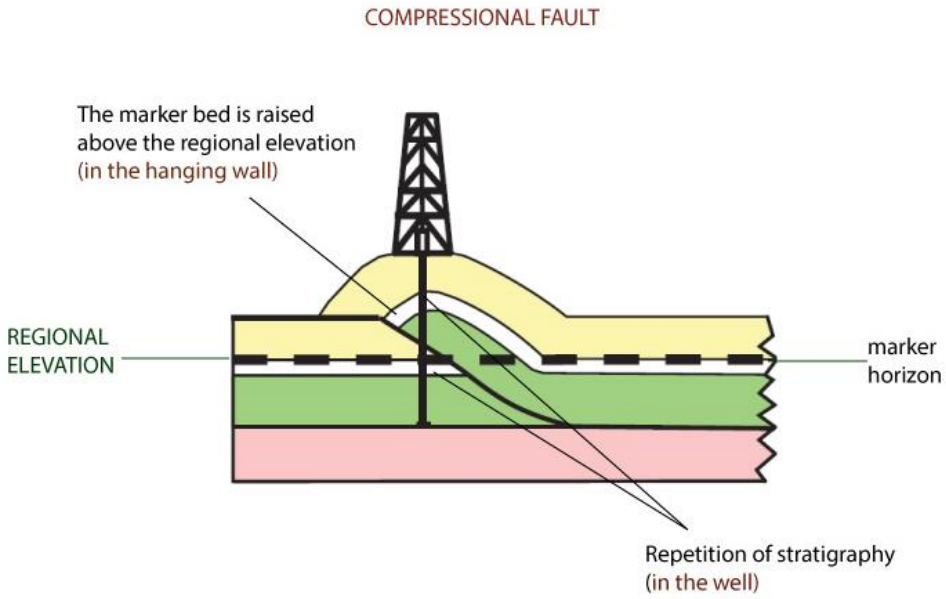

Figure 2.8: Inversion structure after compression. After Cooper and Warren (2010)

2.5.2 Occurrence

Ziegler *et al.* (1995), in their review of the megatectonic setting of intraplate compressional deformations in Africa, Russia and North America, attribute the formation of inversion structures to the collision of plates in orogenic settings that transfer the stress to the continent interiors. They also acknowledge that compressional deformation can occur in non-orogenic settings due to transpressional forces e.g. in the CARS, where transform deformation dominantly occurred with minor compression. They state that inversion occurs mainly in intraplate basins, but other authors such as De Graciansky *et al.* (1989) believe that this could also occur in passive margins with extensional faults. They gave an example of the Alps Mountains, which underwent extension during the opening of the Tethys in the Mid Jurassic as well as the opening of the North Atlantic and later on experienced compression due to the subduction of the oceanic crust in the Late Cretaceous.

Inversion occurs in basins that formed under tensional stress that caused thinning and weakening of the crust. It occurs best during a short-term interval between the extension period and the compression period. This is because the lithosphere requires some time to thermally re-equilibrate (Ziegler *et al.*, 1995).

According to Cooper *et al.*, (1989), the development of inversion basins should follow the requirements below:

1. The basin should be controlled by faults
2. The syn-rift deposits should be recognized
3. There should be a change in regional stress that will cause a reverse on the fault slip, with the uplift only affecting the hanging wall.

Tari *et al.*(2020) classify inversion tectonics into two modes:

Mode I: Occurs where the syn-rift sequence is thicker than the post-rift succession. This often occurs in failed intracontinental basins and proximal passive margins (figure 2.9a).

Mode II: Occurs where the syn-rift sequence is thinner than the post-rift succession (Figure 2.9b). This is common in back-arc basins and in the distal parts of passive margins.

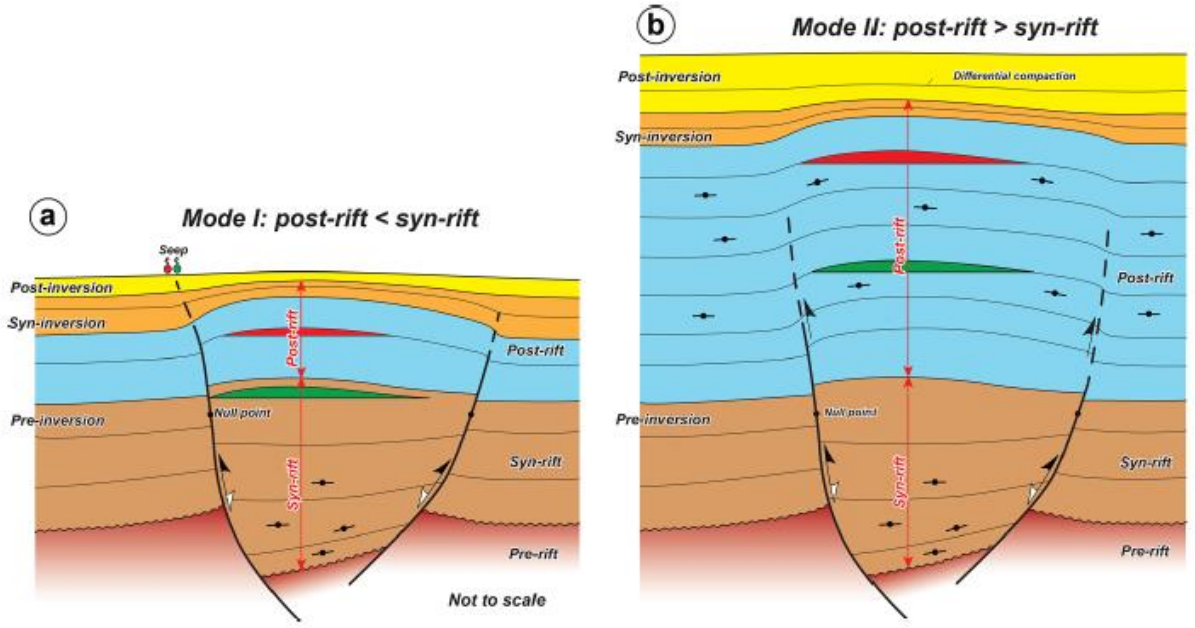

Figure 2.9: The two modes of structural inversion: mode I (a), where the post-rift is thinner than the syn-rift, and mode II, where the opposite occurs (Tari *et al.*, 2020)

2.5.3 Geometric Characteristics

The degree of inversion varies from partial, mild to complete. Mild inversion occurs when deformation takes place only on the shallow parts, turning it into an anticlinorium, while the bottom part remains undeformed. In total inversion, movement along the fault is reversed to its original configuration. For significant inversion to occur, pre-existing weak fault zones must exist (Buiter and Pfiffner, 2003). Figure 2.10 below illustrates the progression of structural inversion from the pre-rift (a) and syn-rift stages (b and c) to the mini-inversion (d) and total inversion (e), up to the post-null point stage of inversion.

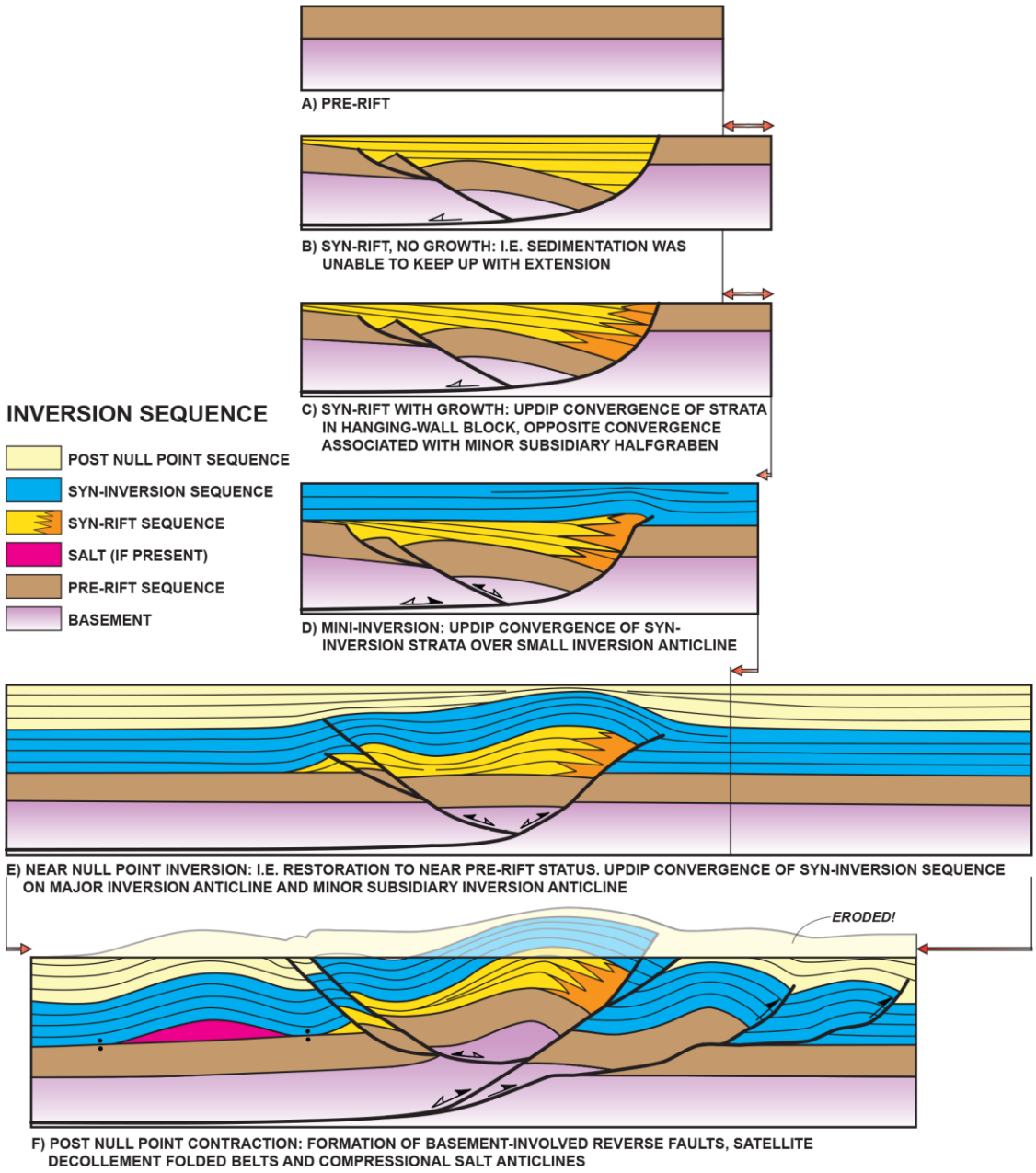

Figure 2.10: An extension of Bally, 1984*'s model of inversion as cited by* Tari *et al.*, (2020)

The essential requirement for an inversion structure is the extensional fault geometry and its subsequent compressional reactivation (Hayward and Graham, 1989). Inversions can be identified in seismic sections where the hanging wall of a fault has marker horizons that display different elevations above and/or below their respective regionals. The accommodation space that is created in the hanging wall during extension is filled with sediments. It is important to understand the initial extensional geometry and sediment distribution before the inversion in order to understand

the petroleum system after the inversion (Cooper and Warren, 2010). For the inversion to be recognized, the syn-rift sediments must be identified in the inversion structure (Cooper *et al.*, 1989).

The pre-rift sequence will have originally been extended by a factor. During inversion, the slip on the fault is reversed, causing the expulsion of the syn-rift deposits. The post-rift is longer since it was deposited on extended strata. After inversion, the post-rift sequence will shorten while the pre-rift will be restored to its pre-extensional level (Hayward and Graham, 1989). Inversion becomes more difficult after the pre-rift has been restored to its pre-extensional level. The shortening of sediments causes folding and backthrusting on the hanging wall. Backthrusts are mainly associated with listric faults rather than planar faults that bound the basin (Buiter and Pfiffner, 2003). This is simulated in a sandbox experiment by Gomes *et al.* (2010) in figure 2.11 to 2.12 below.

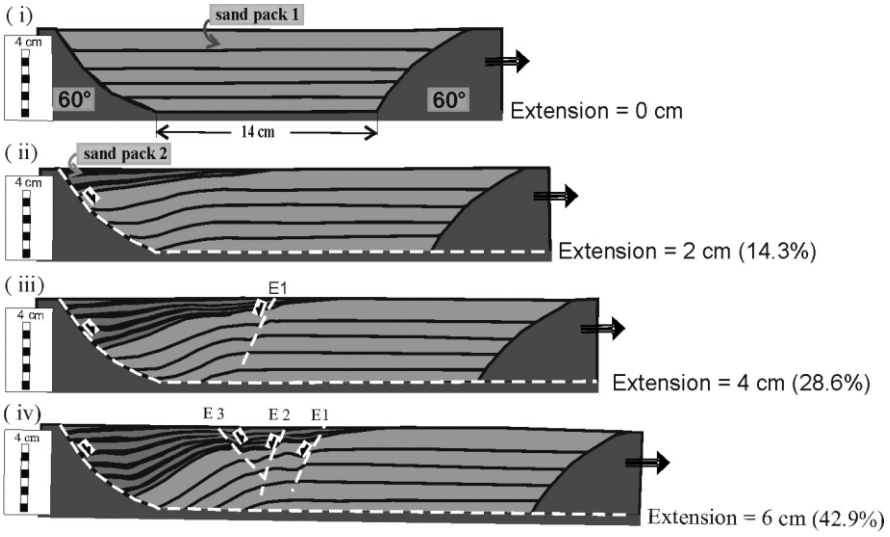

Figure 2.11: Sandbox experiment showing extension phase with normal faults (Gomes *et al.*, 2010)

Figure 2.11 above illustrates the extensional phase; whereby initial extension causes the deposition of syn-rift sediments and synthetic and antithetic faults.

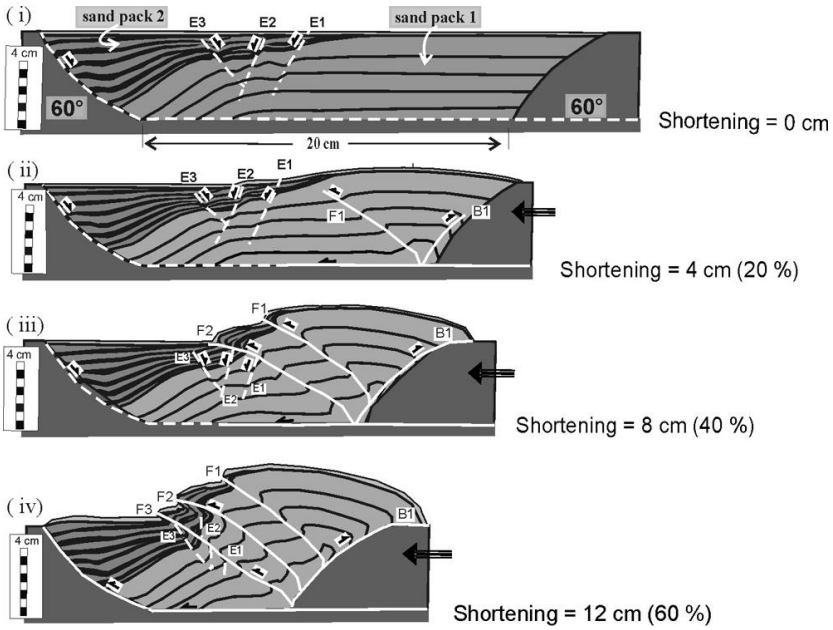

Figure 2.12: Sandbox experiment showing compressional phase during inversion. E1 - E3 are structures that formed during inversion and F1 -F3 are forethrusts while B1 is a backthrust (Gomes *et al.*, 2010)

Figure 2.12 above illustrates the inversion phase whereby shortening causes the formation of inversion anticlines, folds and backthrusts. Inverted half basins produce asymmetrical monoclines facing the footwall. Their crest is located above the syn-rift depocenter as illustrated in the example below.

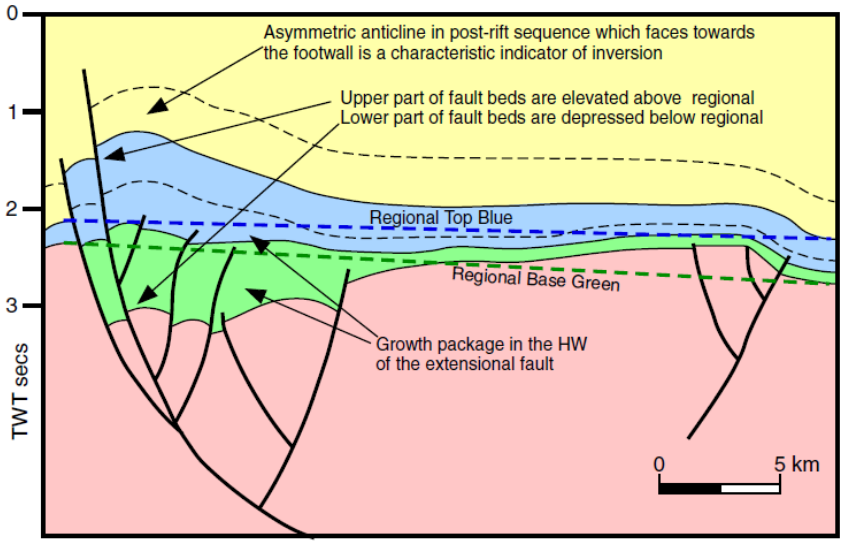

Figure 2.13: Illustration of the geometric characteristics of inversion structures, from Cooper and Warren (2010). *The bold dashed lines represent the regional elevation.*

2.5.4 Significance of inversion structures to the petroleum system

Cooper and Warren (2010) give examples of hydrocarbon exploration case studies in various inversion structures in different tectonic settings such as Western Newfoundland, Canada. Despite the difference in tectonic settings, the geometry of inversion structures is consistent. They state that the effect of inversion structures on the petroleum system depend on the controls from the initial extensional regime as well as the following compressional history that modifies the old trap systems or creates new ones such as footwall shortcuts and inversion anticlines.

The following is a summary of the implications of inversion to the petroleum system, summarised from Cooper and Warren (2010):

Traps

- The fault traps created during the extensional phase may be preserved after inversion
- Mild inversion can create large anticlines that trap hydrocarbons from the nearest source. However, these anticlines may post-date the initial migration from the syn-rift source rocks, creating a charge risk
- New stratigraphic traps can be created through a facies change of reservoir to seal

Migration

- Inversion may modify old trap systems, causing re-migration of hydrocarbons due to the new geometry of the basin
- The hydrocarbons may migrate upwards along non-sealing faults

Reservoir and Source Rocks

- Inversion may lead to the redistribution of reservoirs and source rocks

Seal

The inverted basins that have been uplifted as much as 2 km may be eroded, destroying seals and reservoirs.

Other risks

Inversion may expose light hydrocarbons to meteoric water and cooler temperatures, leading to biodegradation risk

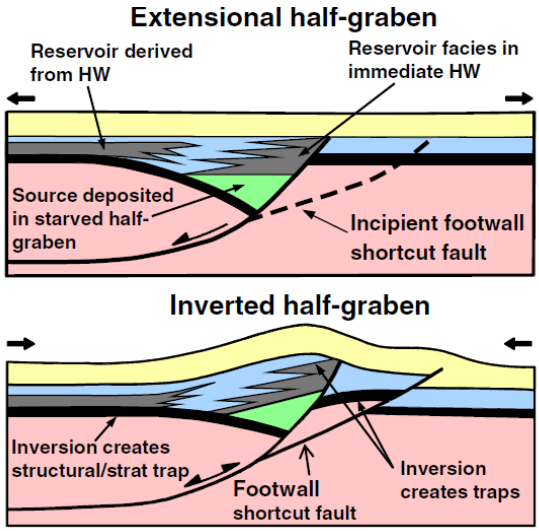

Figure 2.14: Effect of inversion on the petroleum system elements (Cooper and Warren, 2010)

Mild to moderate inversion structures are the preferred petroleum prospects This is because mild inversion creates simple closures with small vertical amplitudes that lie above the extensional depocenters (Tari *et al.*, 2020).

2.5.5 Inversion in the CARS

The CARS (Figure 2.1) consists of several basins that contain inversion structures (Petters and Ekweozor, 1982; Genik, 1993). Genik (1993) suggests that compressional tectonics in the Benue, Bongor and Doba Doseo basin took place during the Santonian. He attributes this compression to the convergence of the African plate and the European plate. However, Ziegler *et al.* (1995) suggest that this inversion formed due to a change in strain distribution due to wrenching rather than the collision of plates.

Inversion in the CARS is mostly pronounced in the ENE–WSW orientated Benue, Logone Birni, Bongor, Doba and Doseo basins. It is least pronounced in the WNW–ESE Termit-Lake Chad, Muglad, Melut and Anza basins. The inversion is minimal in the Eastern African rifts because they are oriented in a NW-SE direction. The Barraga block in South Sudan shows evidence for Cretaceous and Tertiary compressional structures and strike-slip movement (Schull, 1988). Inversion structures occur sporadically in outcrops as well as the subsurface in the Anza basin, western Somalia and the northern and central part of Sudan (Bosworth 1992). The lack of significant inversion in the Eastern African basins such as the Muglad and Melut basins in Sudan favoured the original trap geometries that formed during extension without any re-migration of hydrocarbons. The source rock was deposited and matured early and the hydrocarbons were

trapped shortly afterwards. Since the inversion was not very significant, these source rocks were not fully uplifted and eroded, enabling them to mature within the oil zone. This also ensured the hydrocarbon seal was preserved. In the CARS, inversion anticlines are the main type of traps formed in the E-W oriented basins. However, in N-S oriented basins, extensional fault blocks are the main type of traps formed.

2.6 GAPS IN LITERATURE

Little is known about the inversion structures in the Anza basin. Authors such as Bosworth (1992) and Morley *et al.* (1999) acknowledge the presence of inversion structures in the Anza basin, but they do not go into much detail. Bosworth (1992) studied the Mesozoic and Early Tertiary rifts in Eastern Africa using seismic data and suggested that the Khartoum basin in Sudan and the Anza basin underwent inversion during the Early Tertiary. He attributes this inversion to Late Cretaceous-Early Tertiary wrench faulting. Morley *et al.* (1999) note the presence of pronounced Paleogene inversion anticlines in the central and south-eastern part of Anza basin e.g. in the Hothori-1 and Ndovu-1 well site areas. They conclude that multiple episodes of inversion occurred in the Central and Southern Anza rift. Morley and Wigger (1999) gave a more detailed study of the geometry, magnitude and origin of basin inversion in East African basins such as Rukwa, Turkana and Anza. They mainly used seismic data and focused on the mechanism and geometry of inversion anticlines within the southern part of the Anza basin. They concluded that the inversion structures in the southern part of the Anza graben are more developed than on the northern parts. They also suggest that multiple phases of inversion that alternated with extension occurred. According to their study, the driving force was short, and alternated with periods of extension. No study has established the impact of inversion tectonics on the petroleum system of the basin. This study offers an improved understanding of the stratigraphy and an estimation of the amount of shortening that occurred due to inversion and its impact on the petroleum system of the basin. Furthermore, previous works used data that was acquired in the 70s and 80s. However, this study uses seismic and well data that was obtained in 2008 to 2009 to update the model of the basin.

2.7 SUMMARY

Several studies have been conducted in the Anza basin in order to determine the geologic evolution of the basin (Reeves *et al.*, 1987; Greene *et al.*, 1991; Bosworth, 1992; Dindi, 1992; Bosworth and

Morley, 1994). Table 2-1 below summarizes the current understanding of the evolution of the Anza basin.

Table 2-1: Evolution of the Anza Basin. Summarized from Bosworth, 1992; Bosworth & Morley, 1994; Greene et al., 1991; Reeves et al., 1987; Schull, 1988*;* Dindi, 1992*;* Winn *et al.*, 1993

AGE			EVENT
Pleistocene			Volcanism
NEOGENE		Pliocene	Basalts covered block 10 and the northern parts of block 9 Thermal sag Diabase intrusion
		Miocene	Marine transgression in the SE of Anza basin (in Wal-merer-1 well) Mid Miocene: subsidence of the Central and southern Anza continued
PALEOGENE		Oligocene	Compressional deformation (Inversion anticlines) in the Anza basin
		Eocene	Renewed rifting & subsidence of the Muglad and Anza Basins
		Palaeocene	Late Cretaceous Early Tertiary wrenching, causing anticlines in the Kaisut basin
CRETACEOUS	LATE	Maastrichtian	Brief marine incursion in Central Anza
		Campanian	-Thick rift infill of fluvial, deltaic and lacustrine shale - Wrench-related Shale diapirism in Hothori-1, formation of anticlines. Widespread rifting and subsidence from the Cenomanian to Maastrichtian to Early Tertiary.
		Santonian	
		Coniacian	
		Turonian	
		Cenomanian	
	EARLY	Albian- Aptian	Albian -Aptian unconformity, uplift and Erosion Rifting and subsidence in the Sudan rifts and Lamu,
		Barremian	Rifting
		Hauterivian	
		Valanginian	
		Berriasian	
		Neocomian	Early rifting and deposition of syn-rift sediments. Thermally driven uplift in Anza and erosion of the Jurassic sediments from the rift shoulders. Cretaceous Marine regression
Upper Jurassic			Renewed rifting in Anza Muglad & Melut rift initiation Marine transgression on the Matasade High
Mid Jurassic (Toarcian-Oxfordian)			Madagascar fully separated from Africa. Thermal subsidence and marine incursion
Lower Jurassic			Early rifting between Africa and Madagascar
Triassic			Thermal sag rifting
Carboniferous-Permian			
Precambrian			

CHAPTER 3: MATERIALS AND METHODS

3.1 THE STUDY AREA

3.1.1 Location

The study area is located in the south-eastern part of the Anza basin, Block 9. It lies within latitude $1^0$14’27” N and $1^0$39’54” N and longitude 38^0 52’48” E and $39^0$16’26.4” E. It is positioned in the northern part of Isiolo County, 55 Km NE from Merti town, north-eastern Kenya. The study area covers an area of 1583 Km^2 (figure 3.1).

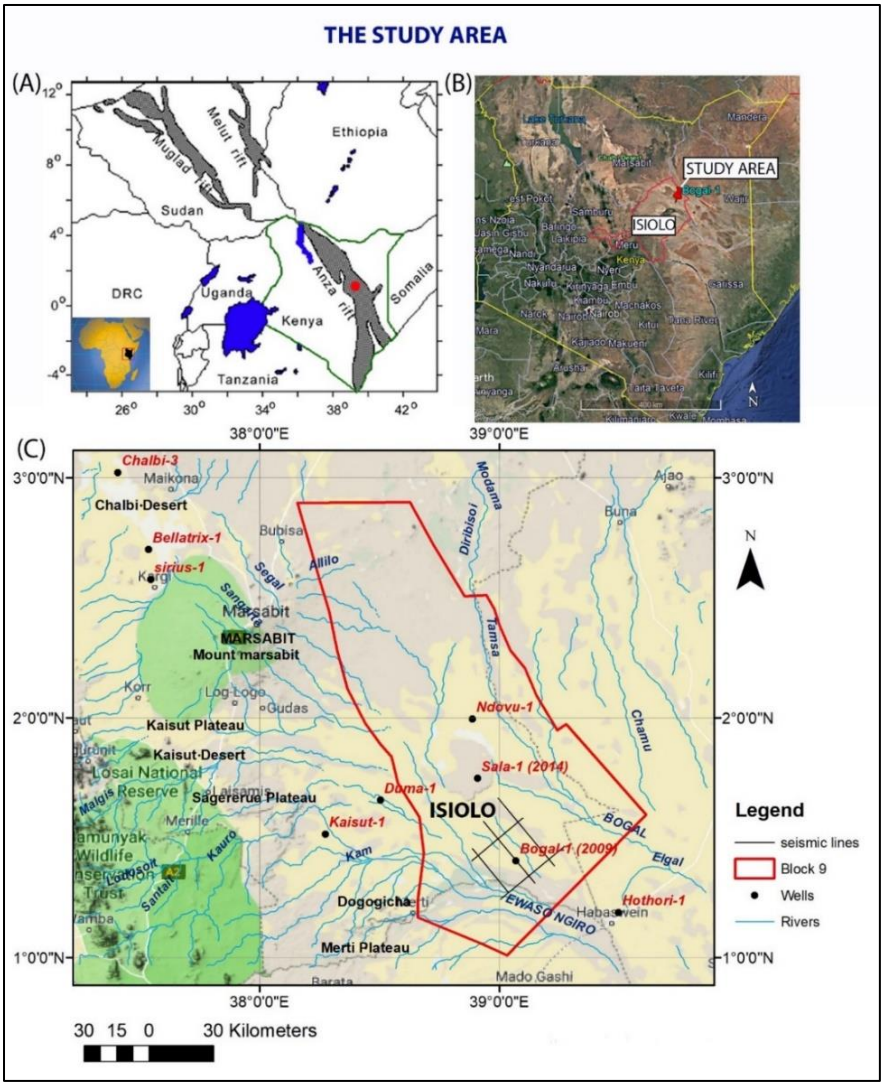

Figure 3.1: The study area: (A) Regional position of the Anza basin, relative to the Sudan rifts, after Bosworth (1992). The red dot shows the position of the Bogal play (B) Location of the Bogal-1 well in Isiolo County, courtesy of Google Earth. (C) Digitized map of Block 9 in the Anza basin showing the five seismic lines used in the study and the position of Bogal-1 well

3.1.2 Physiography and Drainage

The topography of north-eastern Kenya is generally flat. Mount Marsabit is the highest point in the Anza basin. It separates the northern basin and the southern basin. The elevation of Bogal-1 well is 244m above sea level. The neighbouring Ndovu-1, Sala-1, Duma-1 and Kaisut-1 and lie at around 342m, 325m, 323m and 366m respectively. Further towards the north-west, Chalbi-1, Bellatrix-1 and Sirius-1 lie at 372m,375m and 417m respectively. The main river in this area is River Ewaso Nyiro. It is a permanent river that has its source at the Aberdares. This river supplies water to pastoralists in Isiolo, Wajir, Samburu and Laikipia. Seasonal rivers such as Bogal, Elgal, and Tamsa supply water during the rainy reasons. Figure 3.2 illustrates the physiography and drainage system in the Anza basin.

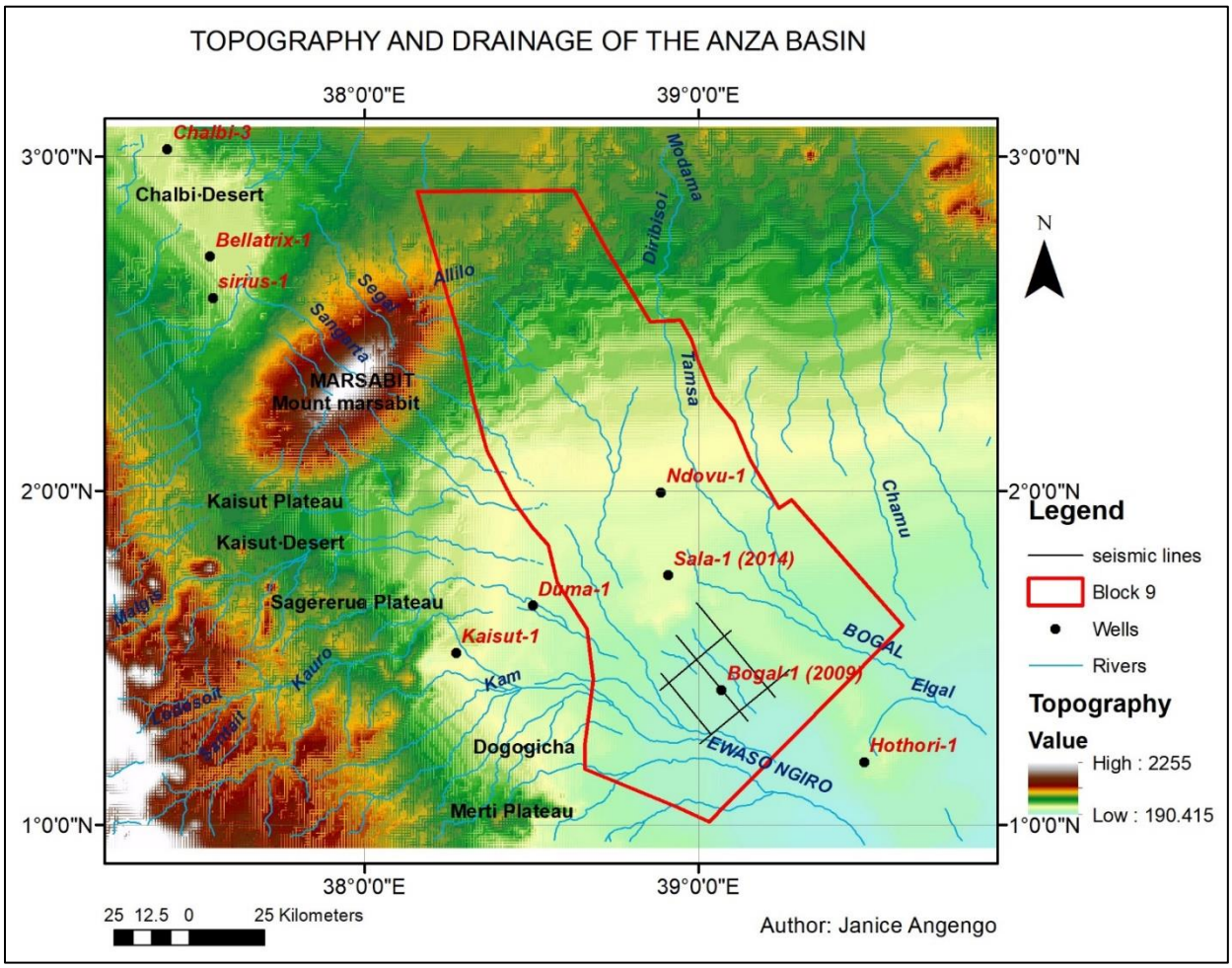

Figure 3.2: Topographic and drainage map of the Anza basin. The study area is enclosed by the seismic lines on the south-eastern part of Block 9. The topography in the study area is generally low, averaging around 190m above sea level. River Ewaso Nyiro and its tributaries extend widely in this area

3.1.3 **Climate**

The North-Eastern Kenya terrain features an arid climate with an average temperature of 30^0 C and an annual rainfall of 200 to 700 mm. There are two main rainy seasons: the long-rain season, which runs from March to May, and a short rain season that extends from mid-October to mid-December. These high temperatures and low rainfall create rampant drought conditions (BGS, 2019). Figure 3.3 below show the average rainfall and temperature in north-eastern Kenya.

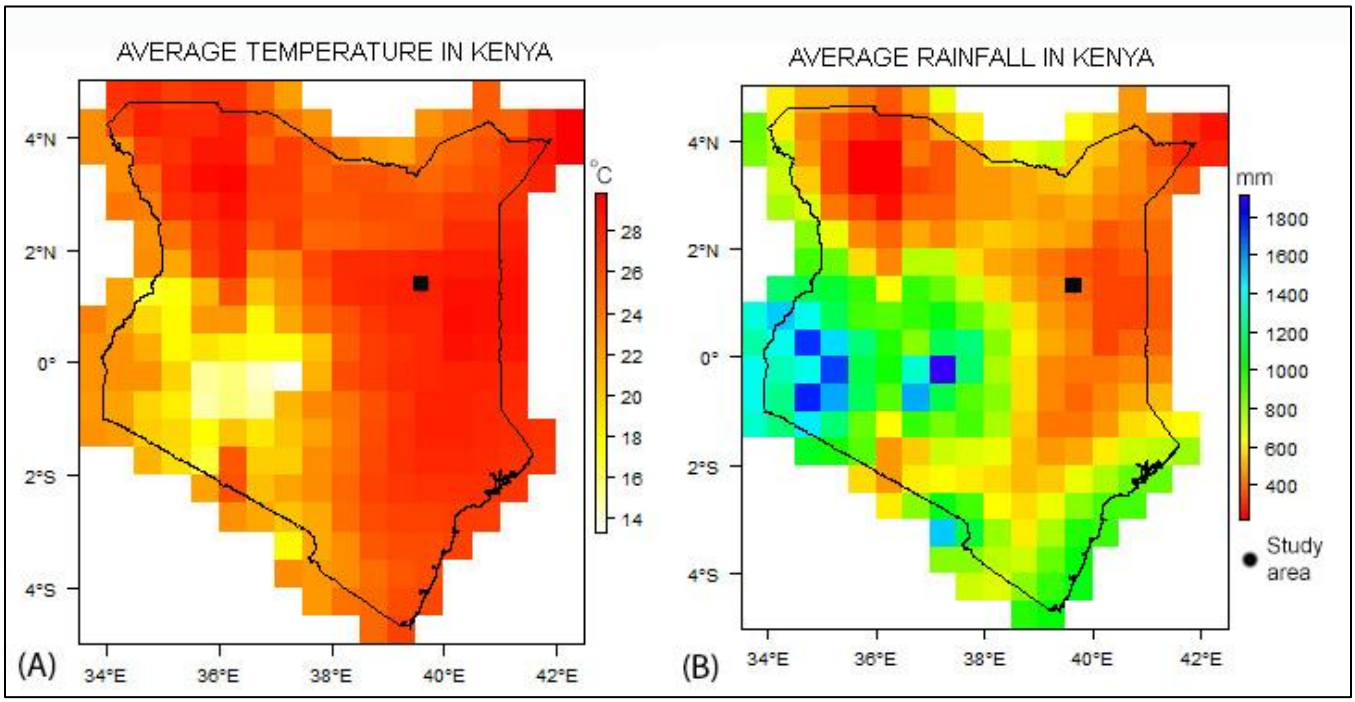

Figure 3.3: Average temperature of 30^0 C (A) and rainfall of 400mm per annum (B) in Kenya (BGS, 2019). *The black square indicates the study area.*

3.1.4 Vegetation

North-Eastern Kenya contains desert-like vegetation with sparsely distributed thorny bushes and shrubs. The deep sandy soils in this area favour the growth of annual grasses and shrubs (Krhoda, 1989). The study area is predominated by *Acacia-Commiphora* stunted bushland, which is the main vegetation type in Isiolo County as shown in figure 3.4 below.

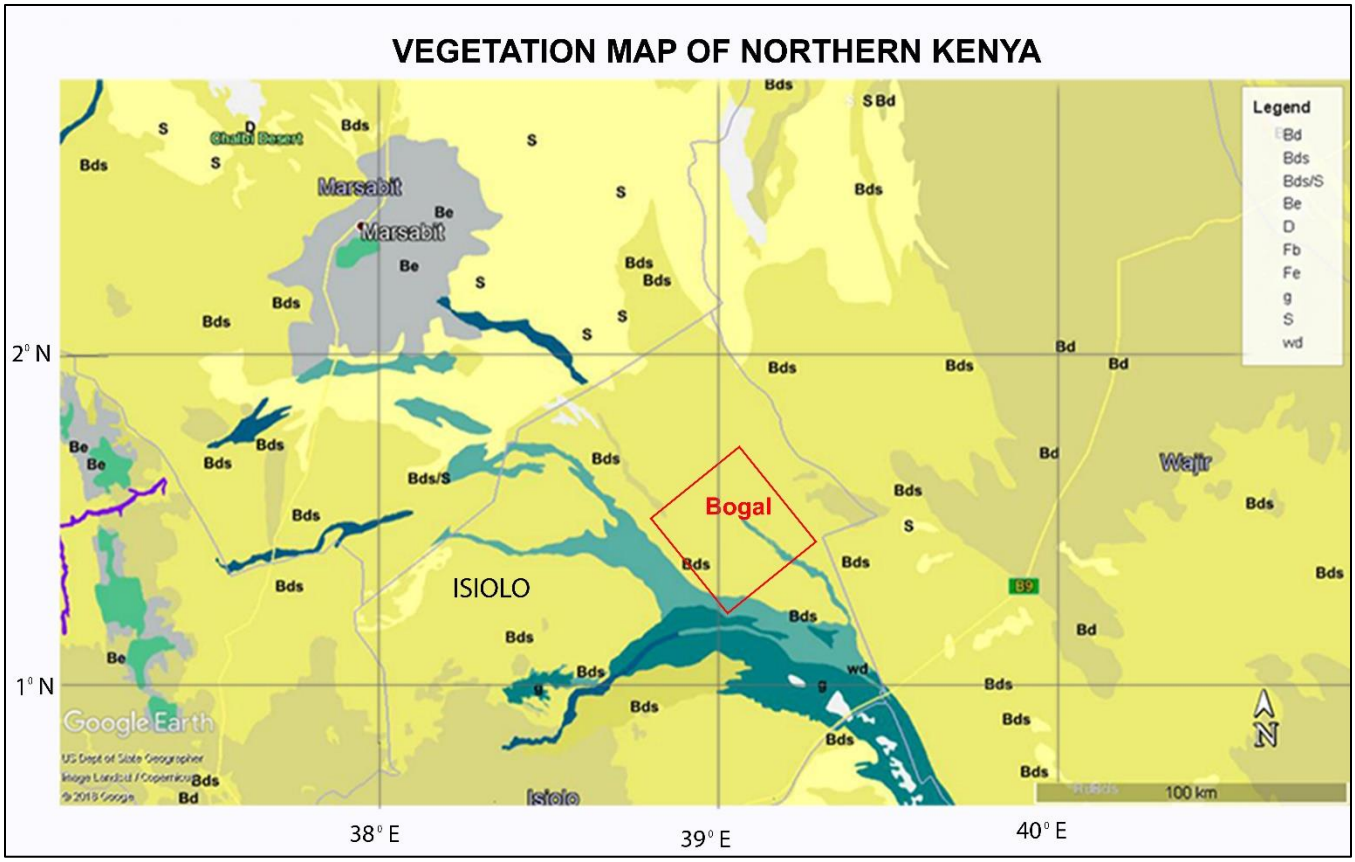

Figure 3.4: Vegetation map of north-eastern Kenya, after Breugel et al. (2015). The study area, highlighted in red, is dominated by Acacia Commiphora bushland

Vegetation description:

Bd: Somalia-Masai *Acacia-Commiphora* deciduous bushland and thicket

Bds: *Acacia-Commiphora* stunted bushland

Be: Evergreen and semi-evergreen bushland and thicket

D: Desert

g: Edaphic grassland on drainage-impeded or seasonally flooded soils

s: Somalia-Masai semi-desert grassland and shrubland

wd: Edaphic wooded grassland on drainage-impeded or seasonally flooded soils

3.1.5 Land Use and Land Resources

Isiolo County is sparsely populated. It is mainly used as an unimproved grazing land or rangeland by the pastoralist community, who move from one place to another in search of better pasture. (figure 3.5).

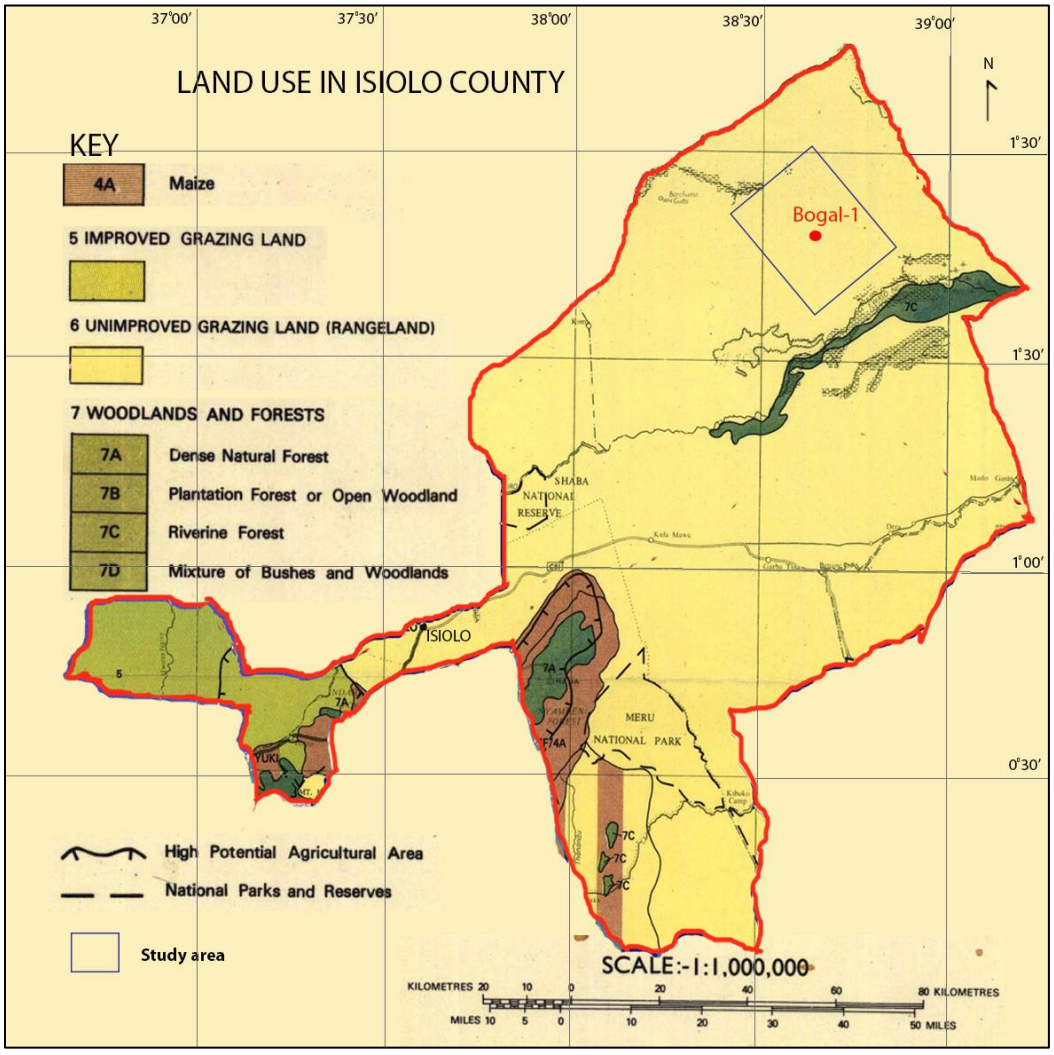

Figure 3.5: Land use map of Isiolo County. Modified from: Survey of Kenya, map no. 500/3/83. The study area, highlighted with a blue square, is used as grazing land or rangeland

3.1.6 Geology

The general geology of the Anza basin consists of Tertiary volcanics in the western part of the basin that cover most of the structures. Quaternary sediments dominate the south-eastern part of the basin. The Anza basin is subdivided into two: the Chalbi desert area, which lies to the northwest

of Mt. Marsabit and the area that lies to the southeast of Mt. Marsabit. Figure 3.6 shows the general geology of the Anza basin.

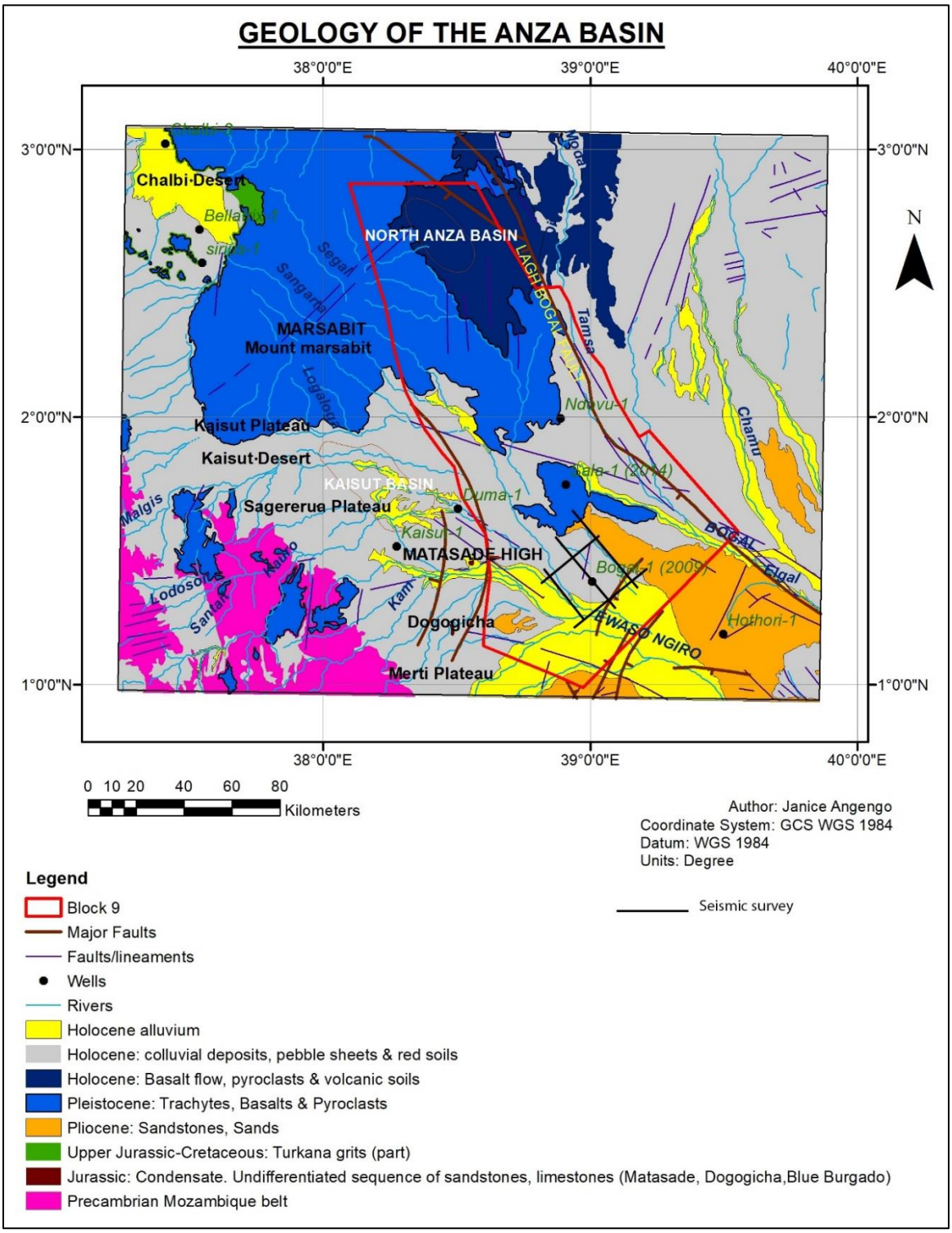

Figure 3.6: Geological map of the Anza basin. Volcanic sediments are present in the NW and Quaternary sediments in the SE. Digitized after Beicip (1987)

3.1.7 Structure

The Bogal structural zone appears as a -35 mGal anomaly that lies on a topographic high in the Yamicha Sag, on the south-eastern part of the Anza basin (Figure 3.7). The satellite gravity map below shows the position of the Bogal inversion structure in the Anza basin.

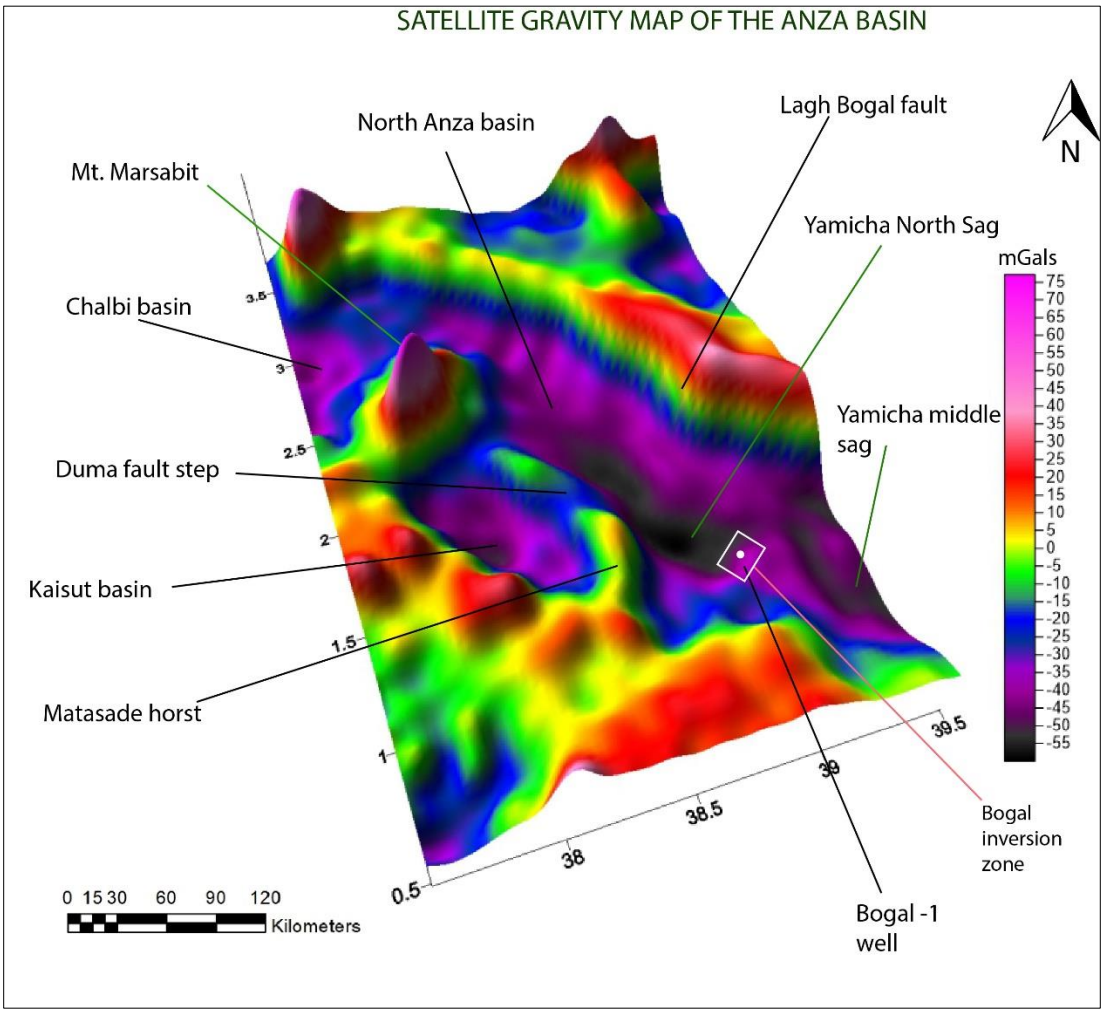

Figure 3.7: DTEM Satellite gravity map of the Anza Basin with the Bogal inversion located on the paleohigh.in the Yamicha Sag. Free air gravity data adopted from http://topex.ucsd.edu/cgi-bin/get_data.cgi after Sandwell and Smith (2009) and Sandwell *et al.*, (2013, 2014)

The extent of the inversion structures is shown in figure 3.8 below.

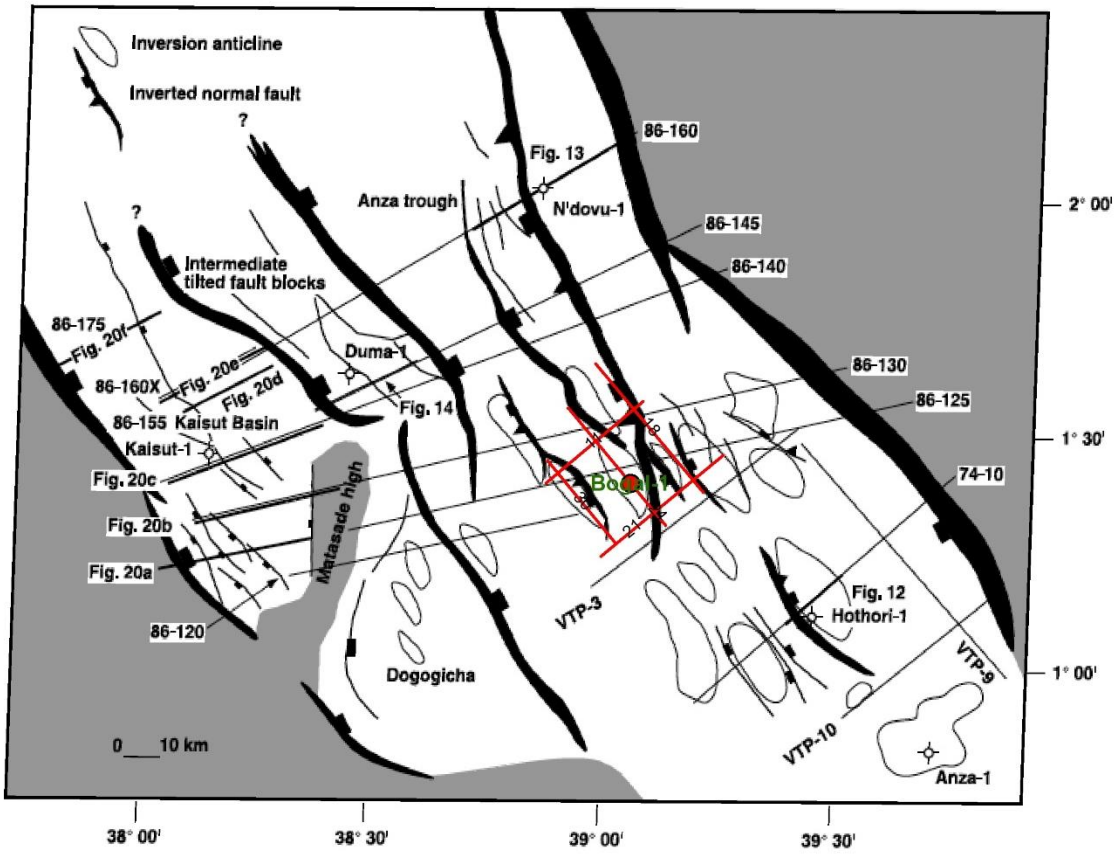

Figure 3.8: The extent of inversion anticlines in central and southern Anza basin. The study area is enclosed with the five seismic lines marked in red. Bogal-1 well is at the centre. Modified from Morley *et al.* (1999).

3.2 GENERAL WORKFLOW

The materials used in this study include 2D seismic data, logs from the Bogal-1 well and well reports, obtained from NOCK. The chart below illustrates the general workflow of the study.

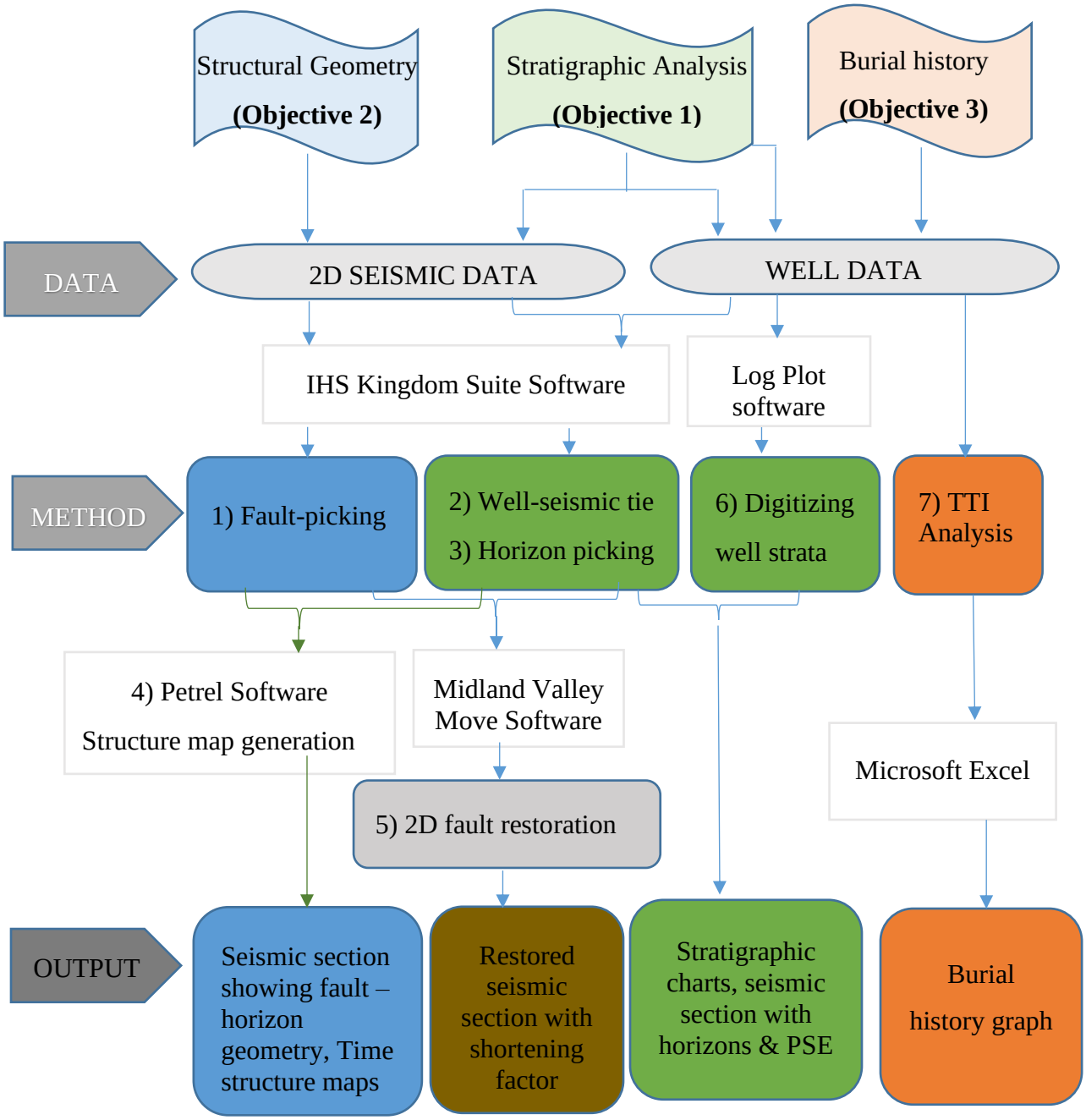

Figure 3.9: General workflow

3.3 STRATIGRAPHIC ANALYSIS

The first objective of this study is to undertake a lithostratigraphic and seismo-stratigraphic interpretation of Bogal-1 well and five profiles from the Bogal structural zone. The goal is to identify the major stratal units, unconformities and the petroleum system elements. The following gives a description of the methods used to achieve this objective.

3.3.1 Dataset and Software

2D seismic data, displayed in figure 3.10 below, as well as borehole data from Bogal-1 well were used in this study. Bogal-1 well is located at latitude $1^0 24' 16.9258''$ N and longitude $39^0 04' 6.1773''$ E. It was drilled in 2009 by CNOOC to a total depth of 5085m, reaching the Lower Cretaceous formation. The well was plugged and abandoned due to fluid losses caused by the extensive fracture network. It encountered gas in two potential pay zones.

Five processed 2D seismic lines covering an area of 1583 Km^2 in the southern part of Block 9 were also used in this study. The seismic data was acquired by CNOOC in 2008. It is of better quality than that of the northern part of the Anza basin due to the absence of shallow subsurface lava.

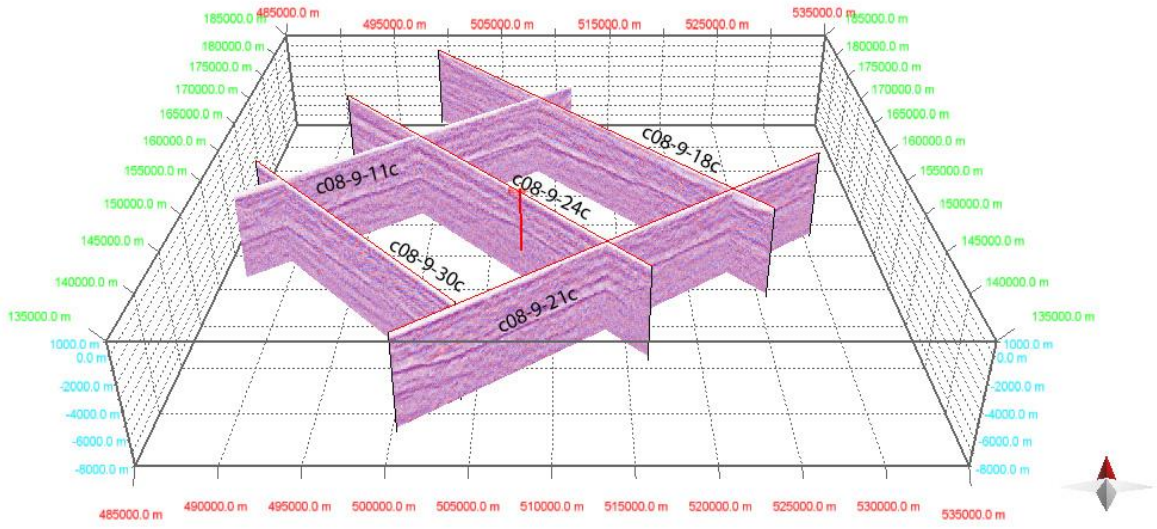

Figure 3.10: 2D seismic lines used in the study. Three lines have a trend that is parallel to the axis of the Anza basin (NW-SE), while two lines, trending NE-SW, cut across the basin. The red line indicates the position of Bogal-1 well. The data is displayed in Petroleum Experts Midland Valley Move software, 2017.

LogPlot software was used to digitize and create the stratigraphic charts based on well cuttings records from CNOOC, while Kingdom Suite software was used to tie the well and seismic data, and for the seismic stratigraphic analysis.

3.3.2 Petroleum System Elements Identification

Borehole data, such as well cuttings and geophysical logs, were used to select the well tops of the stratigraphy in Bogal-1 well. The well cuttings information, such as grain size, colour and sorting, were applied in the inferring of the depositional environments. Potential reservoir zones, seals and source rocks were identified based on their porosities, permeability and TOC properties.

3.3.3 Well to Seismic Tie

Well-to-seismic ties enables correlation of the stratigraphy recorded in the well in depth to that of the seismic data, which is recorded in time. This enables the tying of formation well tops to specific reflectors on the seismic data. The synthetic seismogram was created using sonic and density logs from Bogal-1 well.

Different lithologies in a sedimentary sequence have various densities, hence different velocities. Therefore, acoustic energy passing through these layers will be reflected, depending on the difference in the acoustic impedance of the sedimentary beds. Acoustic impedance is the product of both density and velocity.

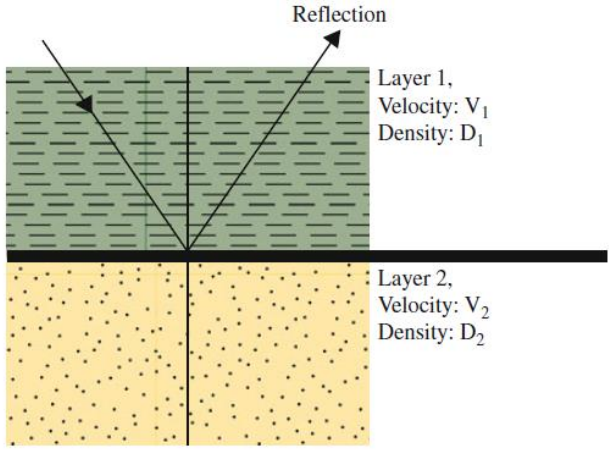

Figure 3.11: Reflection of waves in a sedimentary sequence. The degree of reflection is a function of the acoustic impedance (Bjørlykke, 2010)

The coefficient of reflection is obtained by the formula:

$$\text{Reflection coefficient} = \frac{\rho_2 v_2 - \rho_1 v_1}{\rho_2 v_2 + \rho_1 v_2}$$

……*Equation 1* (Kearey *et al.*, 1991)

Where ρ_1 and ρ_2 are the densities of the two rocks, while v_1 and v_2 are their respective velocities. The greater the difference in density and velocity, the higher the reflection coefficient.

During a seismic-to-well tie, a synthetic seismogram is created by multiplying the sonic and density logs to create an acoustic impedance log. The impedance log creates a reflection coefficient log, which is used to generate a synthetic seismogram. The synthetic is then compared to the real seismic trace. This is illustrated in figure 3.12 below.

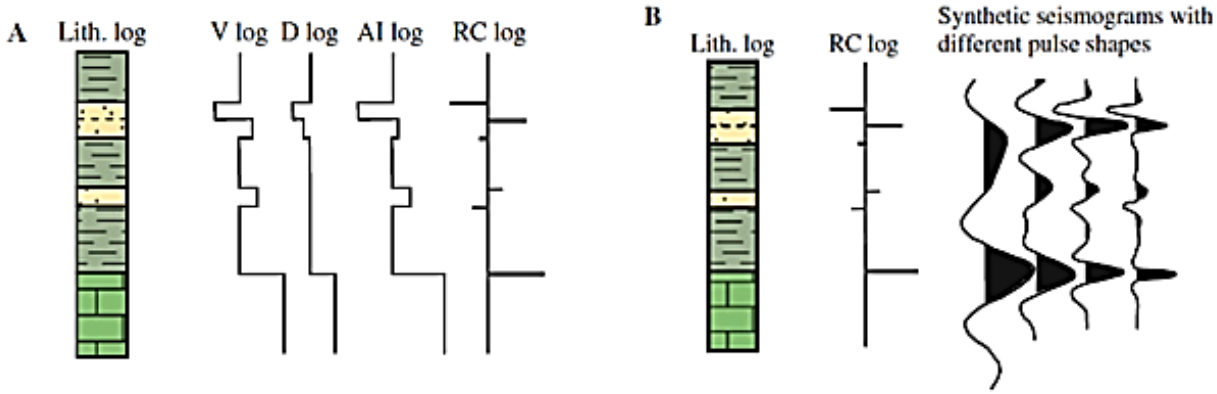

Figure 3.12: The process of creating a synthetic seismogram: The sonic log is multiplied by the density log to obtain an acoustic impedance log, which subsequently creates a reflection coefficient log using equation 1 (A). The reflection coefficient is used to create a synthetic seismogram (B) (Bjørlykke, 2010)

Seismic Facies Analysis

Formation well tops tied to the synthetic seismogram were used to mark major horizons that are laterally consistent along the seismic section. Seismic facies were defined by reflection packages with similar characteristics. According to Nanda (2016) The parameters used in seismic stratigraphy include**:**

1. Reflection amplitude- the strength of the reflections
2. Reflection frequency- the distance between reflections
3. Reflection continuity- this depends on the continuity of the sediments
4. Reflection configuration- this is the shape of the reflection package.

The table below presents the formation tops for Bogal-1 well.

Table 3-1: Formation tops for Bogal-1 well (CNOOC, 2010)

FORMATION	TOP (m)	BASE (m)
Quaternary (Q)	10.5	245
Neogene (N)	245	550
Paleogene (E)	550	1075
Upper Cretaceous (K2)	1075	2563.5
Lower Cretaceous ($K1_1$)	2563.5	3363.5
Lower Cretaceous ($K1_2$)	3363.5	5085

3.4 STRUCTURAL ANALYSIS

The second objective of this study is to examine the structural geometry of the Bogal play based on 2D seismic data interpretation and fault restoration.

3.4.1 Dataset and Software

The five processed 2D seismic lines described in section 3.3.1 above were used to achieve this objective. The IHS Kingdom Suite software, 2017, was used to delineate the fault structures and major horizons, while Petroleum Experts Move, 2017, was used for the seismic restoration process. Petrel 2017 was used to generate time structure maps, while satellite gravity data was used to position the Bogal play relative to the other local anomalies within the Anza basin.

3.4.2 Structural Geometry Analysis

Structural features such as faults and inversion anticlines were identified in the seismic sections based on the reflection patterns. Faults were deduced by detecting terminated reflections, abrupt changes in seismic patterns, abrupt changes in dip, fault plane reflections and stratigraphy offsets.

3.4.3 Fault Restoration

Structural restoration is a technique used by structural geologists for decades to unravel the structural and stratigraphic history of a basin and to validate seismic interpretations. It works by removing deformation in geological sections. First, a depth-converted seismic section containing

faults and horizons was created using interval velocities from the vertical seismic profile (VSP) presented in appendix 1. The relationship between time and depth is presented in the graph in appendix 2. It was restored by matching hanging wall and footwall cut-offs and unfolding using an appropriate kinematic algorithm in Petroleum Experts Move software, 2017. This process assumed that no material moved into or out of the section during restoration. The lengths of the selected horizons were calculated using the section analysis tool before and after restoration to estimate the amount of shortening that took place during the deformation.

The algorithm applied for fault restoration depends on the type of deformation that took place. The simple shear, trishear and fault parallel flow algorithms can all be used to restore inverted basins. Flower structures, which are a common feature in inverted basins, are formed in triangular shear zones due to the downward convergence of deformation as illustrated in figure 3.13 below (Cristallini *et al.*, 2004). Erslev (1991) defines trishear as "distributed shear in a triangular shear zone". The trishear algorithm available in the Move software was therefore considered suitable for fault restoration in the Bogal play.

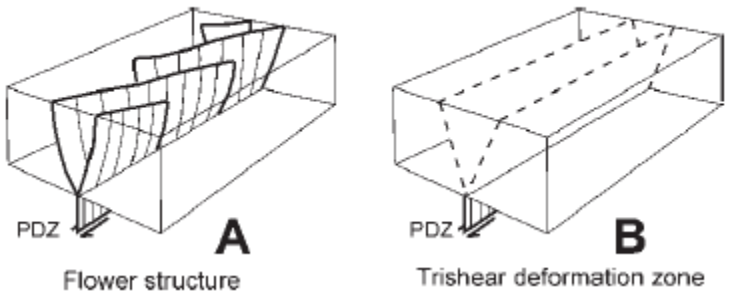

Figure 3.13: Concept of trishear deformation in flower structures (Cristallini *et al.*, 2004)

Once the fault restoration was complete, the beds were unfolded. The flexural slip and simple shear algorithms can be used to unfold the geological section. The simple shear algorithm assumes that the deformation took place diffusely throughout the hanging wall. It is mostly applied in geological settings where ductile deformation took place or where semi-consolidated rocks occur.

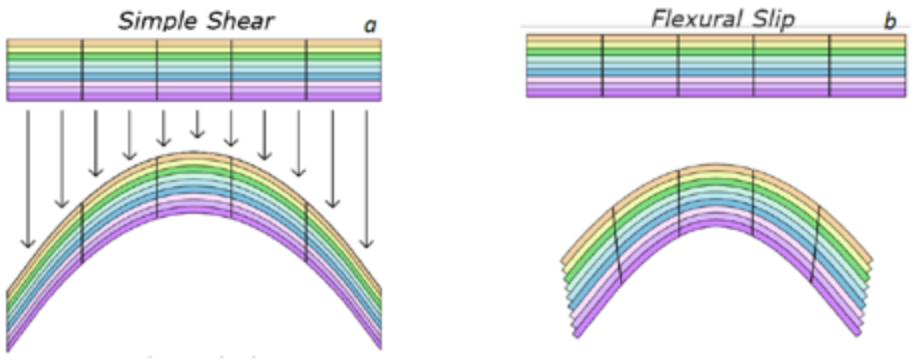

Figure 3.14: Simple shear (a) and Flexural slip (b) deformation styles applied in unfolding beds. Images from Midland Valley Move Knowledge Base (2017)

Flexural slip models deformation as discrete slip between beds. It preserves line length and area (Rowan and Kligfield, 1989). It is applied in geological settings where fully lithified rocks occur, and therefore chosen for this study.

3.5 BURIAL HISTORY ANALYSIS

Burial history analysis aims at reconstructing the vertical movement of sediments in a basin. It quantitatively describes the geologic history of a basin (Hinte, 1978). This study adopts the Lopatin-Waples method, which involves the construction of burial history graphs, and the calculation of TTI values that estimate the onset of petroleum generation. TTI analysis provides information on the timing of petroleum generation and the type of hydrocarbon produced.

3.5.1 Dataset

Data required for TTI analysis include:

- Bottom-hole temperature
- Well formation tops
- Sediment thickness
- Sediment age
- Sedimentation rates

3.5.2 TTI Analysis

Time and temperature have an effect on organic matter. The Lopatin method establishes the depth of the onset of petroleum generation. It assumes that for every 10^0C increase in temperature, the

rate of petroleum generation reaction doubles. Therefore, if the temperature interval is 10 ^{0}C above the reference, the rate of petroleum generation will double, while if it is 10^{0}C below the reference, the rate of petroleum generation will go half as fast (Barker, 1996). A temperature factor δ is therefore given for every interval n, where:

$$\delta = r^n \quad \text{……..} \textit{Equation 2 (Barker, 1996)}$$

where r=2 and the index value n= 0 for the 100°-110°C base interval.

Table 3-2 below gives a list of temperature factors for every 10^{0}C interval.

Table 3-2: Temperature factors for every 10 ^{0}C used in the Lopatin method (Barker, 1996)

TEMPERATURE INTERVAL (^{0}C)	δ	
20 - 30	2^{-8}	1/256
30 - 40	2^{-7}	1/128
40 - 50	2^{-6}	1/64
50 - 60	2^{-5}	1/32
60 - 70	2^{-4}	1/16
70 - 80	2^{-3}	1/8
80 - 90	2^{-2}	1/4
90 - 100	2^{-1}	1/2
100 - 110	2^0	1
110 - 120	2^1	2
120 - 130	2^2	3
130 - 140	2^3	4

The Time Temperature Index (TTI) is a maturity value obtained by assuming that the maturity increase in any 10 ^{0}C temperature interval is directly proportional to the amount of time spent in that temperature interval, but will vary according to the nth power of the temperature, i.e.

$$\Delta \text{ Maturity (TTI)} = (\Delta T_i)\,(r^{ni}) \text{……} \textit{Equation 3 (Barker, 1996)}$$

Where T_i = Time spent in the temperature interval

r^{ni} = temperature factor in the interval

The total maturity is the sum of the individual maturity indexes for every 10^0C interval.

The steps in the Lopatin method include:

STEP 1: Construction of burial graphs.

The depths of the major rock units that are penetrated by the well are plotted as a function of time. Their present depths are plotted against their respective ages in a straight line, assuming that there was a steady burial from their time of deposition to the present. With this assumption, all the units below the first unit (unit 1 in figure 3.15), within the same time window, are represented by parallel lines. This process does not take into account the effects of compaction or water loading.

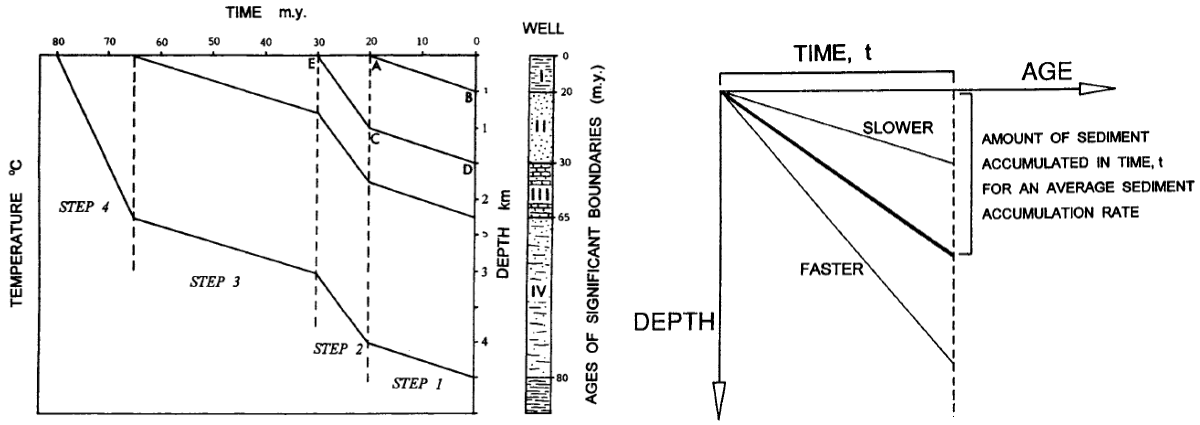

Figure 3.15: Construction of burial curves (Barker, 1996)

The resulting graph shows the sedimentation rates of the units. A higher gradient represents rapid burial, while a smaller gradient represents slower burial rates. A negative gradient implies that an uplift occurred.

The ages of sediment deposition are obtained from biostratigraphic data of the Anza basin, based on palynological data from (Sewe, 1995) and the Geological Society of America (GSA) chronostratigraphic timescale. Two uplift and erosional phases identified from Fission Track Analysis (FTA) aged 20 to 10Ma and 70 to 60Ma (Foster and Gleadow, 1996) were included.

Table 3-3: Formation ages and erosion history for sediments in Bogal-1 well based on Sewe (1995; Foster and Gleadow (1996) *and the GSA geological timescale*

Formation	**Abbreviation**	**Reference**	**My**	**Thickness**
Quaternary	Q	GSA	2.6 - 0	245
Neogene	N	GSA	10 – 2.6	305
Erosion		Foster (1996)	20 -10	-310
Paleogene	E	GSA	60 - 20	525
Erosion		Foster (1996)	70 - 60	-800
Upper Cretaceous	K2	Sewe (1995)	100-70	1488.5
Lower Cretaceous	$K1_1$	GSA	126-100	800
Lower Cretaceous	$K1_2$	Sewe (1995)	145-126	1721.5

STEP 2: Creation of a temperature grid for every 10^0C. It is assumed that the geothermal gradient remains constant though time.

Waples (1980, 1985) gave a general relationship of TTI values with other maturity indicators and their relation to petroleum maturation as described in the table 3-3 below:

Table 3-4: TTI- Vitrinite reflectance correlation and hydrocarbon type (Waples, 1985)

TTI	**R_0**	**Hydrocarbon (80% probability)**
50	0.90	Normal oil
75	1.00	Normal light oil
180	1.35	Condensate - wet gas
500	1.75	Wet gas
900	2	Dry gas

Uplifts decrease the temperature factor. The TTI values are always positive because maturity increases regardless of burial or uplift. However, the rate of maturation decreases with uplift and cooling (Waples, 1985).

The following table summarizes the methods and software used to achieve the objectives of the study.

Table 3-5: Summary of the data and software used in this study

Task	Output	Software
Desktop Study	Digitized geological map	ESRI ArcGIS
	Topographical map	ESRI ArcGIS
	Gravity map	Surfer 14
Structural interpretation	Seismic sections	IHS Kingdom Suite 2017
	Structural restoration sections	Petroleum Experts Move 2017
	Structure maps	Petrel 2017
Stratigraphic interpretation	Seismic facies sections	IHS Kingdom Suite
	Stratigraphic chart	LogPlot
Burial history	Burial graph	Excel, Adobe illustrator

CHAPTER 4: RESULTS AND DISCUSSIONS

This chapter presents the results obtained from the procedures described in chapter three.

4.1 STRATIGRAPHY AND PETROLEUM SYSTEM ELEMENTS

The stratigraphy of Bogal-1 well is composed of Cretaceous, Tertiary and Quaternary sediments. The well reached a total depth of 5085m in the Lower Cretaceous formation. The strata consist of interbedded layers of sandstone, mudstone, siltstone, claystone, micro-conglomerate, pebblestone, with minor gypsum occurrences. Igneous intrusions of basalt and diabase are present in the Lower Cretaceous formation. Tables 4.1 to 4.4 were plotted in LogPlot software based on lithological charts adapted from CNOOC. They were modified to include the petroleum system elements, depositional environments and tectonic sequences.

4.1.1 Lower Cretaceous Sediments (2563.5m - 5085m)

Lower Cretaceous sediments are the thickest units encountered by the Bogal-1 well section (2522m). They are subdivided into the following sub-sections:

i) ***$K1_4$ (4760m-5085m)***: This presents the deepest sediments encountered by the well section. It comprises thin layers of sandstone and mudstone. The mudstone is brown, partly grey, soft, and slightly calcareous. The sandstone layers are medium grained and fine grained, unconsolidated, and well sorted. This interval represents the major source rock interval of the Bogal play. Geochemical data indicates that the mudstones contain type II Kerogen and are mature, suggesting that they are of marine origin, and produce both oil and gas.

ii) ***$K1_3$ (4035m- 4760m)***: This interval is predominated by massive sandstone beds with minor mudstone and gypsum. A 14m thick layer of basalt is present between 4028m and 4042m. It occurs again between 3520m and 4760m. This basalt is black, contains white speckles in some parts, and is unevenly fractured. The thin mudstone layer is brown, partly grey, firm, brittle, flaky and partly calcareous.

The massive sandstone is mainly medium-grained, light grey in colour, unconsolidated, well sorted and sub-angular. It has low porosity and permeability values that range from 1.09% - 7.71% and 0.1 mD - 2.02 mD respectively. This indicate low reservoir quality. Nonetheless, gas was encountered in this interval. This implies that the permeability of this

reservoir is mainly caused by the large fracture network. The thin bed of gypsum indicates a brief shallow marine incursion of the area occurred in the Early Cretaceous.

A massive, bedded diabase sill, 100m thick, lies between the massive sandstone between 4415m and 4515m. It is dark grey, yellowish-green in part and partly speckled in white and has a greasy lustre. It exhibited some gas shows. The basalt is black and waxy with no gas shows. The basalt and diabase intrusions may be of Tertiary age (Bosworth and Morley, 1994).

iii) $K1_2$ (3206m-4035m): Consists of alternating thin layers of sandstone, mudstone and micro-conglomerate. The mudstone is brownish-purple and light grey in some parts and slightly calcareous. It changes to light brown-light grey- greenish grey in some parts of the lower section, implying a transition from an oxidizing environment to a moderately reducing one. This section contains thin beds of gypsiferous mudstone that is light grey in colour, greenish-grey in some parts and is slightly calcareous. Arenaceous mudstone is also present in this section. It is light grey, greenish-grey in some parts, soft and sticky. Source rock evaluation of the mudstones indicate type II and type III kerogen that ranges from mature, immature to excessive maturity. The TOC values are between 0.02 and 0.19 (CNOOC, 2010), indicating poor source rocks.

The fine-grained sandstone is unconsolidated, light grey in colour, sub rounded and moderately sorted. It is mainly composed of quartz and minor feldspar. This interval has low porosity values that range from 4.87% to 10.46% and low permeability that ranges between 0.24 and 3.46 mD. This is not sufficient to be of reservoir quality. However, 2.08% and 1.34% gas was encountered in this interval. The low porosity and permeability might have been supplemented by the numerous fracture network.

iv) $K1_1$ (2563m-3206m): Consists of fine and medium-grained sandstone and mudstone beds. The sandstone is light grey in colour, well sorted, unconsolidated and sub-angular. They have fair porosities of up to 15.5%. The mudstone volume is greater than the sandstone. It is brown and light grey in some sections and partly arenaceous. These sediments may have possibly been deposited in a deltaic environment. These thick mudstone layers with poor permeability (2.7md to 7.16md) possibly form a hydrocarbon seal. TOC data reported by CNOOC indicate mature source rocks present at the lower part of this interval. 6.75% maximum gas was encountered in this section.

Table 4-1 and 4-2 below present a summary of the lithostratigraphy, paleoenvironment, tectonic sequence and petroleum system elements of the Lower Cretaceous sediments developed in the Bogal Play.

Table 4-1: A generalized lithological, palaeoenvironmental, tectonic sequence chart with corresponding petroleum system elements (PSE) of the Lower Cretaceous section

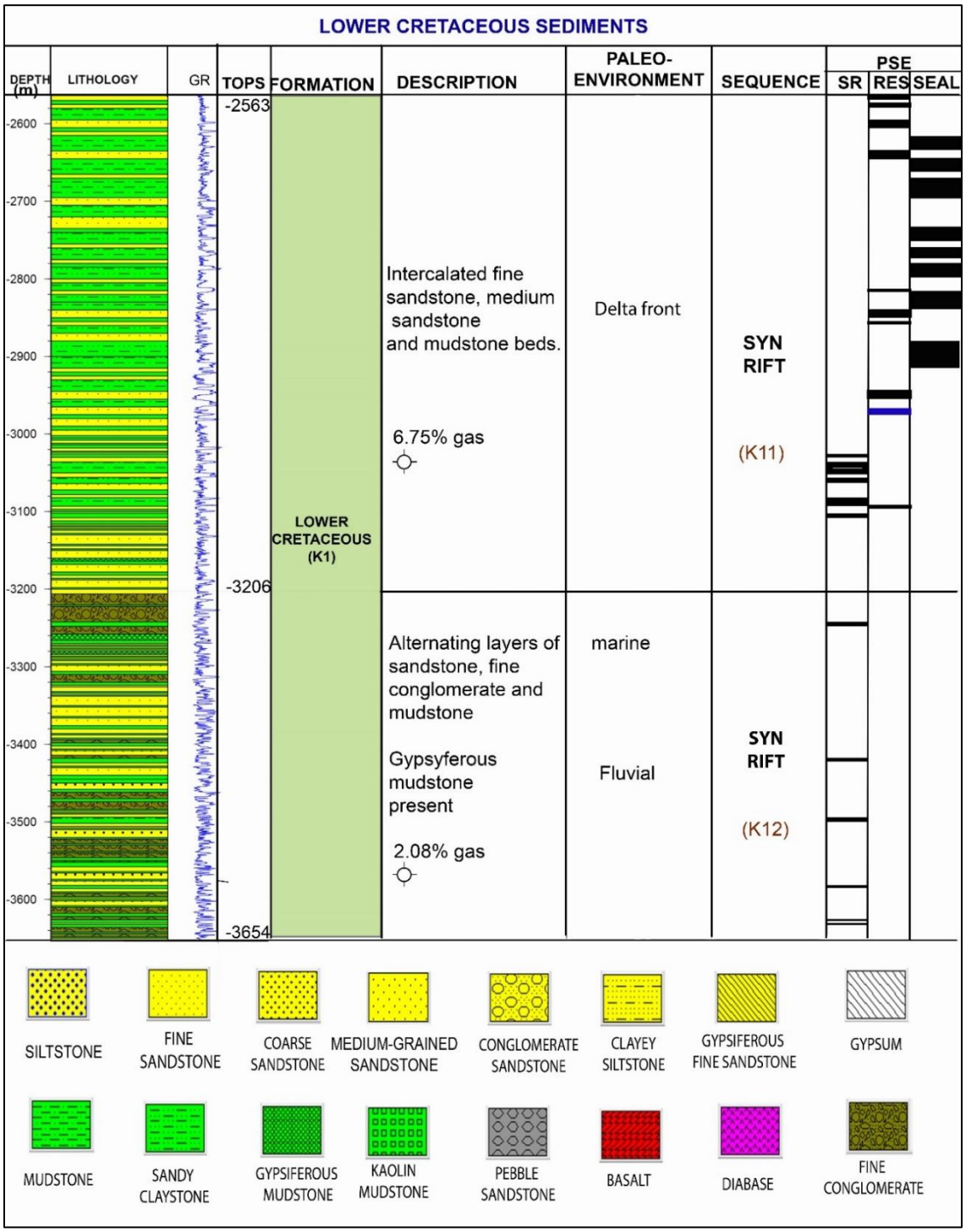

Table 4-2: A generalized lithological, palaeoenvironmental, tectonic sequence chart with corresponding petroleum system elements (PSE) of the Lower Cretaceous section (continuation)

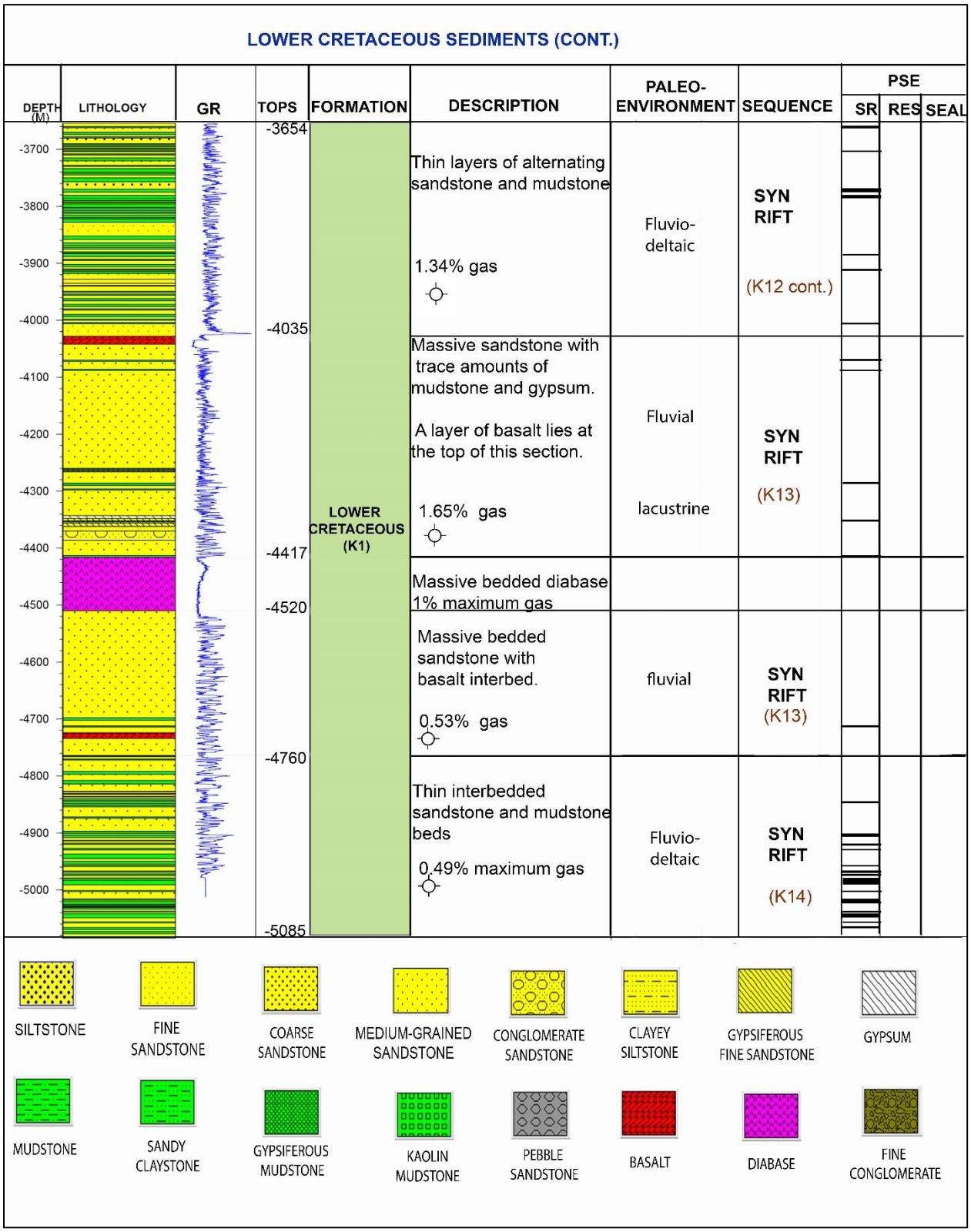

4.1.2 Upper Cretaceous Sediments (1071m-2563m)

The Upper Cretaceous sediments are 1492m thick. They consist of alternating layers of course, medium and fine sandstone, siltstone, silty mudstone, gypsiferous mudstone and micro-conglomerate that were deposited in fluvial, deltaic and marine environments. The porosity and permeability of the upper part of the Upper Cretaceous are very low, qualifying this section as a potential top seal of the Bogal play. The lower part of this section contains sandstones with fair porosities and poor permeability. The highest porosity value is 17%. The permeability is likely to be induced by the extensive fracture network in the Upper Cretaceous sediments.

The Upper Cretaceous sediments are subdivided into two intervals:

i) ***$K2_2$ (1857m- 2563m):*** The bottom part of this interval comprises alternating layers of fine sandstone, siltstone and mudstone. The mudstone is brown and light grey in some parts, soft-moderately firm, and slightly calcareous. The siltstone is light grey, medium consolidated while the sandstone is fine, light grey, unconsolidated. The transition from a silty facies at the bottom to a sandy facies with upward coarsening at the top of this interval implies a regressional phase. The porosities in this interval range from fair (9.8%) to good (17.24%) while permeability ranges from poor to good (2.18 md to 20.51md). This interval makes up the reservoir of the Bogal play. The mudstones in this section have poor permeability (0.55md to 1.22 md), making them possible seals. Gas was encountered in this interval.

   The top part of this section is predominated by fine-grained, medium-grained and minor coarse sandstone interbedded with thin mudstone beds. The mudstone is brownish-red, partly light grey and slightly calcareous. The sandstone is light grey, unconsolidated, sub-angular and well sorted. Their porosities range from 8% to 17% with permeability of up to 11.6%. This section contains the highest porosities within the Bogal play. The fair permeability might be supplemented by the extensive fractures in the Upper Cretaceous sediments, thereby classifying this section as a fractured sandstone reservoir of the Bogal play. Some gas was encountered.

ii) ***$K2_1$ (1075m-1857m)***: Composed of unconsolidated sandstone interbedded with mudstone, gypsiferous mudstone and fine conglomerate. The sandstone in this interval changes from fine-grained in the lower part, to medium-grained in the mid-section and finally, coarse-grained in the upper parts. The coarse sandstone is light grey, unconsolidated, sub-angular, well-sorted and is mainly composed of quartz and feldspar with argillaceous cement. It is interbedded with a 50m thick layer of grey, unconsolidated, well sorted and sub-angular micro-conglomerate. The fine and medium-grained sandstones are light grey, unconsolidated, sub-angular and well sorted.

A thick mudstone layer lies at the bottom part of this interval. It is brownish-red, light grey in some parts, soft to moderately firm, slightly calcareous and sub blocky. The brownish-red mudstone suggests that deposition was in an exposed flood basin. These thick mudstone layers could possibly be the hydrocarbon seal of the Bogal play.

Another mudstone layer lies at the top part of this interval. It is green-grey and light grey in some parts. The light grey implies an oxidizing environment, probably in shallow water. A thick layer of gypsiferous mudstone, light grey to greenish grey, lies at the top of this section. The gypsiferous mudstone may have possibly been deposited in a shallow marine environment.

The source rock potential of this interval is unknown due to the lack of TOC data.

Table 4-3 below gives a summary of the lithostratigraphy, palaeoenvironment, tectonic sequence and petroleum system elements of the Upper Cretaceous sediments developed in SE Anza. Reservoirs with fair porosities ranging from 10% to 15% are marked in black, while the ones with good porosities that range from 15% to 20% are marked in blue.

Table 4-3: A generalized lithological, palaeoenvironmental, tectonic sequence chart with corresponding petroleum system elements (PSE) of the Upper Cretaceous section

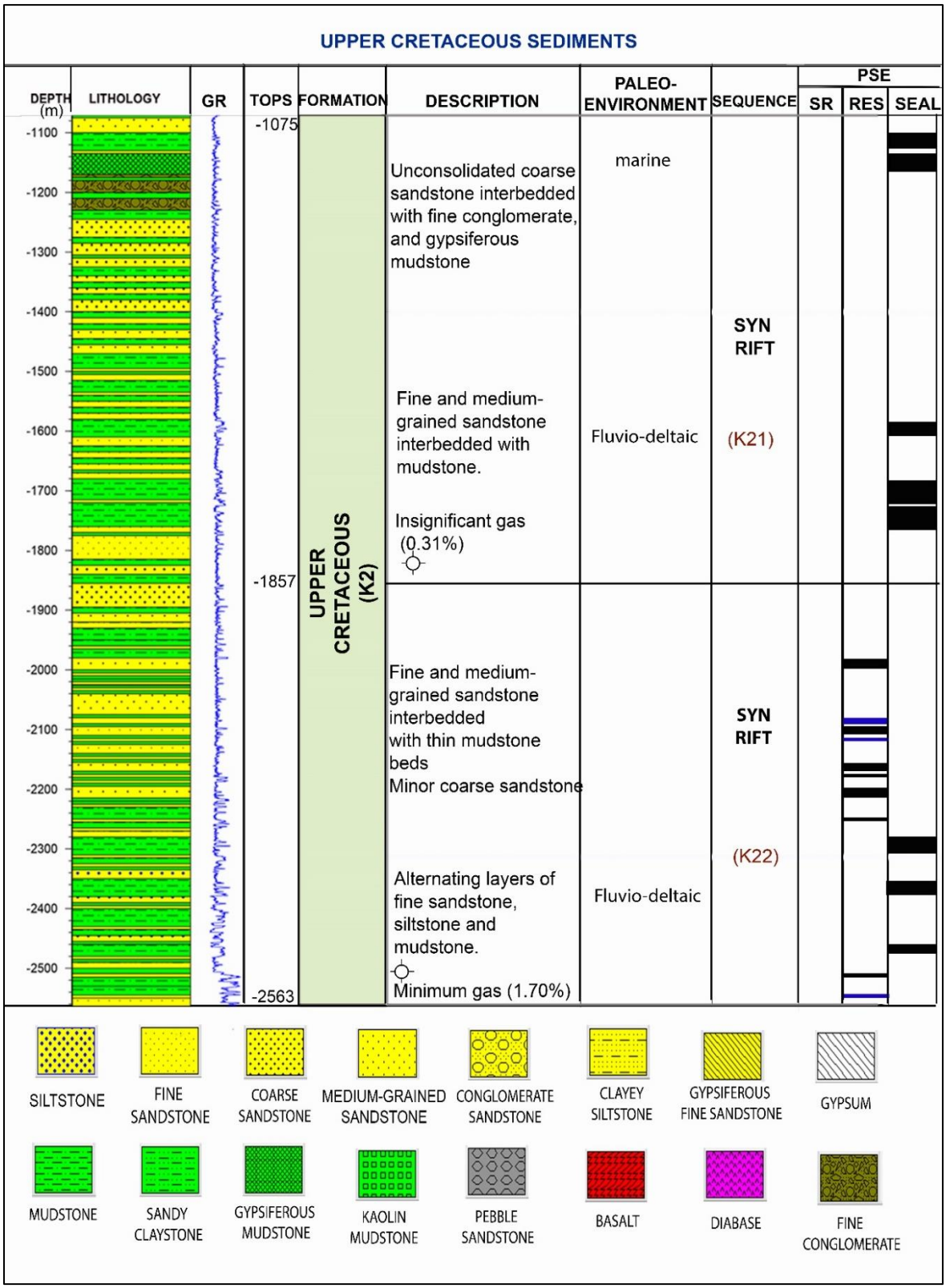

4.1.3 Quaternary and Tertiary Sediments

Paleogene (550m -1075m)

Paleogene sediments are 525m thick. They are predominantly composed of thick beds of grey micro-conglomerate intercalated with thinner beds of greenish-grey/ partly purplish-red mudstone with minor gypsum. The total conglomerate thickness is 335m, while the total mudstone thickness is 190m.

The upper part consists of alternating layers of greenish-grey/ partly purplish red mudstones and fine conglomerate with pyrite traces indicating the presence of a moderately reducing and partly oxidizing environment. The middle part of the section is dominated by thick layers of sub-angular to sub rounded and well-sorted micro-conglomerate. This lithology suggests deposition in a braided river environment during a renewed rifting phase. Minor mudstone that occurs in between the thick conglomerate may have been deposited as floodplain deposits. The lower section consists of alternating layers of fine conglomerate and greenish-grey/ partly purplish-red mudstone similar to the upper section.

The Paleogene sediments make up the syn-rift sequence. They form the overburden rocks of the Bogal play.

Neogene (245m – 550m)

Neogene sediments have a total thickness of 305m. They comprise interbedded layers of unconsolidated micro-conglomerate, pebblestone, medium to course sandstone and mudstone. The micro-conglomerate has a cumulative thickness of 85m. It is grey, sub-angular, unconsolidated, well sorted, and is predominantly composed of quartz. The sandstone has a total thickness of 40m. It is medium to course-grained, light grey, unconsolidated, sub-angular, well sorted and is mainly composed of quartz and minor feldspar coated by an argillaceous cement. The pebblestone is grey, unconsolidated, sub-angular, well sorted and predominantly consists of quartz. It has a total thickness of 27m. This section might have been deposited during a high-energy event such as flooding. The mudstone is light grey (at the top), and greenish grey (lower part) suggesting a transition from an oxidizing environment to a moderately reducing environment. It has a total thickness of 153m.

The Neogene and Quaternary sediments make up the post-rift sequence.

Quaternary Sediments (50m - 245m)

Quaternary sediments in Bogal-1 well are characterized by a 195m layer of alternating course sandstone, fine conglomerate and mudstone. The total sandstone thickness in this interval is 35m. It is light grey, coarse grained, unconsolidated, sub-angular, well sorted and is mainly composed of quartz, feldspar with an argillaceous cement. The micro-conglomerate has a total thickness of 90m. It is grey, unconsolidated, moderately sorted and sub-angular. It is mainly composed of quartz. The thick layers of coarse sandstone and conglomerate suggest that these sediments may have been deposited by in a braided river environment. The mudstone has a total thickness of 70m. It is yellowish-grey and partly red in colour, suggesting an oxidizing environment.

Table 4-4 below gives an overview of the lithostratigraphy, palaeoenvironment and tectonic sequence of the Quaternary, Paleogene and Neogene deposits developed in the SE Anza basin. These strata form the overburden rocks in the Bogal Play.

Table 4-4: A generalized Lithological, palaeoenvironmental, tectonic sequence chart for the Quaternary and Tertiary section in SE Anza basin

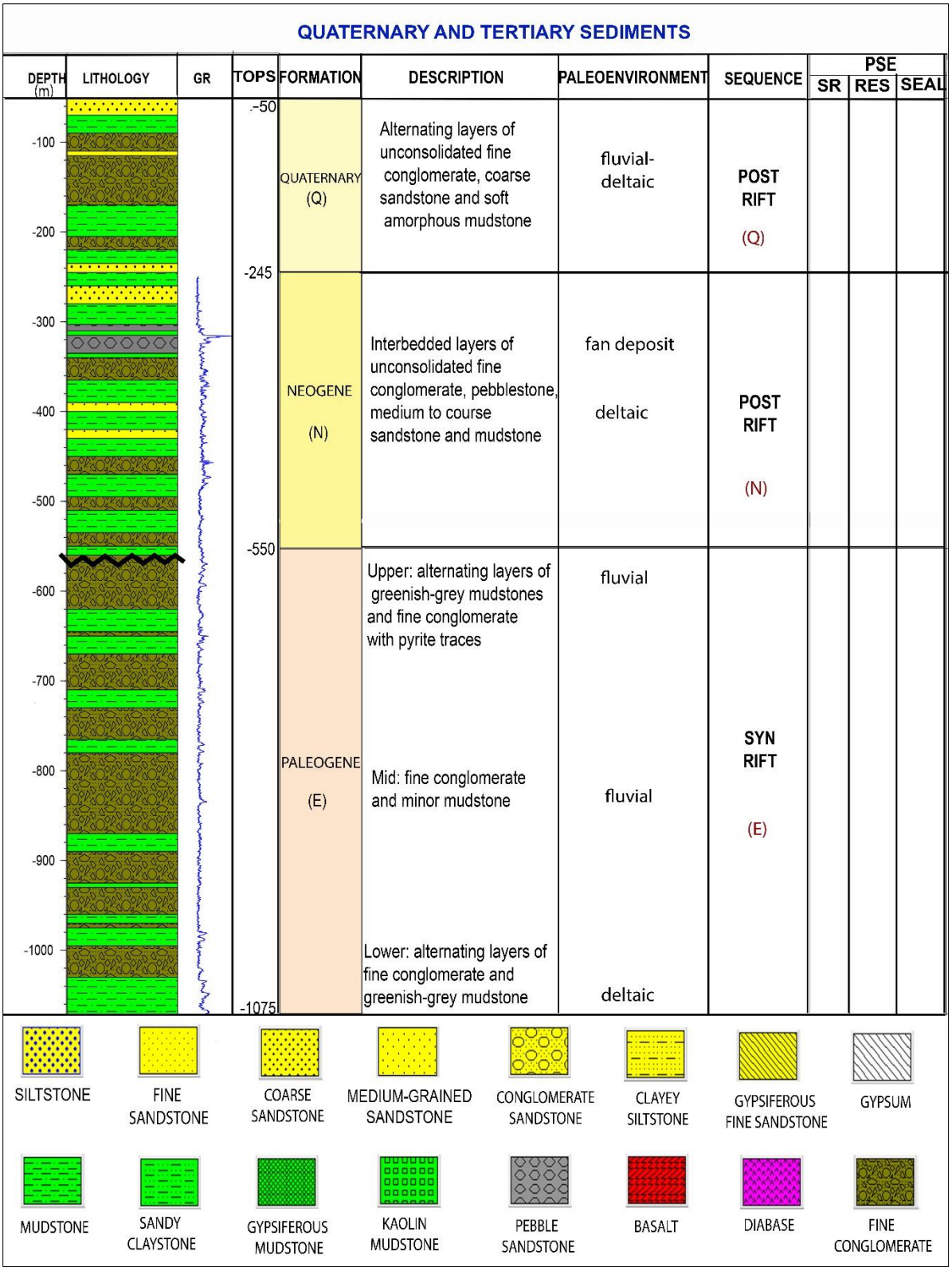

Well to seismic Tie

A well to seismic tie produced a synthetic seismogram with a good correlation value of 0.7. The formation tops marked in the synthetic seismogram were used to mark the major horizons in the seismic sections.

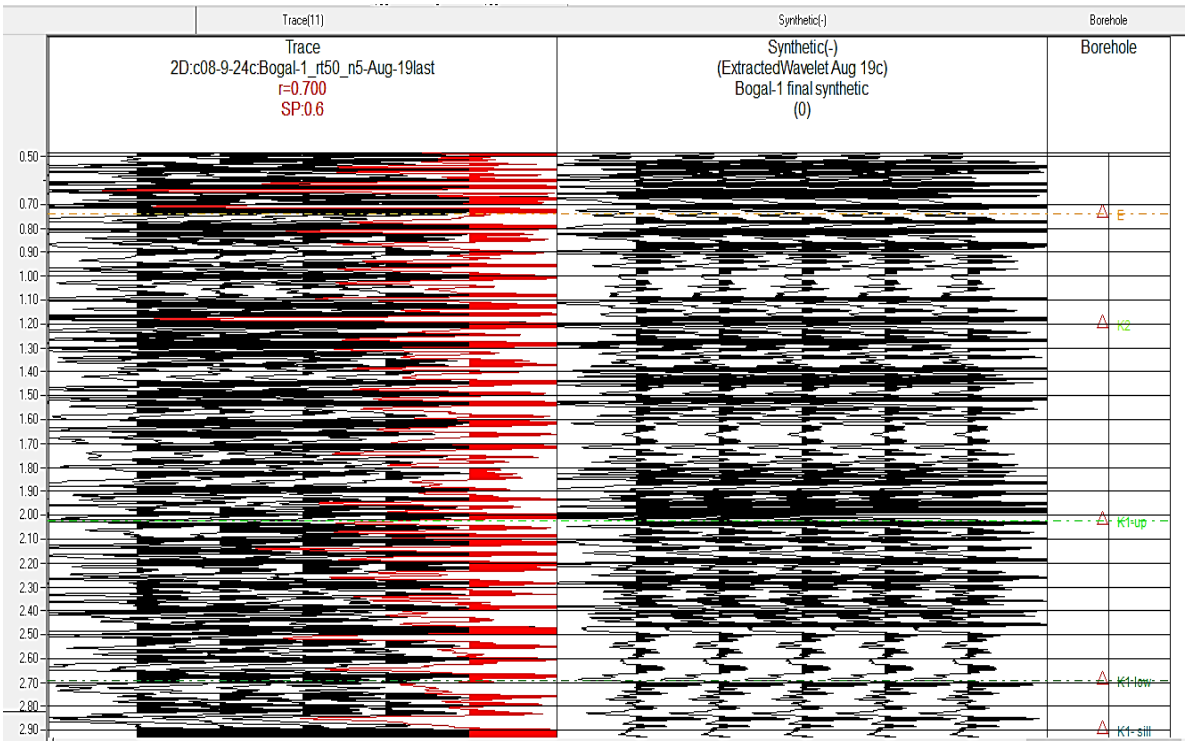

Figure 4.1: Synthetic seismogram for Bogal-1 well showing a correlation value of 0.7

4.1.4 Seismic Stratigraphy

The seismic stratigraphy shows the areal distribution of the sediments discussed above. The Jurassic, Triassic and Carboniferous- Permian sediments represent the first syn-rift sequence. The Lower Cretaceous and Upper Cretaceous represent the second and third syn-rift sequences respectively. The Paleogene represents the fourth syn-rift sequence while the Neogene and Quaternary sediments represent the post rift. Pre-rift sediments are represented by the Precambrian basement (figures 4.3 to 4.12 below).

Quaternary (Q): Represented by a reflection package of low amplitudes, discontinuous, parallel, high frequency reflections. This package represents interbedded layers of course sandstone, mudstone and fine conglomerate. This package is part of the post-rift sequence due to its undeformed, horizontal, continuous state.

Neogene (N): Represented by a thin package of low amplitude, parallel, high frequency reflections in the NW and high amplitude, parallel, medium frequency reflections in the SE. This represents a facies change. The Neogene is also part of the post-inversion /post-rift sequence because of its undeformed state.

Paleogene (E): Marked by low amplitude, medium frequency, parallel, semi-continuous reflections on the NW side and higher amplitude, medium frequency, parallel and continuous reflections. The Paleogene makes up part of the syn-rift sediments. An angular unconformity lies at the boundary between the Upper Cretaceous and the Paleogene sediments.

Upper Cretaceous: The Upper Cretaceous has two seismic units: $K2_1$ and $K2_2$.

$K2_1$: A thick package of high amplitude, low frequency, continuous, parallel reflections at the top and SE side. The beds are horizontal in the NW side, however, they dip eastwards in the SE side. This layer represents the thick mudstone beds that could possibly form the sealing rock in the Bogal play.

$K2_2$: A low amplitude, low frequency, continuous, parallel reflections at the bottom NW side. This change in reflection pattern represents a facies change.

Lower Cretaceous: Four seismic facies are identified in this section.

$K1_1$: marked by high amplitude, low frequency, parallel, continuous reflections.

$K1_2$: marked by high amplitude, low frequency, parallel, continuous reflections. It is separated from $K1_1$ by a strong reflection.

$K1_3$: marked by low amplitude, low frequency, parallel, semi-continuous reflections. It represents a massive sandstone layer.

$K1_4$: marked by low frequency, medium amplitude, parallel, continuous reflections. This package represents the source rocks of the Bogal play.

Igneous intrusion: Marked by a high amplitude, low frequency, continuous reflection. Well cuttings indicate that this igneous intrusion is a diabase sill.

Pre-Cretaceous seismic facies

Four reflections below the diabase seal could possibly represent the Jurassic, Triassic, Carboniferous-Permian sediments and the basement. These sediments were not encountered by the well; therefore, their boundaries are uncertain.

Jurassic (?)

This is represented by low amplitude, high frequency, chaotic, subparallel, discontinuous reflections. Sediments thicken south-eastwards.

Triassic (?)

The package consists of low amplitude, hummocky, sub-parallel, semi- continuous reflections. It is separated from the Jurassic by a strong, high amplitude reflection.

Carboniferous-Permian (?)

It is separated from the Triassic by a strong, high amplitude reflection. It consists of low amplitude, low frequency, hummocky, discontinuous reflections.

Precambrian Basement (?)

This package is represented by low amplitude, low frequency, hummocky, discontinuous reflections that are separated from the Carboniferous-Permian by a high amplitude reflection.

4.2 STRUCTURAL ANALYSIS

A map view of the seismic survey is presented in figure 4.2 below.

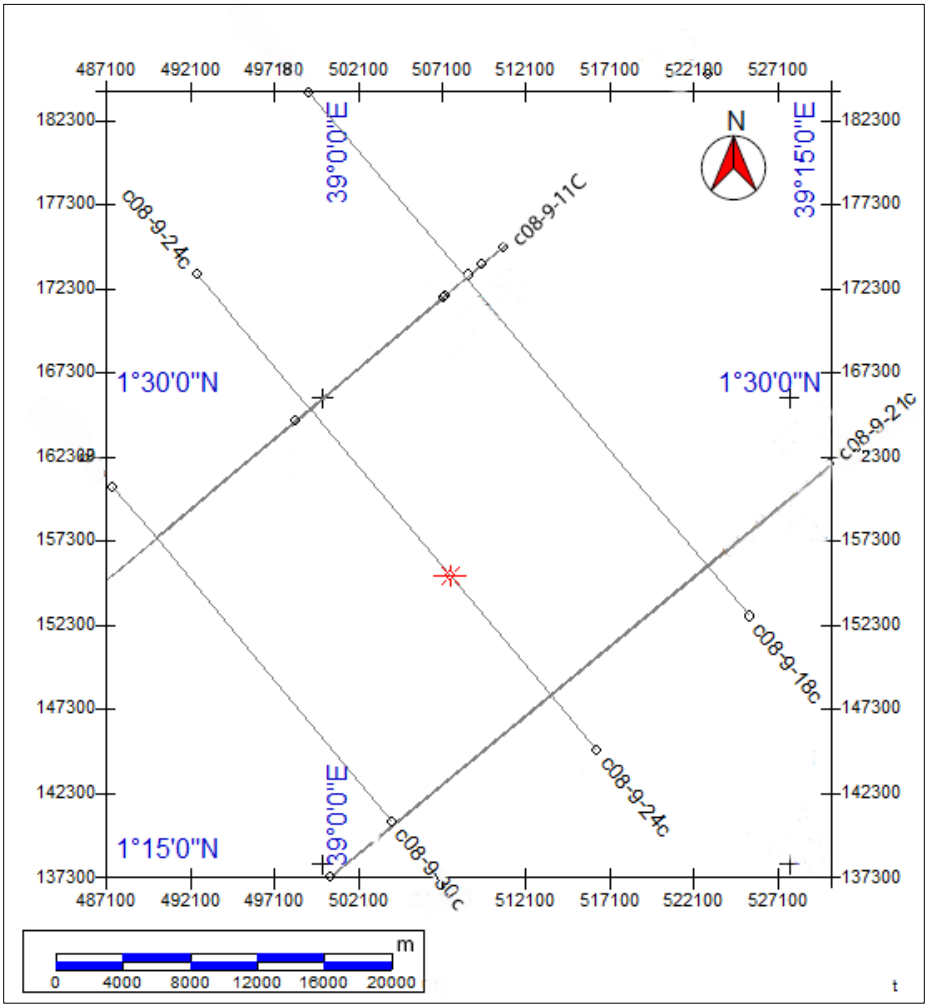

Figure 4.2: Basemap of the seismic survey

Line C08-9-11c

This line trends in a NE-SW direction, cutting across the strike of the Anza basin. Listric and planar faults dip to the north-east and south-east, forming flower structures (Figure 4.3b). Shortening occurred in a NE-SW direction, resulting in the formation of two inversion anticlines on the Cretaceous sediments. The Cretaceous sediments appear to be more deformed than the pre-Cretaceous, implying that the inversion is mild. They form a prominent anticline on the south-western side and a minor asymmetric one on the north-eastern side.

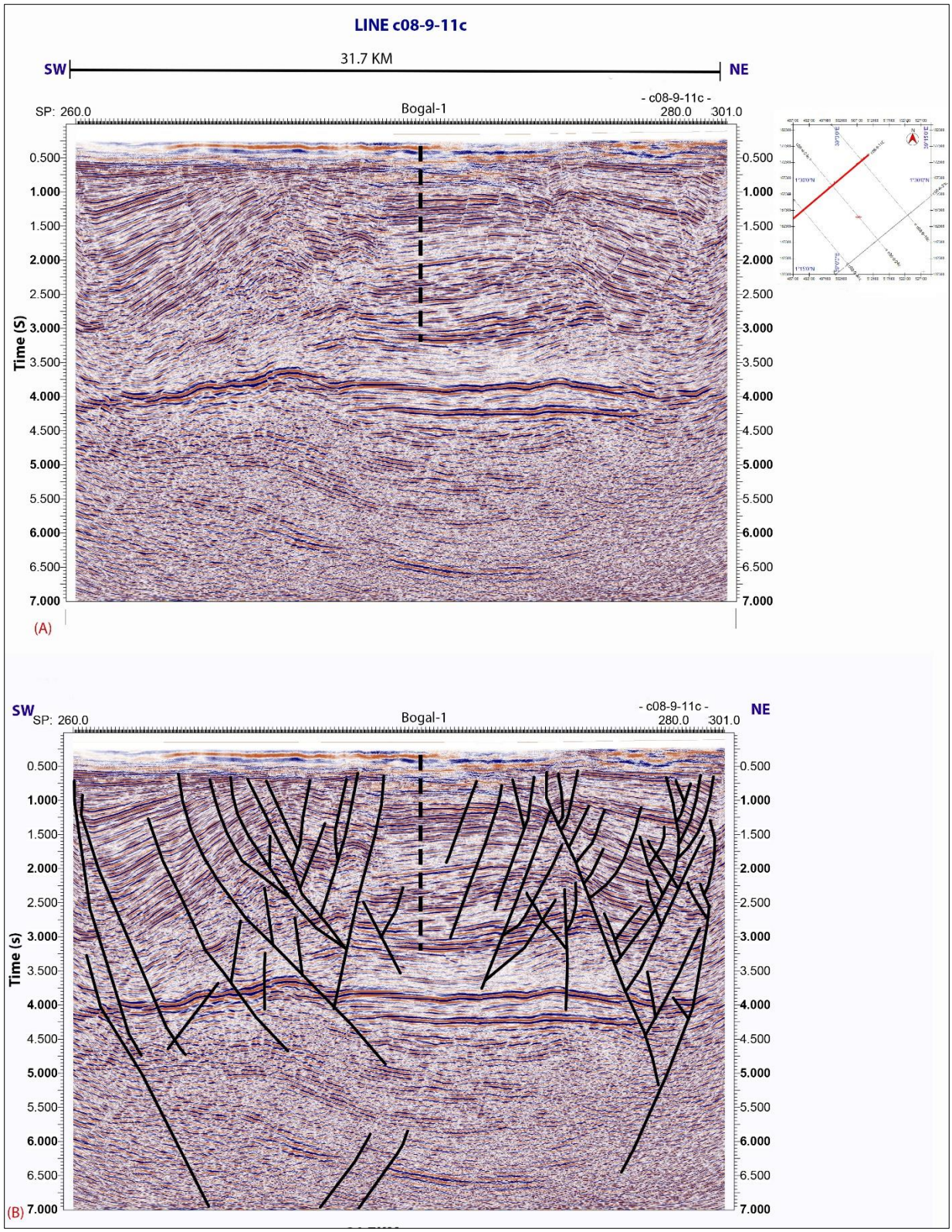

Figure 4.3: Uninterpreted seismic section (A) and fault picks in line c08-9-11c (B). The inset picture shows the position of the seismic line

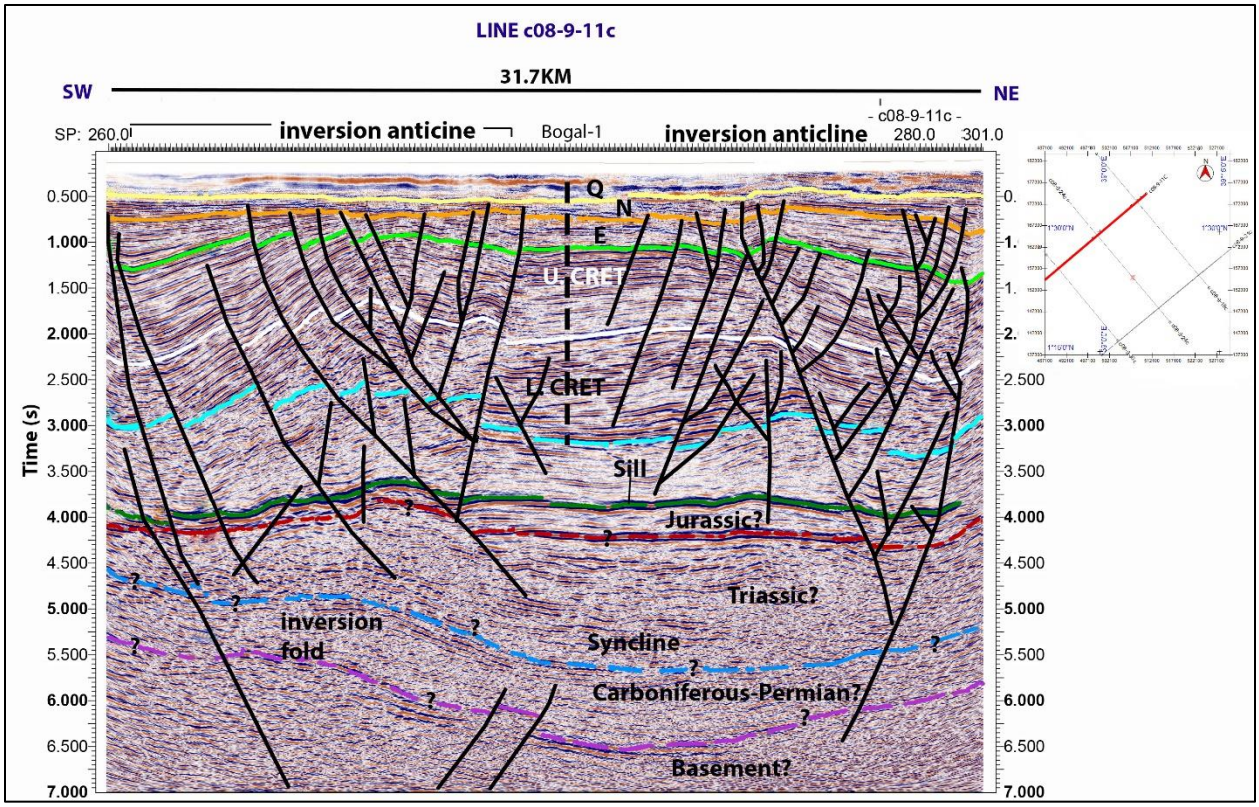

Figure 4.4: Interpreted faults and horizons in line c08-9-11c showing an inversion anticline on the south-western side and an inversion monocline on the north-eastern side. Inversion is more prominent on the Cretaceous sediments (Z=2). (Abbreviations: Q- Quaternary, N- Neogene, E-Paleogene)

Synthetic faults on the western side dip to the north-east, while antithetic faults dip to the south-west. However, on the eastern side of the seismic section, synthetic faults dip to the south-west, while antithetic faults dip to the north-east. A negative flower structure appears on the south-western side while a hybrid flower structure, which forms due to a combination of both normal and reverse faults, is present on the northeastern side of the seismic section. Hybrid flower structures are indicators of wrenching. They may be associated with Late-Cretaceous- Early Tertiary wrenching that took place in the Anza Basin. They formed due to the combination of translation, transtension and oblique rifting in a locally compressional environment.

Line C08-9-21c

Line 21, which is parallel to 11c, shows similar structures. Listric faults that dip to the northeast and south-west, form negative flower structures. Two inversion anticlines appear on the south-west and in the middle. These anticlines are formed by reverse faulting, with shortening occurring in a NE-SW direction (Figure 4.5).

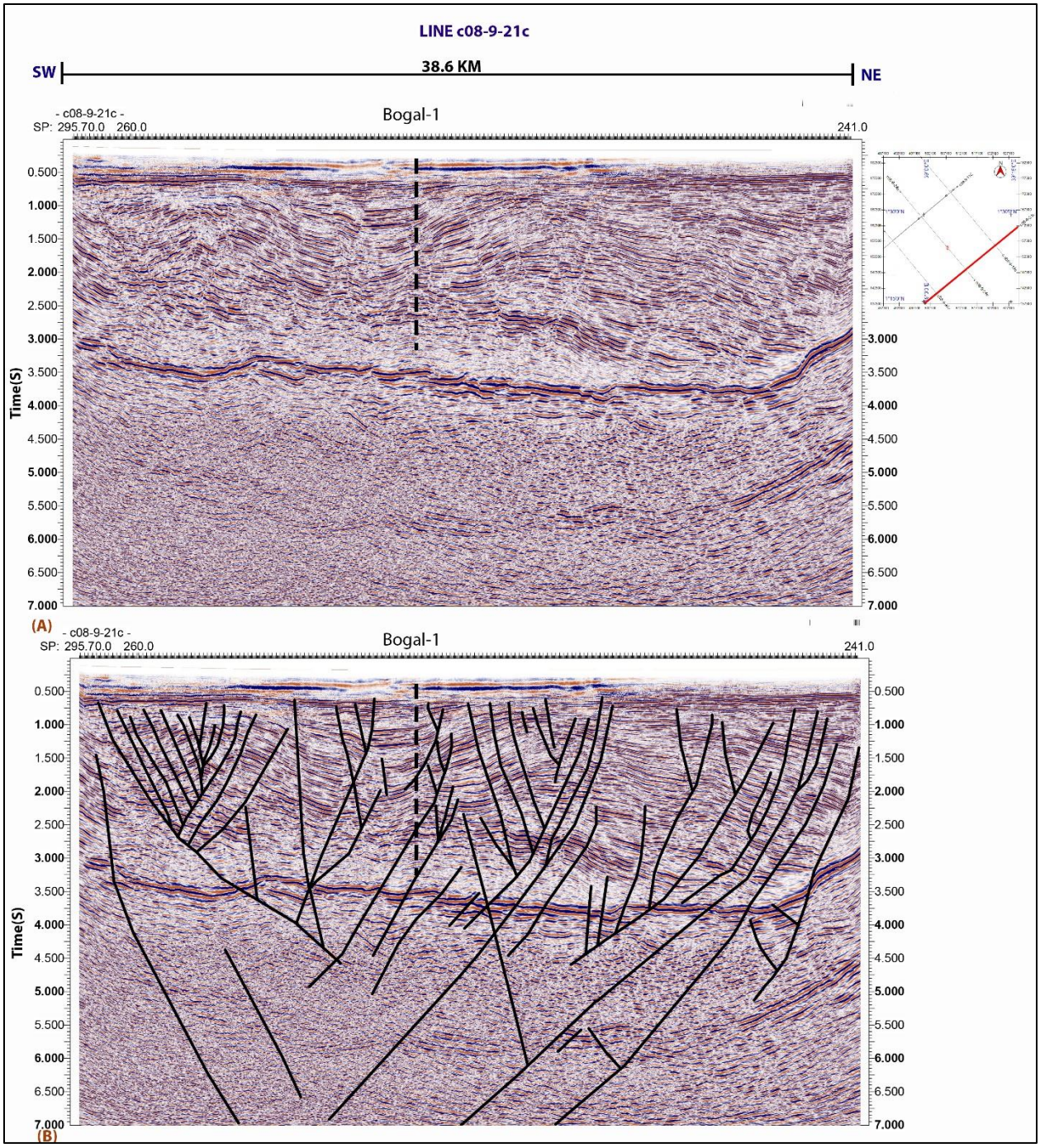

Figure 4.5: Uninterpreted seismic section (A) and fault picks in line c08-9-21c (B) The inset picture shows the position of the seismic line

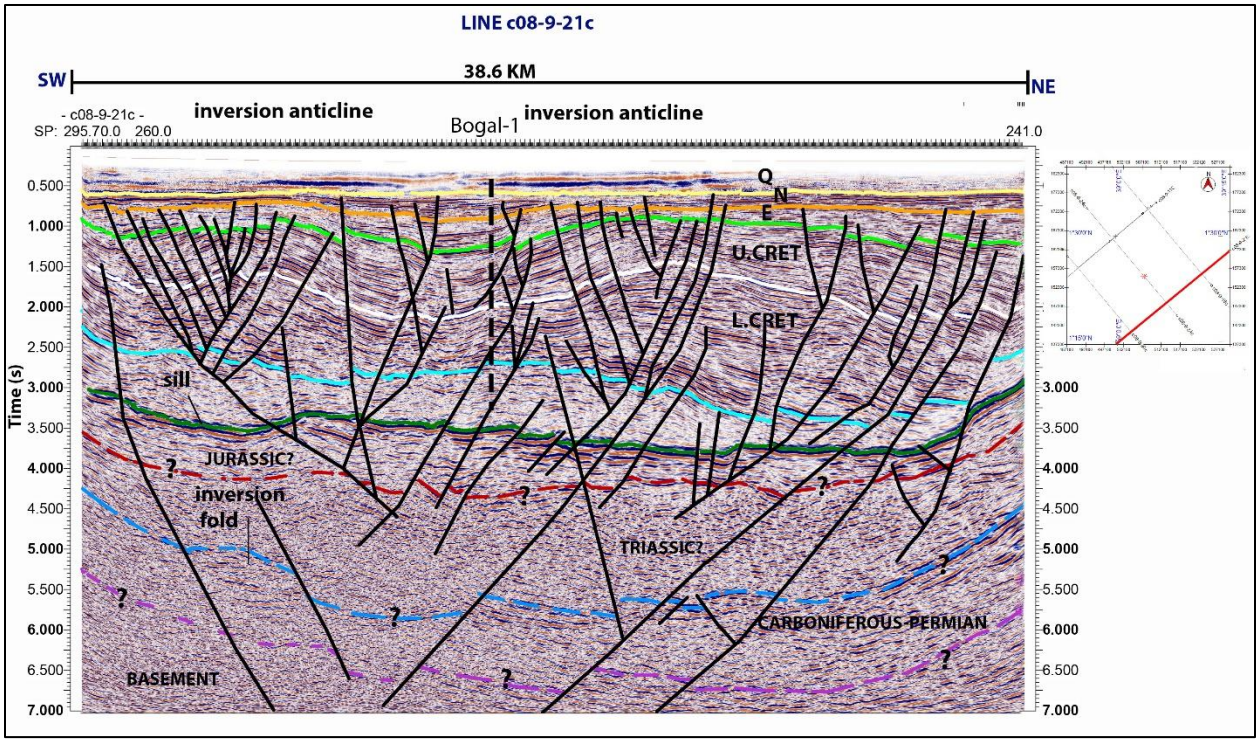

Figure 4.6: Interpreted faults and horizons in line c08-9-21c

Synthetic faults in the flower structure on the left side of the seismic section dip to the north-east, while antithetic faults dip to the south-west. However, synthetic faults on the right side of the seismic section dip to the south-west, while antithetic faults dip to the north-east.

The anticlines are more prominent on the Cretaceous sediments than in the pre-Cretaceous section where inversion appears to be minimal. An inversion fold is present alongside the major fault that lies in the south-west.

Line C08-9-30

Line 30 trends in a NW-SE direction, parallel to the axis of the Anza basin. Majority of the faults dip in a SE direction, with a few dipping to the NW. They form a negative flower structure. The Cretaceous sediments are generally horizontal, while the pre-Cretaceous are involved in the formation of a gentle syncline. An anticlinal structure can be observed on the southeastern side of the prominent high-reflection diabase sill.

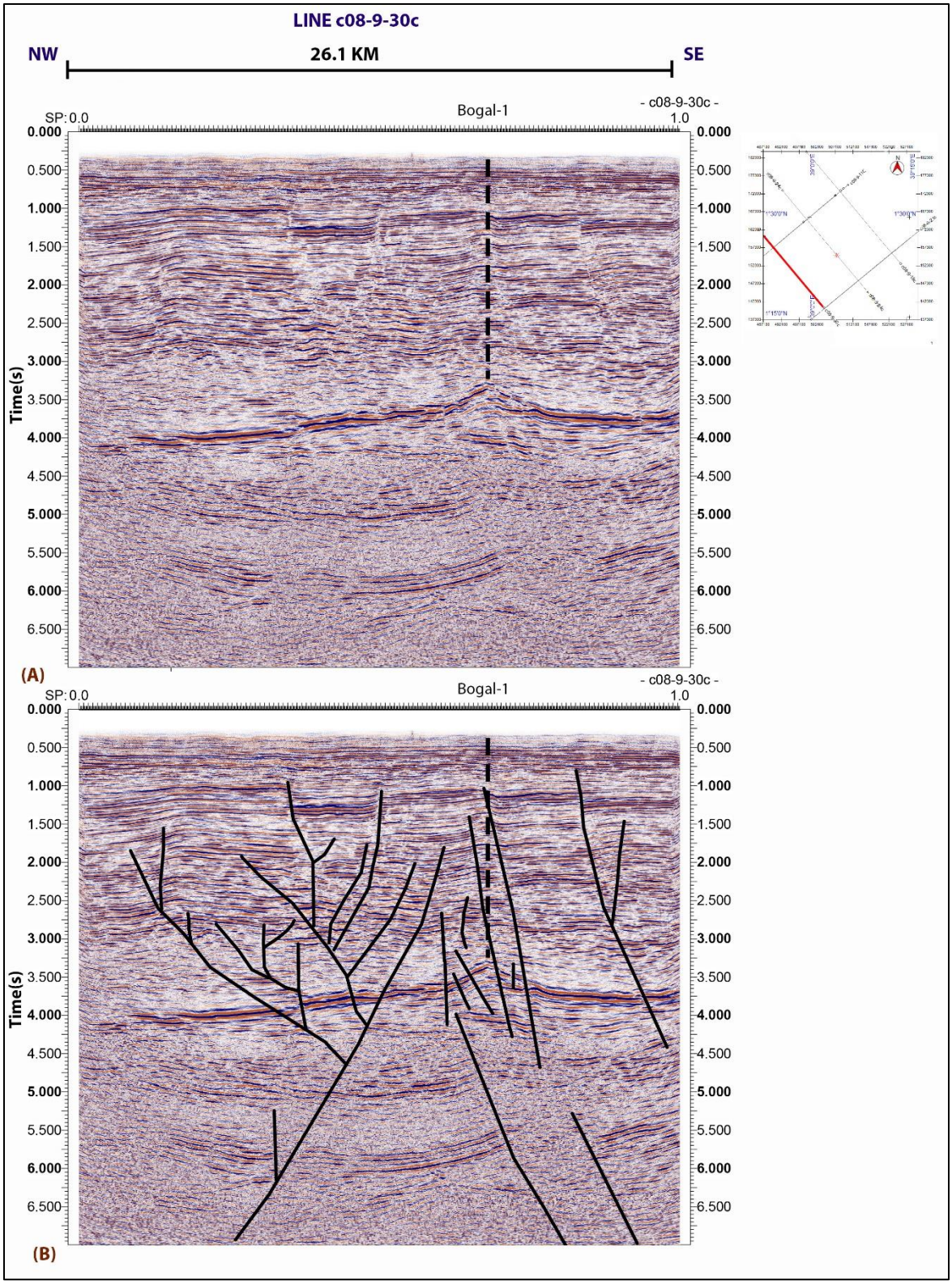

Figure 4.7: Uninterpreted seismic section (A) and fault picks in line c08-9-30c showing a negative flower structure (B)

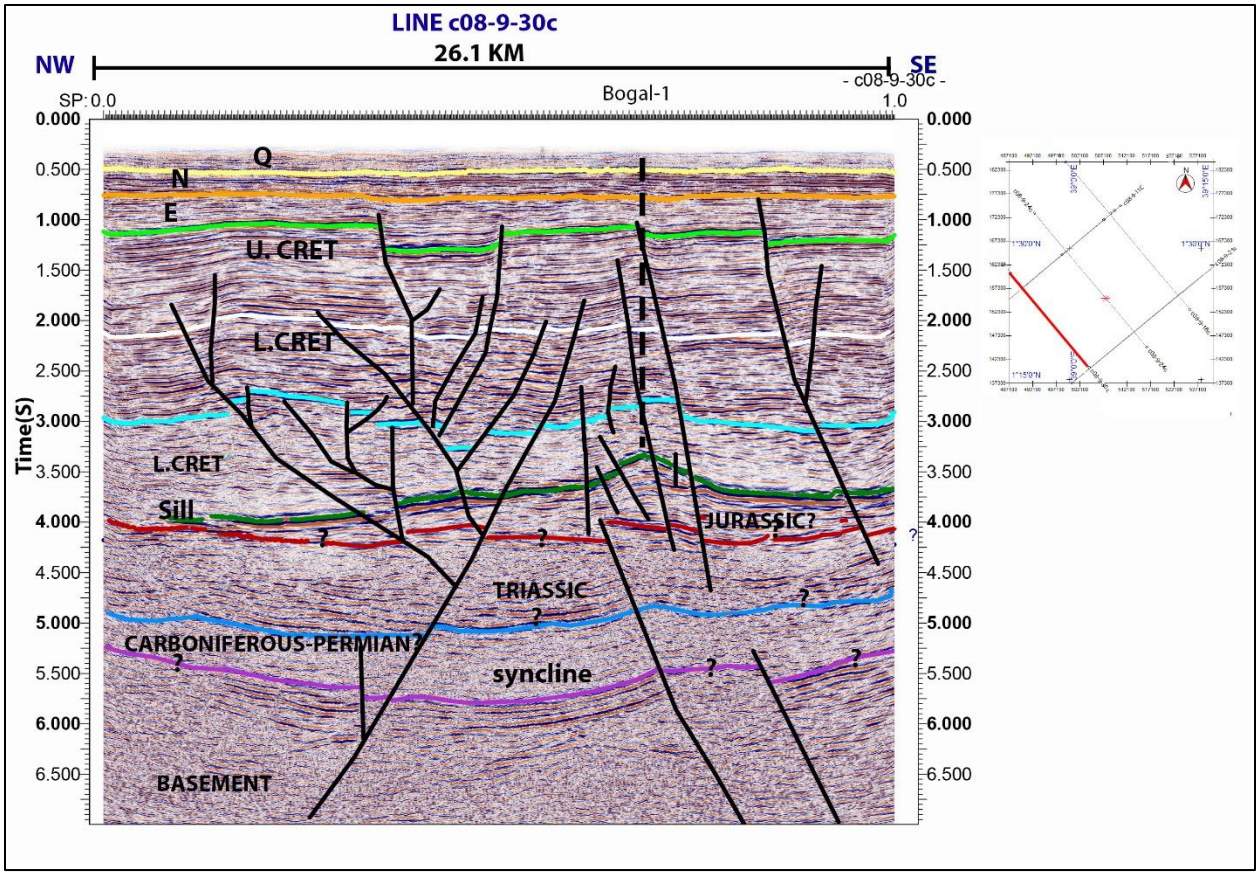

Figure 4.8: Interpreted faults and horizons in line c08-9-30c. (Q- Quaternary, N- Neogene, E-Paleogene)

Line C08-9-24

Line 24 also trends parallel to the axis of the Anza basin. The anticlinal feature identified in line C08-9-30 is more prominent in this section. Hybrid flower structures are present in this section. Synthetic faults dip in a southeast direction, while antithetic faults dip towards the north-west. The Cretaceous sediments have very shallow dips that are almost horizontal on the north-western side of the section. They dip south-eastwards on the south-eastern side of the section.

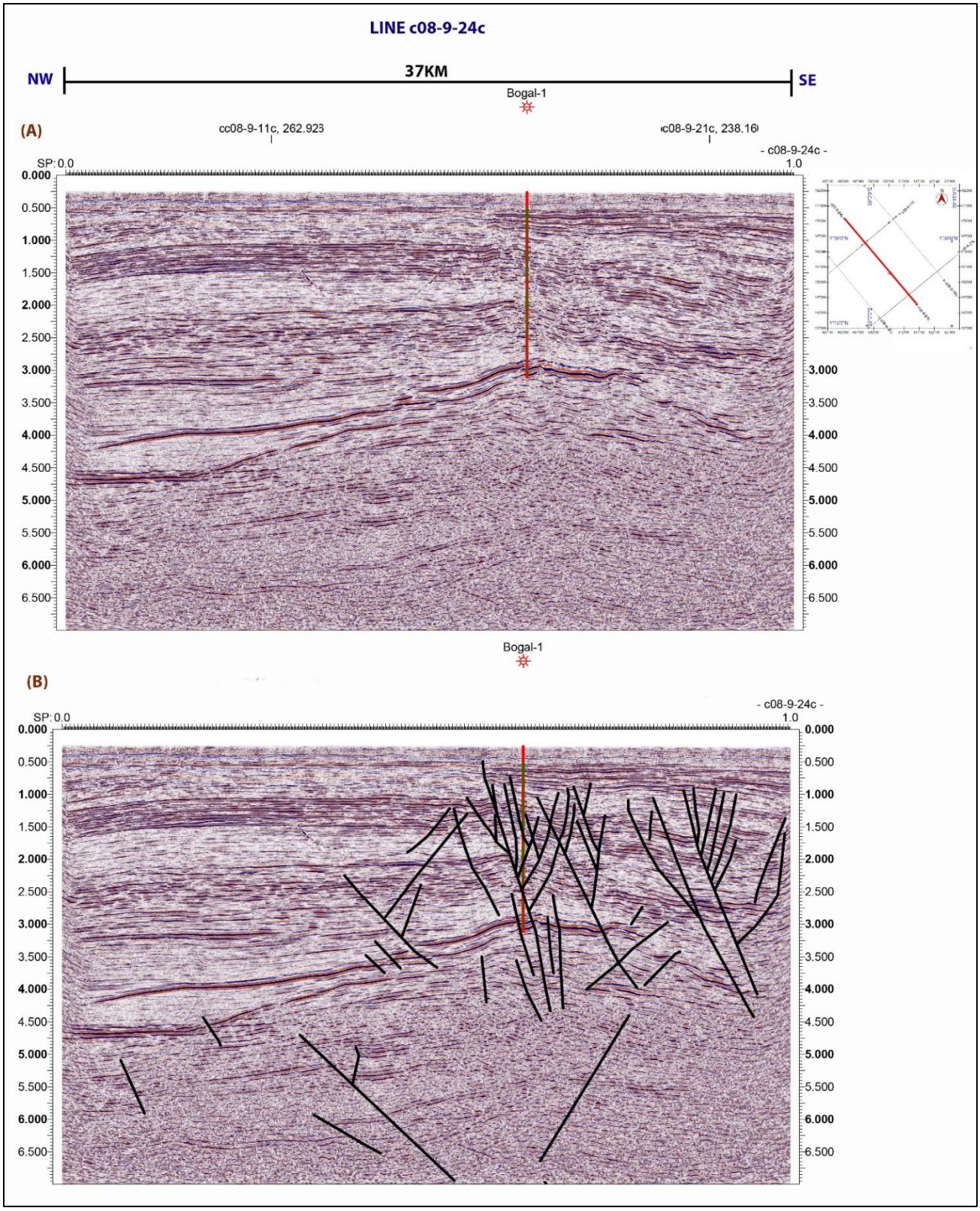

Figure 4.9: Uninterpreted seismic section (A) and fault picks in line c08-9-24c (B)

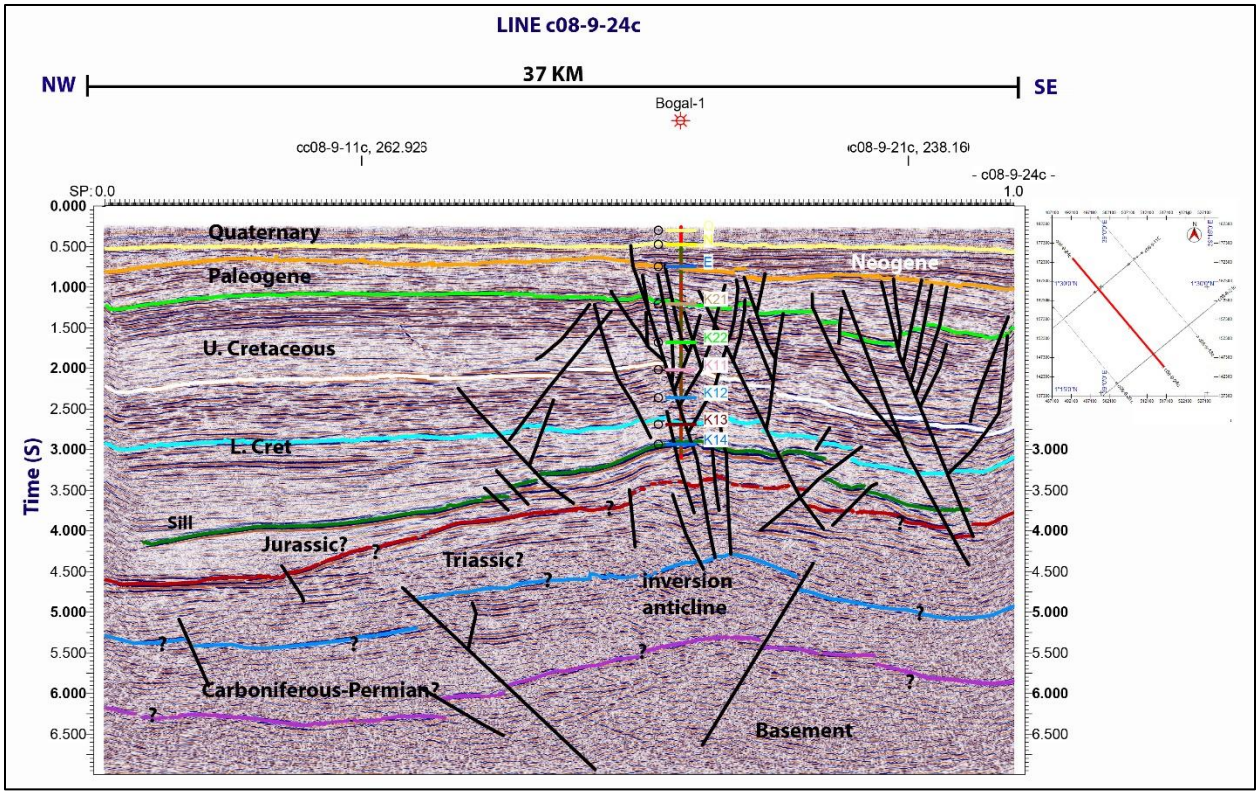

Figure 4.10: Interpreted faults and horizons in line c08-9-24c

Line C08-9-18

This seismic line trends parallel to the Anza basin. It shows similar structures to the ones present in line c08-9-24c and c08-9-30c. This section contains numerous faults that form flower structures. Synthetic faults dip to the northeast while antithetic faults dip to the north-west. Inversion is evident in both the Cretaceous and Pre-Cretaceous sediments in this section.

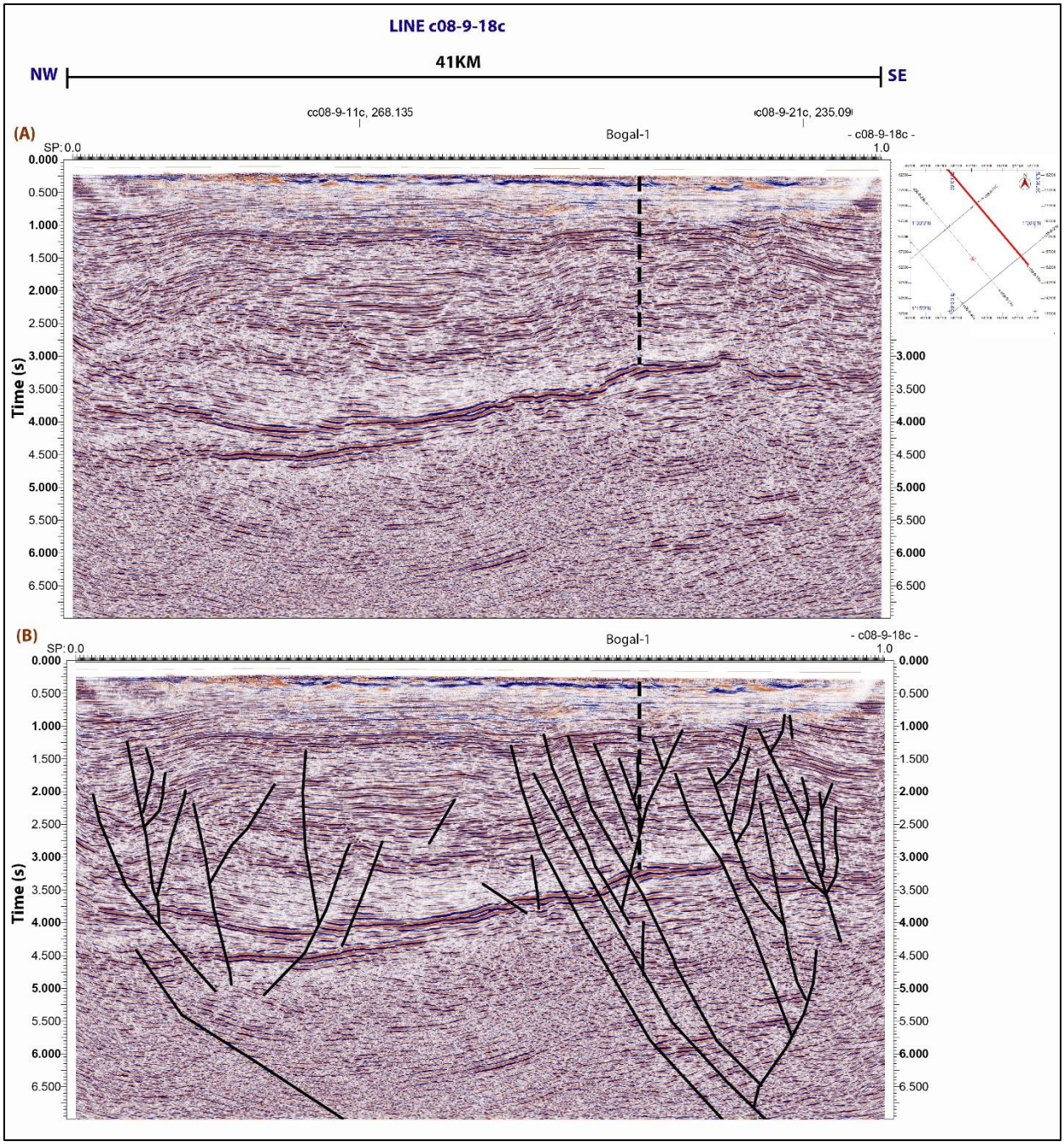

Figure 4.11: Uninterpreted seismic section (A) and fault picks in line c08-9-18c (B)

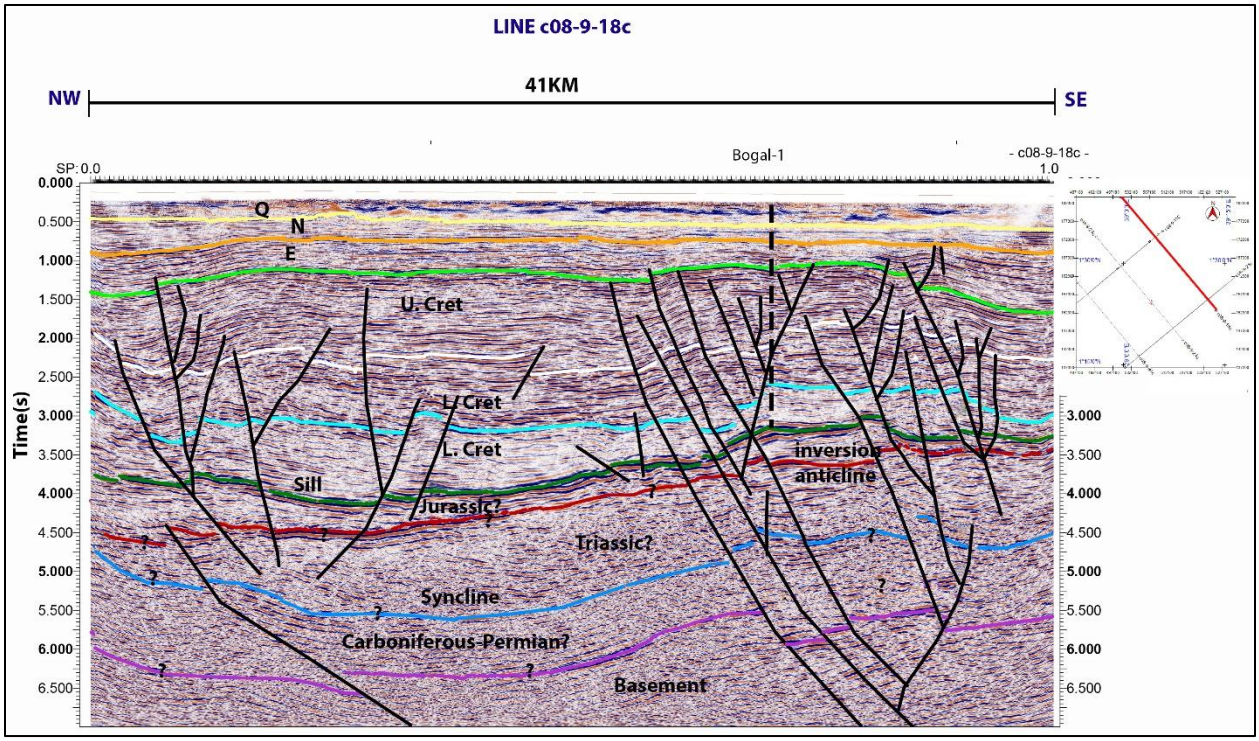

Figure 4.12: Interpreted faults and horizons in line c08-9-18c

The interpretation of the five seismic sections above indicate that the Bogal play experienced mild inversion in a dominating extensional setting. Depth conversion of the seismic sections using vertical seismic profile data reveal that the sediment thickness is around 13.5 Km (Figure 4.13).

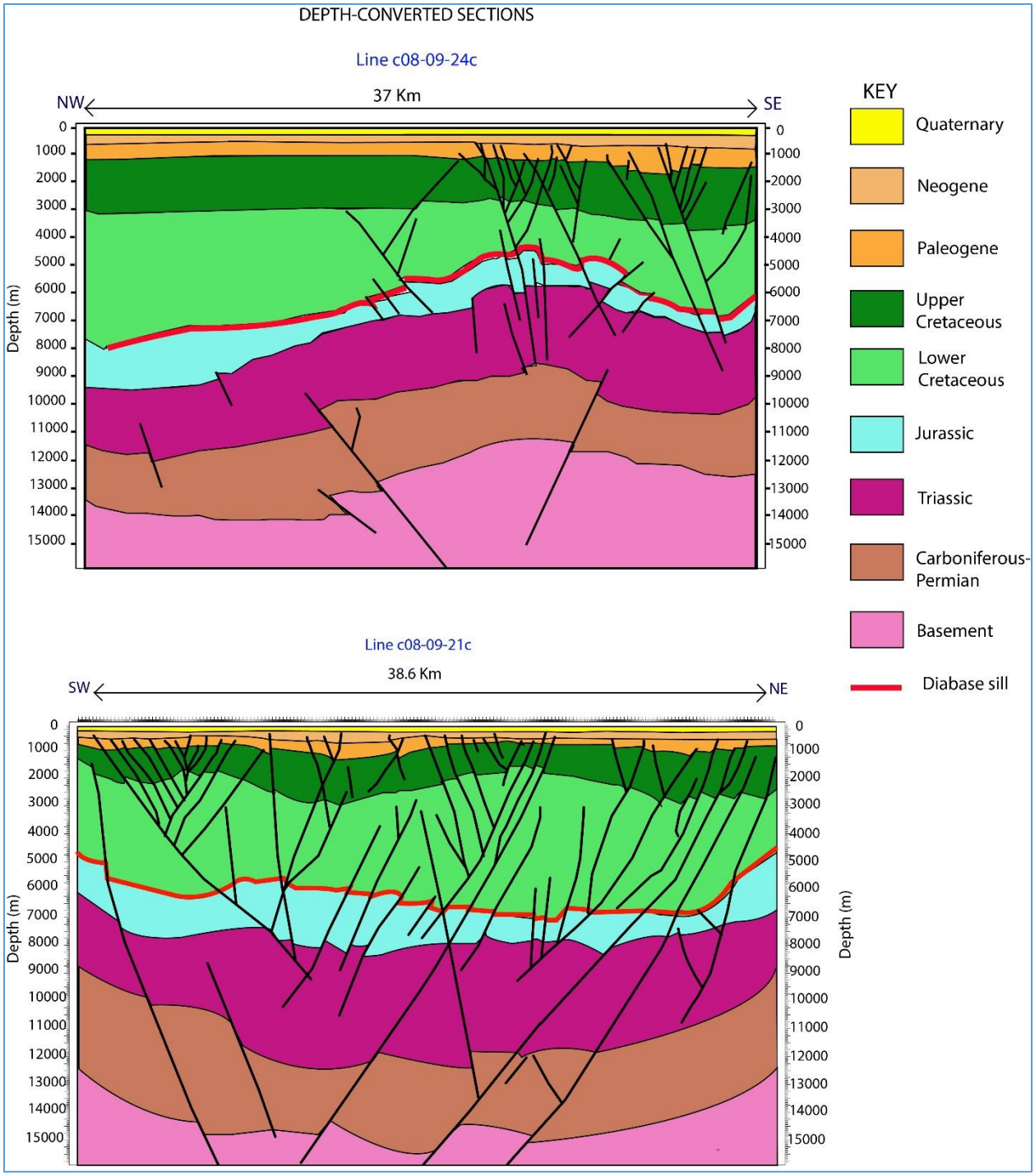

Figure 4.13: Depth-converted illustrations of line c08-09-24c and c08-09-21c.

In summary, figures 4.14 and 4.15 below show the structural geometry, distribution of the potential source rocks, reservoirs and seal as well as the pre-rift, post-rift and syn-rift sequences in the Bogal play.

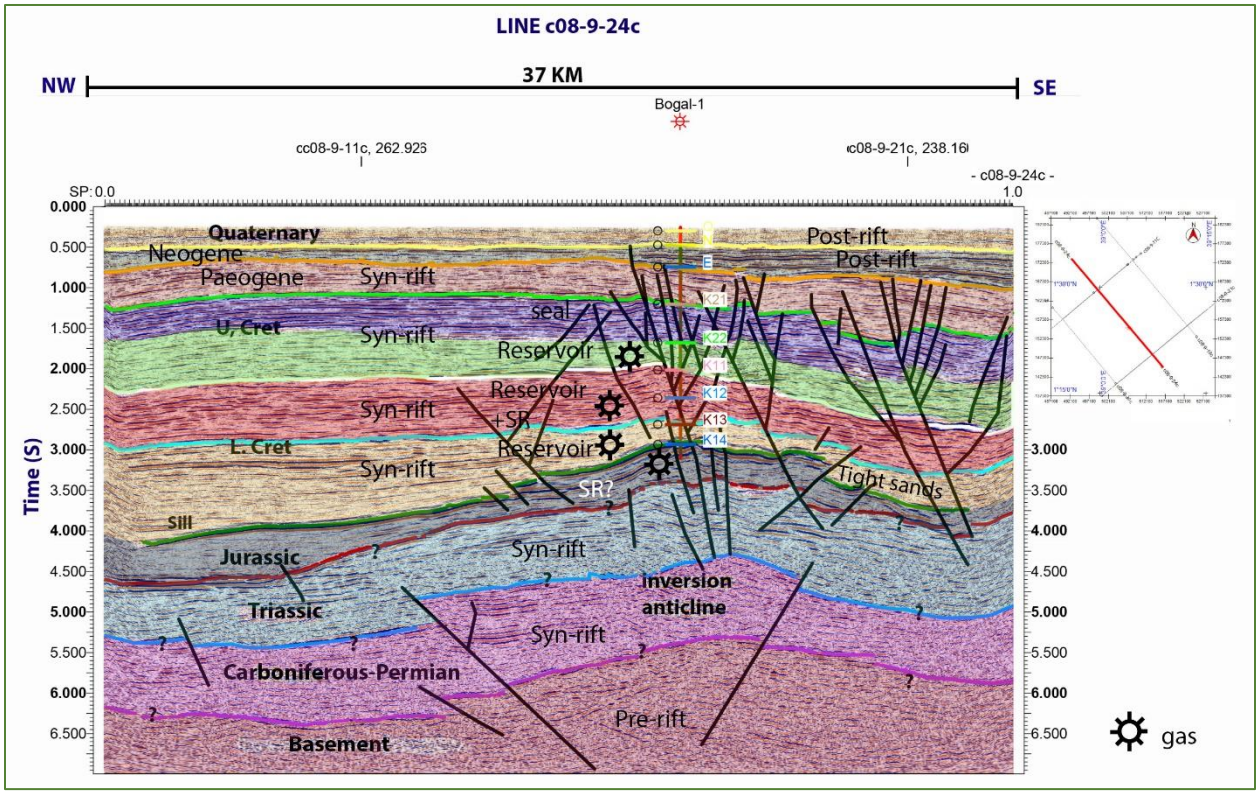

Figure 4.14: Seismic stratigraphy and PSE of line c08-9-24c

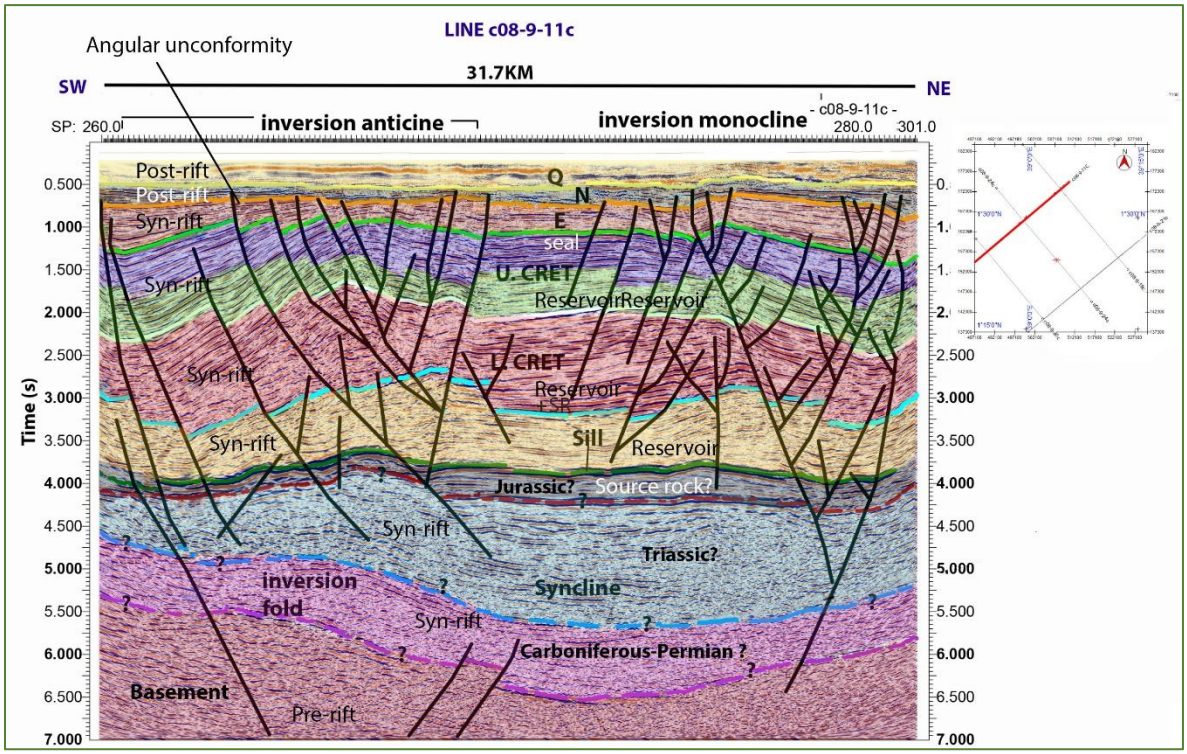

Figure 4.15: Seismic stratigraphy and PSE of line c08-9-11c

Time structure maps for the sill, Lower Cretaceous and Upper Cretaceous horizons, that were created from the five seismic lines, are presented in the figures below.

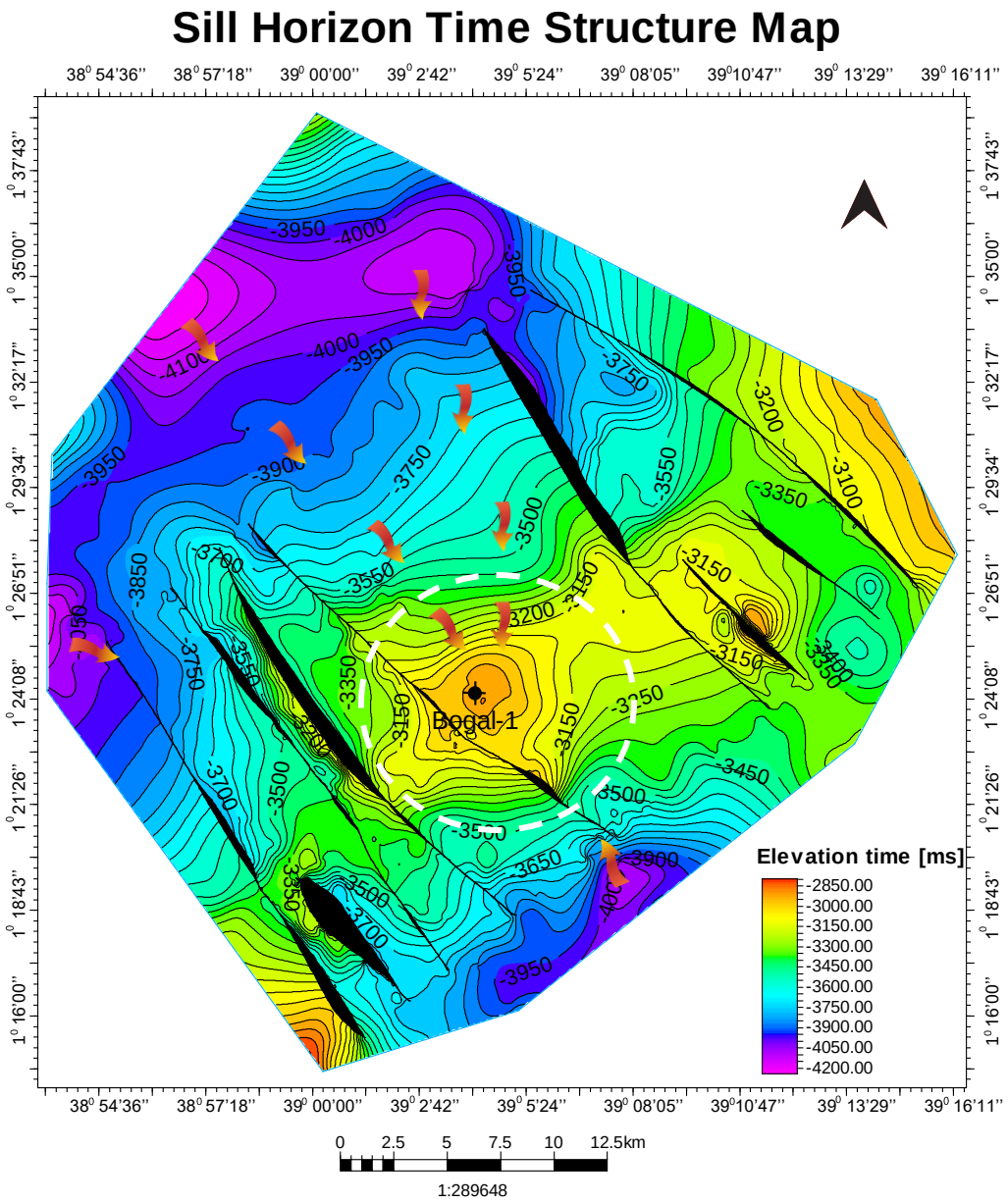

Figure 4.16: Time Structure map for the sill horizon.

Figure 4.16 shows an inversion anticline of approximately 58.1 km^2 represented by the structural high at the centre of the horizon covered by the sill intrusion (encircled in white). Below this horizon are thin layers of Lower Cretaceous source rocks and possibly Jurassic source rocks. The

tip of this anticlinal closure is the hydrocarbon trap on which Bogal-1 well was drilled. High angle normal faults that trend in a NW-SE direction cut across all three horizons. They probably act as conduits to the upper horizons, which have low porosity and permeability values. The arrows indicate possible hydrocarbon migration routes.

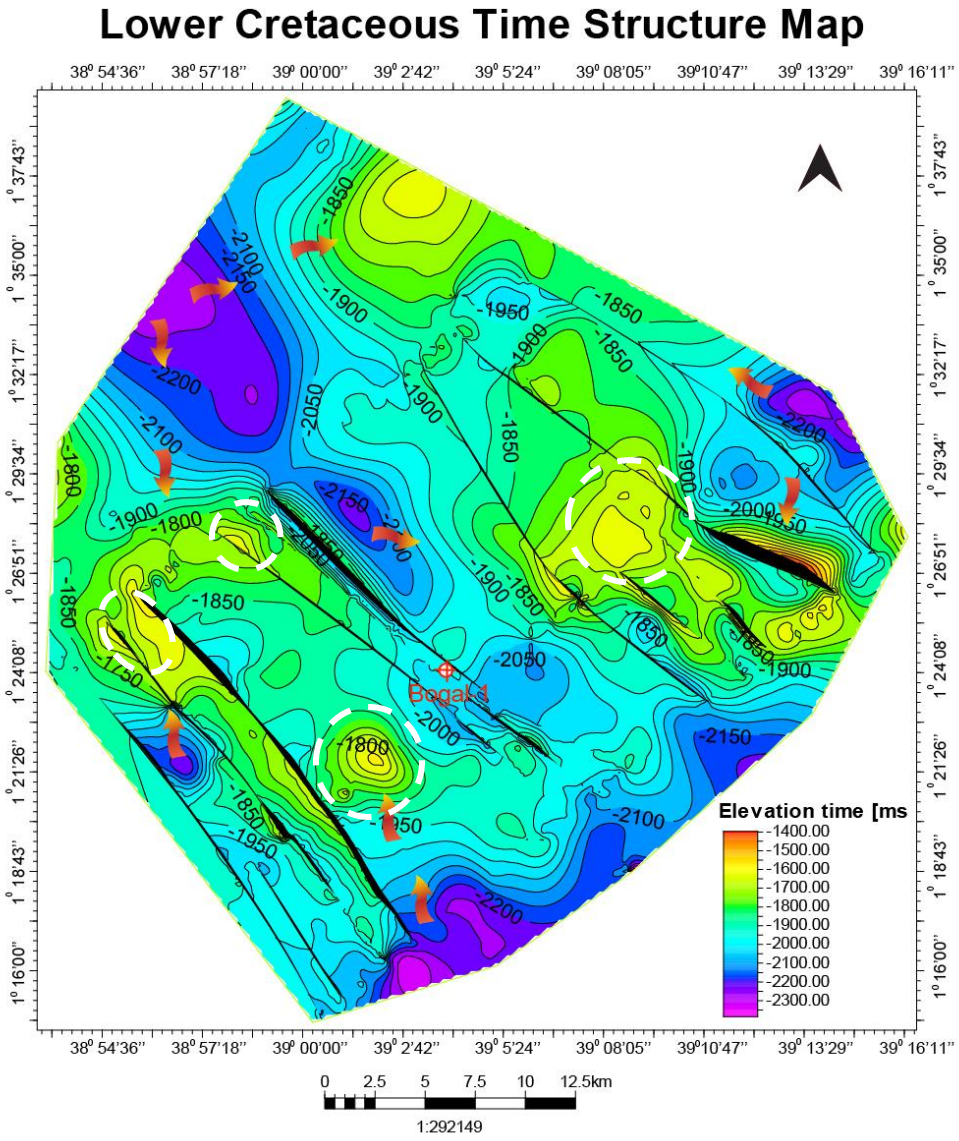

Figure 4.17: Time-Structure map for the Lower Cretaceous horizon

Figure 4.17 represents the top of the Lower Cretaceous horizon. Inversion structures are represented by the structural highs located on the north, west and east of the study area (marked by white circles). They have an area that ranges from 13 km^2 to 51 km^2. These are inversion

anticlines that possibly act as hydrocarbon traps. Potential source rocks lie at the bottom of this horizon, while potential reservoir and sealing rocks are located just above these source rock. The faults act as hydrocarbon conduits that transfer hydrocarbons from the lower part of this section to the anticlinal traps above.

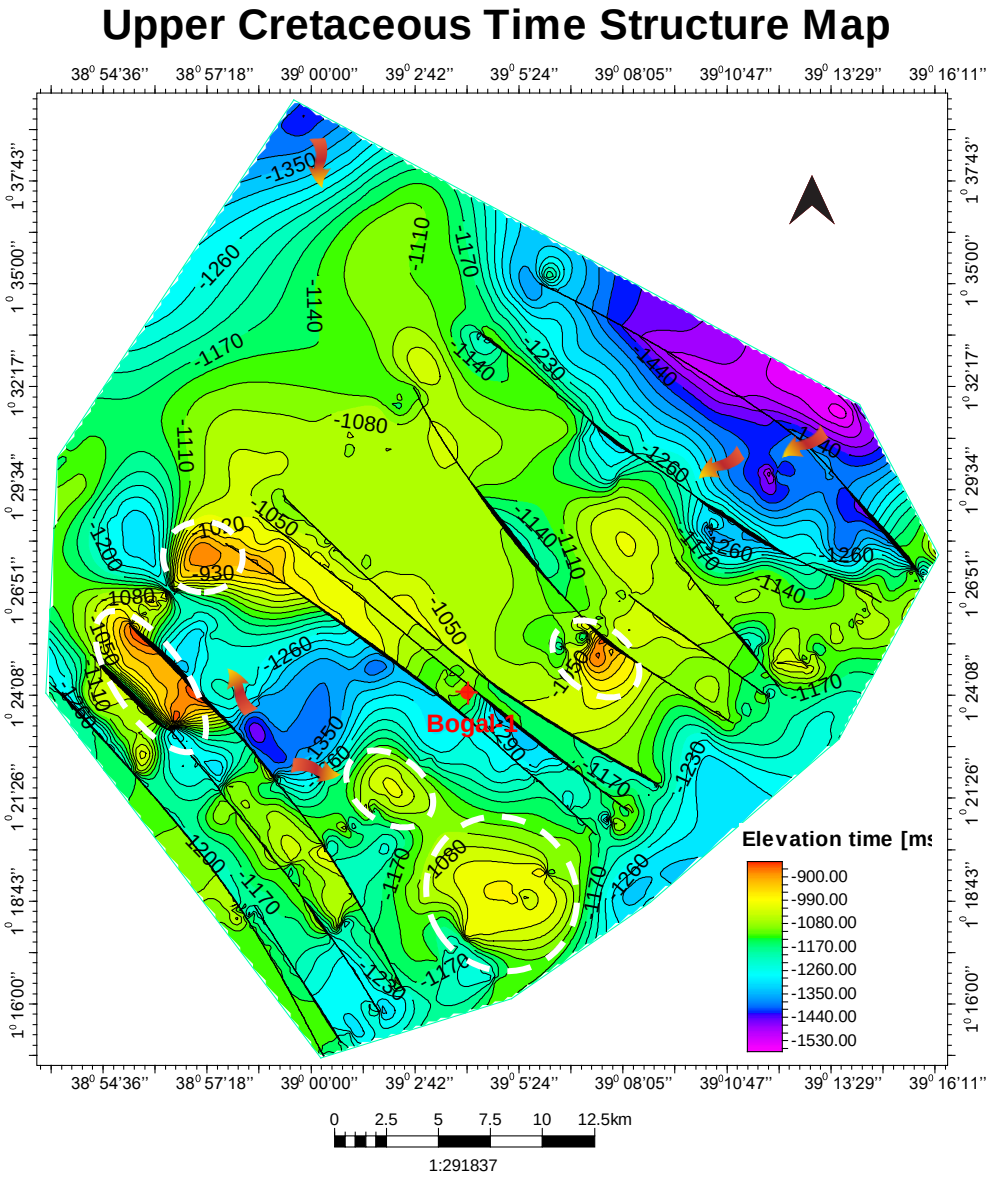

Figure 4.18: Time Structure map for the Upper Cretaceous horizon

Figure 4.18 represents the time structure map for the Upper Cretaceous horizon. This layer is assumed to be the main seal in the Bogal play. Some of the hydrocarbons that seeped through the

conduit faults may have been trapped in the structural highs, while others might have leaked up to the unconformity that lies above this horizon. Inversion structures with areas that range from 48 Km^2 to 7.1 Km^2 are represented by the structural highs encircled in white. They form potential hydrocarbon traps.

4.2.1 Structural Restoration

The Upper Cretaceous and Lower Cretaceous horizons were restored using the trishear algorithm in Petroleum Experts Move software, version 2017. The results show that the Upper Cretaceous (K2) had a length of 30,923.2 m; the upper part of the Lower Cretaceous ($K1_1$) had a length of 30,723m while the lower part of the Lower Cretaceous ($K1_2$) had a length of 31,562.2 m before restoration (Table 4-5).

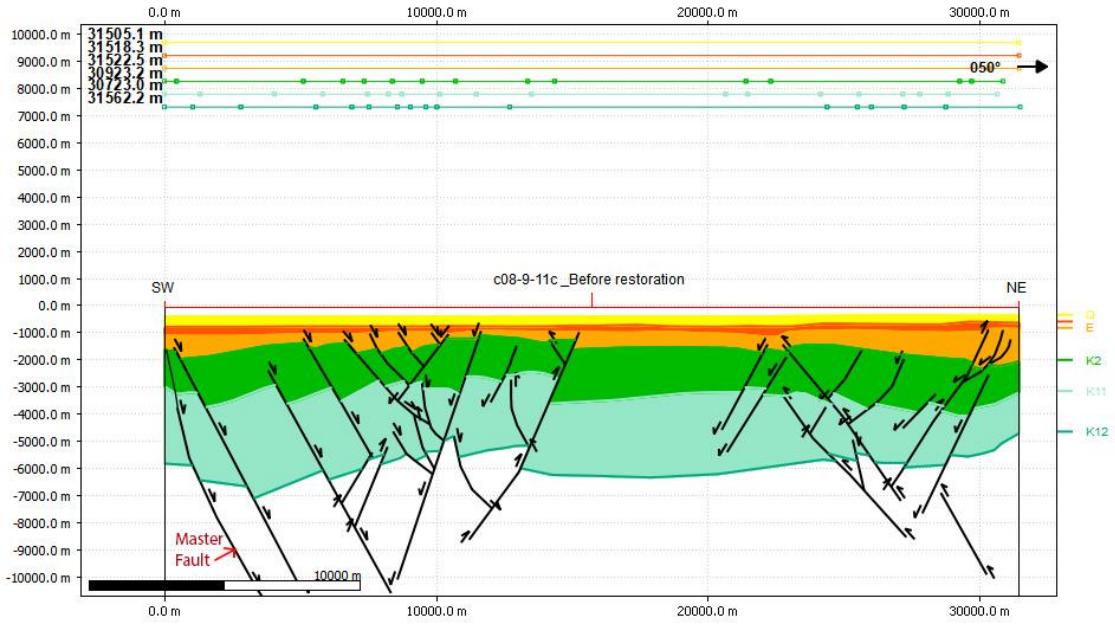

Figure 4.19: Seismic line c08-9-11c before restoration. The arrows show the direction of movement

Table 4-5: Length of the horizons before restoration

UNIT	AGE (Ma)	LENGTH (m)
$K1_2$ (Lower Cretaceous-lower)	131	31,562.2
$K1_1$ (Lower Cretaceous-upper)	100	30,723
K2 (Upper Cretaceous)	66	30,923.2

After decompaction of the top horizons and fault restoration, the Upper Cretaceous (K2) had a length of 31,798.7 m; the upper part of the Lower Cretaceous ($K1_1$) had a length of 32,564 m, while the lower part of the Lower Cretaceous ($K1_2$) had a length of 33,988.9 m (Table 4-6).

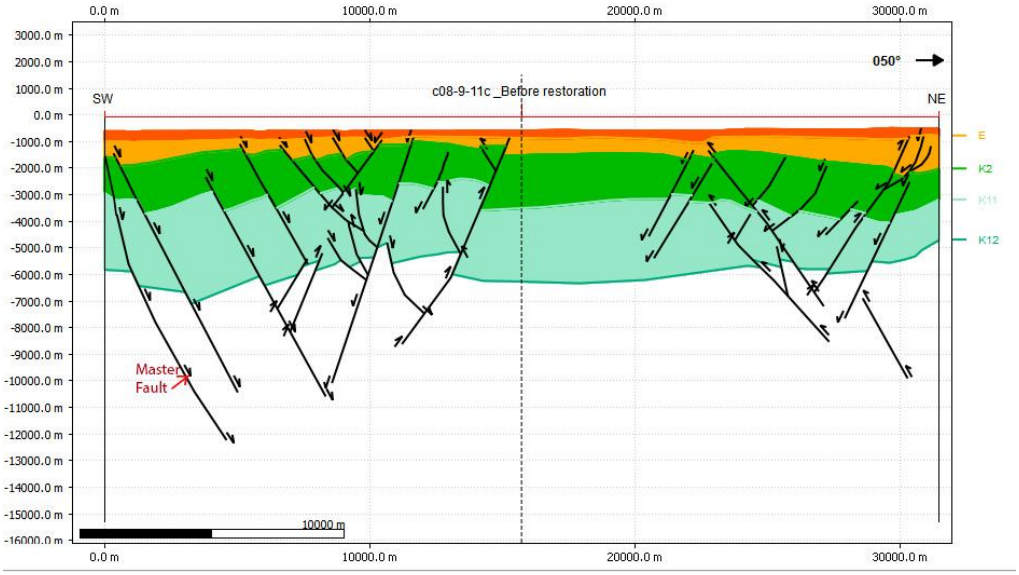

Figure 4.20: Seismic line c08-9-11c after decompaction of the Quaternary post-inversion strata

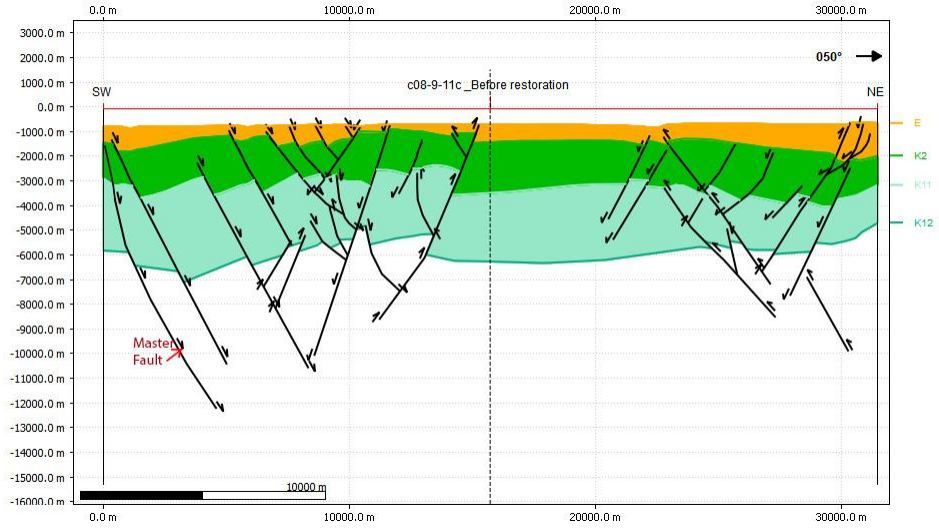

Figure 4.21: Seismic line c08-9-11c after decompaction of the Neogene post-inversion strata

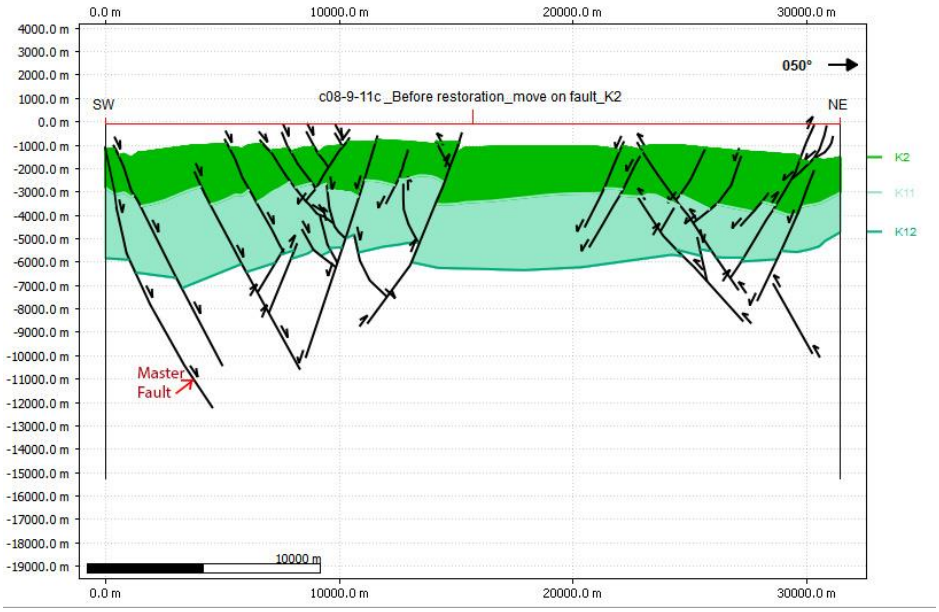

Figure 4.22: Seismic line c08-9-11c after restoration and decompaction of the Paleogene syn-inversion strata

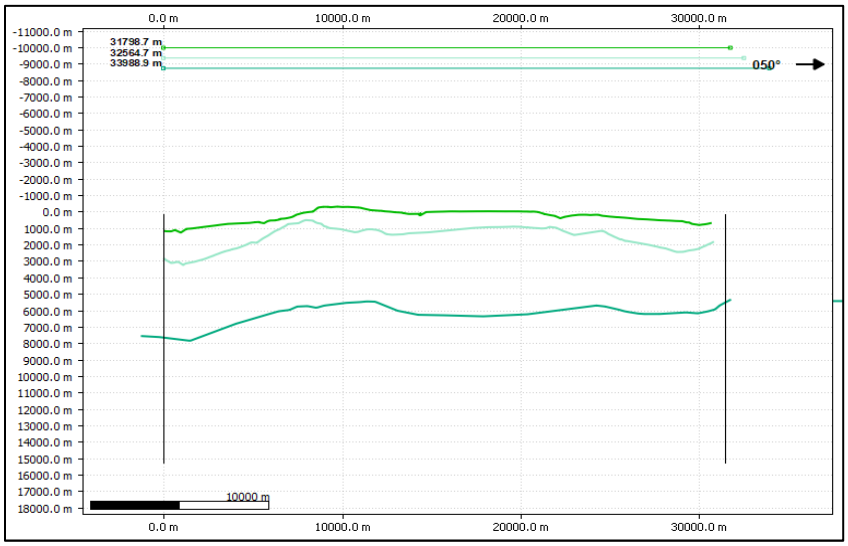

Figure 4.23: Seismic line c08-9-11c after restoration of the Cretaceous horizons. The image shows the bed lengths before inversion tectonics occurred

Table 4-6: Section analysis after fault restoration

UNIT	AGE (Ma)	LENGTH (m)
$K1_2$ (Lower Cretaceous-lower)	131	33,988.9
$K1_1$ (Lower Cretaceous-upper)	100	32,564.7
K2 (Upper Cretaceous)	66	31,798.7

Comparison between the lengths of the horizon, before and after fault restoration:

Table 4-7: An estimation of the shortening factor of the Bogal inversion area

UNIT	BEFORE (M)	AFTER (M)	SHORTENING (M)	% SHORTENING
$K1_2$ (Lower Cretaceous-lower)	31,562.2	33,988.9	2,426.70	7.139684
$K1_1$ (Lower Cretaceous-upper)	30,723	32,564.7	1,841.70	5.65551
K2 (Upper Cretaceous)	30,923.2	31,798.7	875.50	2.753257
AVERAGE			1,714.63	5.182817

The values above indicate that the inversion caused a shortening of 1,714.63m, which gives a percentage decrease of 5.2% from the original bed lengths thereby classifying the inversion as mild.

4.3 BURIAL HISTORY

Sedimentation rate

The graph below shows sediment accumulation rates for the Bogal-1 well. The bottom part of the Lower Cretaceous underwent rapid burial of 90.6m/Ma and a slower burial rate of 30.8m/Ma for the upper section. The Upper Cretaceous accumulated at a rate of 49.6m/Ma. An uplift episode followed, indicated by the unconformity between 70Ma and 60Ma (figure 4.24). The Paleogene accumulated at the slowest rate of 13m/Ma. It was followed by another uplift episode during the Pliocene. The Neogene followed with a higher accumulation rate of 41m/Ma, while the Quaternary experienced the highest accumulation rate of 94m/Ma.

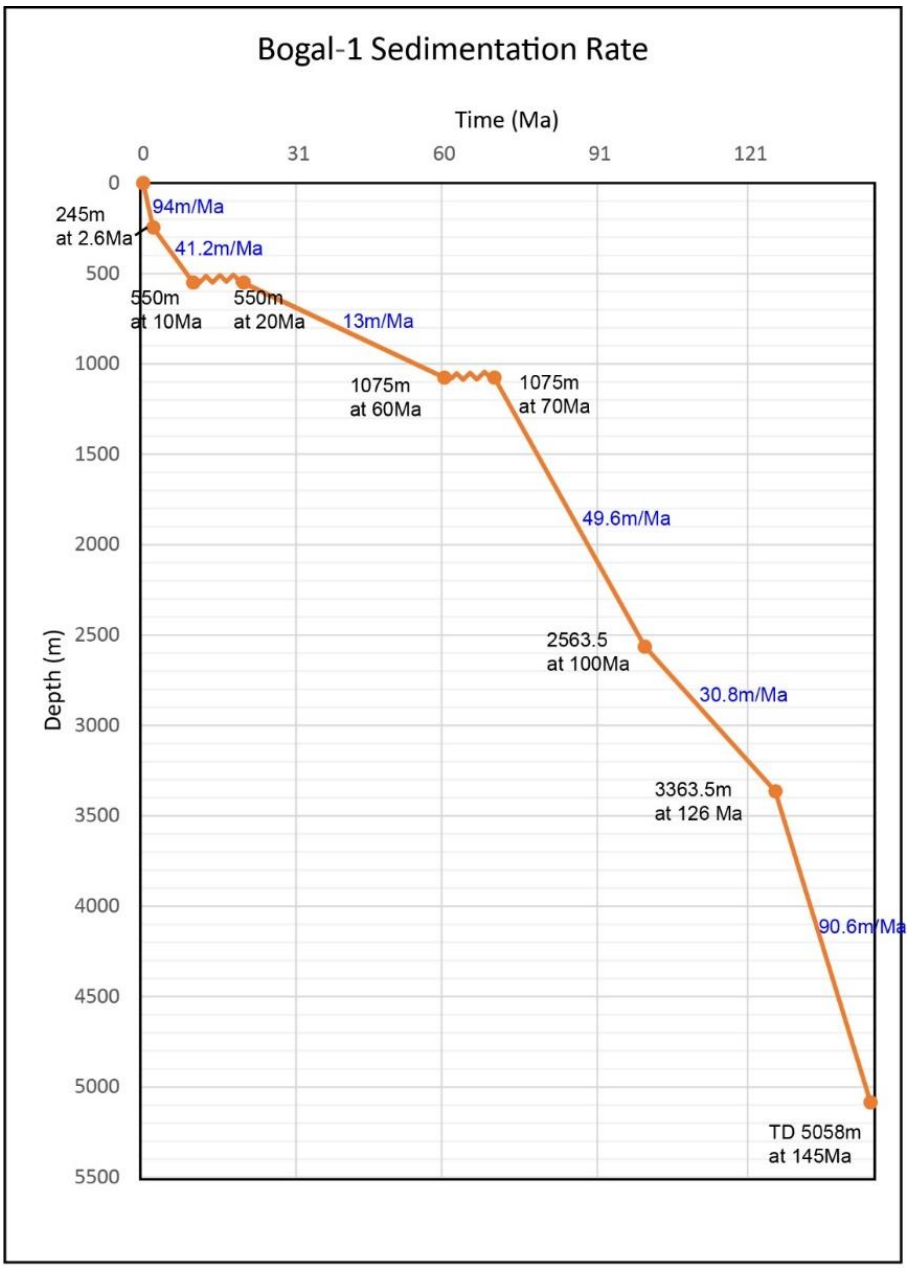

Figure 4.24: Sedimentation rate for Bogal-1 well

Burial Curves

The burial curves for Bogal-1 well are presented in figure 4.25 below. The steep gradients of the Cretaceous units represent dramatic rifting episodes followed by an uplift phase that occurred during the Cretaceous-Paleogene. This was followed by gentle rifting during the Paleogene and another uplift episode during the Pliocene.

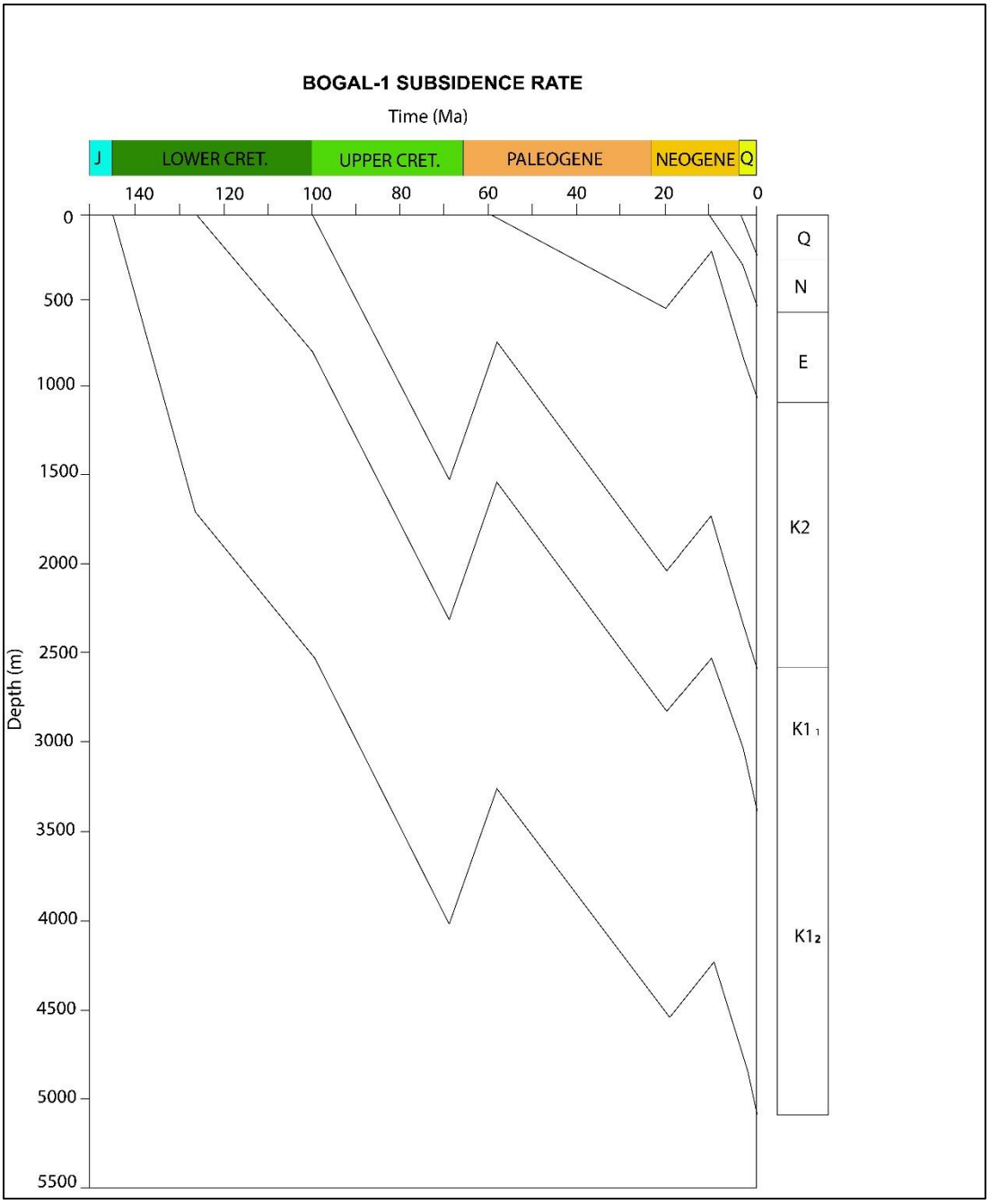

Figure 4.25: Burial curve for Bogal-1 well

The graph below shows the superposition of the temperature grid on the sedimentation rates as discussed in chapter 3, section 3.32. The temperature gradient for Bogal-1 is 23.8^0C/Km as presented in appendix 3.

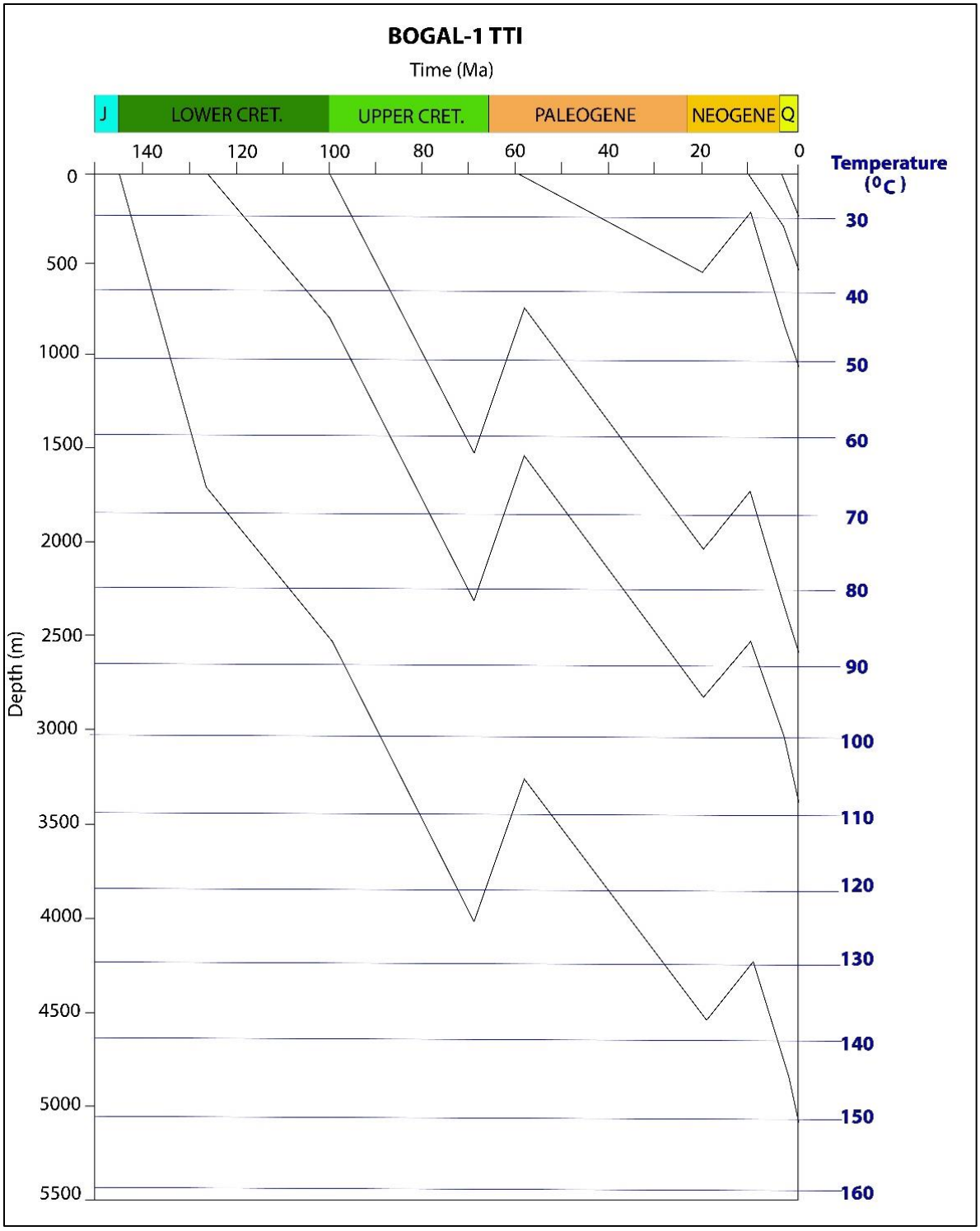

Figure 4.26: Superposition of the temperature grid on the burial curves

TTI Calculations for the Upper Cretaceous Sediments

The TTI value of 6.04 corresponds to a vitrinite reflectance of 0.55. This implies that the upper Cretaceous rocks are located within the early oil window, which began in the Late Miocene, approximately 8Ma, and are therefore immature. The sediments within the early oil window are located between 2050m and 2575m.

Table 4-8: TTI calculations for the Upper Cretaceous sediments

TEMPERATURE INTERVAL (^{0}C)	TEMPERATURE FACTOR δ	INTERVAL TIME (Ma)	INTERVAL TTI	CUMULATIVE TTI
20-30	2^{-8}	4	0.015625	0.015625
30-40	2^{-7}	9	0.0703125	0.0859375
40-50	2^{-6}	21	0.328125	0.4140625
50-60	2^{-5}	38	1.1875	1.6015625
60-70	2^{-4}	19	1.1875	2.7890625
70-80	2^{-3}	18	2.25	5.0390625
80-90	2^{-2}	4	1	6.0390625

TTI Calculations for the Lower Cretaceous Sediments

A TTI value of 457 corresponds to a vitrinite reflectance of 1.60, implying that the Lower Cretaceous source rocks are probably mature and are currently located within the wet gas window, between a depth of 4300 to 5085m. The maturation and expulsion might have occurred in the Oligocene, approximately 27 Ma.

Table 4-9: TTI calculations for the Lower Cretaceous Sediments

TEMPERATURE INTERVAL (^{0}C)	TEMPERATURE FACTOR δ	INTERVAL TIME (Ma)	INTERVAL TTI	CUMULATIVE TTI
20 -30	2^{-8}	2	0.0078125	0.0078125
30 - 40	2^{-7}	5	0.0390625	0.046875
40 - 50	2^{-6}	4	0.0625	0.109375
50 - 60	2^{-5}	5	0.15625	0.265625
60 - 70	2^{-4}	7	0.4375	0.703125
70 -80	2^{-3}	12	1.5	2.203125
80 - 90	2^{-2}	12	3	5.203125
90 - 100	2^{-1}	8	4	9.203125
100 - 110	2^{0}	18	18	27.203125
110 - 120	2^{1}	35	70	97.203125
120 - 130	2^{2}	18	72	169.203125
130 - 140	2^{3}	24	192	361.203125
140 - 150	2^{4}	4	64	425.203125
150 - 160	2^{5}	1	32	457.203125

4.4 DISCUSSION

Stratigraphic analysis reveals that the Bogal area contains thick Cretaceous and significantly thinner layers of Tertiary and Quaternary sediments. This shows similarities with the surrounding wells such as Duma-1 and Ndovu-1. Jurassic sediments in this area lie deeper than 5085m. The Quaternary and Neogene sediments show no evidence of deformation. They were deposited horizontally and uniformly on top of the Paleogene beds, making them the post-rift sequence of the Bogal area. The limited thickness as well as the lack of structures in the post-rift sequence implies that there is little chance for significant hydrocarbon entrapment. The Cretaceous and Paleogene strata make up the syn-rift sequences. The Cretaceous sediments appear to be more deformed than the Paleogene. This implies that the deposition of the Paleogene may have been synchronous with inversion. The pre-rift sequence is assumed to be the Precambrian basement. An angular unconformity separates the Neogene post-rift and the Paleogene syn-rift sediments. Its lateral extent over the entire Bogal area makes it a potential stratigraphic trap for hydrocarbons.

The Upper Cretaceous sediments are 1492m thick. They consist of interbedded layers of course, medium and fine sandstone, siltstone, silty mudstone, gypsiferous mudstone and fine conglomerate that may have been deposited in a fluvio-deltaic environment. Upper Cretaceous reservoirs contain porosity values that range from 9.8% to 17.24% and poor permeability values that range from 2.18 mD to 20.51 mD. These porosity values match with those found in other wells in Block 9 such as Ndovu-1, which recorded gas in the low permeability sediments with porosity values of 10% to 12%, and Duma-1, which also recorded some gas shows in reservoirs of low porosities ranging from 6% to 13% (Africa Oil Corp, 2008). Higher porosity values of about 30% and permeability values of up to 223 mD have been recorded in the northern part of the Anza basin. The intense fracture network formed during inversion might have supplemented the low porosity and permeability values in the Bogal Play. Fractured reservoirs are dominant in the Upper and Lower Cretaceous sections. The laterally extensive, thick Upper Cretaceous mudstones could possibly form the main sealing rocks of the Bogal Play. Upper Cretaceous shales in other parts of the Anza basin form a regional seal. However, its lateral extent is limited in some areas such as in the Bellatrix, Duma and Kaisut structural zones. TTI analysis of the Upper Cretaceous sediments in obtain a value of 6.04. This implies that they are located at the onset of the early oil window, which began in the Late Miocene (Tortonian ~8Ma)). TTI analysis of the neighbouring Duma-1 well gives a value of 0.34 for the Upper Cretaceous (Campanian-Maastrichtian), suggesting that they

are also immature (Sewe, 1995). Further towards the north-west of the Anza basin, Sewe (1995) obtained a value of 10.08 for the Maastrichtian source rocks, while Waga and Mwachoni (2019), attained a close value of 9.99 for the Campanian-Maastrichtian source rocks in Bellatrix-1 well. Sirius-1 well also attained maturation up to the onset of the early oil window, with TTI values of 8.54 for the Maastrichtian source rocks (Sewe, 1995), and 2.14 for the Campanian to Maastrichtian source rocks (Waga and Mwachoni, 2018). Maturation of the Upper Cretaceous source rocks within the peak oil window has only been attained by the Turonian to Santonian sediments in Bellatrix-1 well, where a TTI value of 45.99 was obtained (Waga and Mwachoni, 2018). Table 4-9 below compares the TTI values in the Anza basin.

The Lower Cretaceous section contains the thickest sediments in the Bogal Play. They are 2522m thick and consist of intercalating layers of sandstone, mudstone, micro-conglomerate and minor gypsum. The Lower Cretaceous mudstones that lie at the deepest section of the well make up the main source rock interval of the Bogal Play. Geochemical data from CNOOC indicates that the mudstones contain type II Kerogen and are mature, suggesting that they are of marine origin, and produce both oil and gas. However, TTI analysis obtains a value of 457.2, implying that these source rocks matured within a wet gas window that lies between depths of 4300 and 5085m. The maturation and expulsion might have occurred in the Oligocene (Chattian ~ 27 Ma). TTI analysis of the Lower Cretaceous strata in Duma-1 obtain a value of 336, suggesting that maturation also occurred within the wet gas window. However, the Ndovu-1 well, which neighbours Duma-1 and Bogal-1 gives TTI values of 12.65 (Aptian-Albian) and 112.35 (Hauterivian-Barremian), implying that the Lower Cretaceous source rocks matured within the early oil and the late oil windows respectively (Sewe, 1995). Further, towards the south-east of the Anza basin, the Albian sediments in the Anza-1 well attained a TTI value of 15.38, suggesting that maturation occurred within the early oil window. Towards the north-western side of the basin, Bellatrix-1 obtained a value of 140.66 (late oil window) for the Albian source rocks (Sewe, 1995), while the neighbouring Chalbi-3 well attained a significantly lower value of 6.57 (onset of early oil) for the Albian source rocks (Waga and Mwachoni, 2018). The Lower Cretaceous strata in Sirius-1 well matured in the peak oil window, with a TTI value of 33.2 (Sewe, 1995). However, according to Waga and Mwachoni (2019), the Lower Cretaceous matured only up to the onset of the early oil window. Aptian source rocks in Chalbi-3 well matured within the peak oil window, while the Barremian attained TTI values that range from 2.82-72.32, suggesting maturation occurred up to the onset of the late oil window (Waga and Mwachoni, 2018). Commercial amounts of hydrocarbons were discovered in

the Neocomian-Lower Albian sediments that make up the source, seal and reservoir rocks in the Sudan rift basins.

Relatively thick mudstone layers that possibly form secondary seals in the Lower Cretaceous are interbedded with the tight sandstone reservoirs that contain low porosity values that range from 4.87% to 10.46% and low permeability that range between 0.24 and 3.46 mD.

A 100m thick diabase sill is identified as a high amplitude seismic reflection that cuts through the Lower Cretaceous sediments. This sill has been identified in seismic sections across the Anza basin. It is believed to be of Tertiary origin.

Structural analysis reveals that the Bogal area experienced mode I type of tectonic inversion, where the extensional syn-rift sequence is thicker than the post-rift sequence. Large inversion anticlines with wavelengths of approximately 16 km occur across the strike of the Anza basin. Morley *et al.* (1999) acknowledged the presence of similar inversion anticlines with wavelengths greater than 10 km on the southern part of the Anza basin. Most of these anticlines are symmetrical. However, an asymmetrical anticline is present in seismic line c08-9-11c (figure 4.4). It may have been controlled by a master syn-rift fault. Structural inversion of the Cretaceous sediments took place in a NE-SW direction, while inversion of the pre-Cretaceous sediments took place in a NW-SE direction. This suggests that there were two phases of inversion in the Bogal area. The inversion anticline in section c08-9-24, c08-9-18 and c08-9-30 may be older than the ones in sections c08-9-11 and c08-9-21. The inversion phase occurred during the Late Cretaceous to Early Tertiary. High angle normal listric faults are dominant in the Bogal area. They connect with planar faults to form Positive, negative and hybrid flower structures that form viable structural traps for hydrocarbons. Positive flower structures are characterized by antiforms. They form in areas of converging crust or transpression, while negative flower structures, characterized by synforms, form in areas of diverging crust or transtension. Negative flower structures are formed by a combination of extensional and strike-slip motion, while positive flower structures are formed by a combination of compression and strike-slip movement. Hybrid flower structures form due to a combination of extension, compression and strike-slip strain under a locally compressive environment. The inversion in Bogal may have therefore been caused by both translational and compressional stress. However, the translational stress appears to be more dominant than the compressional stress. The translation took place in a NW-SE direction while the compression took

place in a NE-SW direction. Morley and Wigger (1999) postulated the cause of inversion to be pertabations of stresses that caused the opening of the Red Sea. However, they acknowledged that the duration of the spreading of the Red sea, which lasted for millions of years, did not match with the inversion episodes, which were much shorter. Therefore, they suggested that the compression in the Anza basin may have been initiated locally by the maturity of the rift itself as well as regional stresses from the opening of the Red Sea. They suggest that the inversion in the Anza graben took place multiple times due to fluctuations in paleostress. The first phase occurred after the major extensional phase, followed by another minor extensional phase and a final inversion phase.

Fault restoration of the Cretaceous sediments estimates shortening of approximately 1,714.63 m. This equates to a shortening factor of 5.2%, thereby categorizing the inversion as mild. Inversion is less pronounced in the NW-SE trending basins of the CARS due to their orientation. The extensional geometry of the basin was preserved. This can be observed in seismic line 21 and 11. The source rocks of the Bogal Play were uplifted by the inversion (figure 4.14), thereby causing a decrease in the rate of maturation. The numerous faults that cut through the tight reservoirs provided migration pathways for hydrocarbons.

Table 4-10: A comparison of the TTI values obtained from this study and those of Sewe (1995) *and* Waga and Mwachoni (2019).*The numbers in brackets show the approximate time for the beginning of hydrocarbon expulsion*

		Bogal-1	Bellatrix-1		Sirius-1		Ndovu-1	Anza-1	Duma-1	Chalbi-3
Author		Angengo	Sewe (1995)	Waga & Mwachoni (unpublished)	Sewe (1995)	Waga & Mwachoni (unpublished)	Sewe (1995)	Sewe (1995)	Sewe (1995)	Waga & Mwachoni (unpublished)
U. Cretaceous	Maastrichtian	6.04 ***(~8Ma)***	10.08	9.99 ***(~13Ma)***	8.54	2.14			0.34	
	Campanian									
	Santonian			45.99 ***(~46-37Ma)***		2.45-7.03 ***(~12Ma)***				
	Coniacian									
	Turonian									
	Cenomanian									
L. Cretaceous	Albian	457.203 ***(~27Ma)***	140.66		33.2		12.65	15.38	335.97	6.57 ***(~26-23Ma)***
	Aptian									40.47 ***(~100-91Ma)***
	Barremian						112.35			2.82-72.32 ***(~106Ma)***
	Hauterivian									
	Valanginian									
	Berriasian									
Oil window (m)			2500-3479 TD		1500-2639 TD		2550-4267 TD	2550-3662 TD	1500-3100 TD=3333	
Gas window (m)		4275 -5085 TD								

KEY:

Immature	Early oil	Peak oil	Late oil	Wet gas	Dry gas

Comparison with the Sudan basins

Inversion tectonics in the Sudan rifts took place during the Santonian and Late Eocene (ElHassan and El Nadi, 2015; ElHassan *et al.*, 2017). This has been identified in the Baggara basin, located in the north-western side of the Muglad rift. This basin is filled with fluvial and lacustrine sediments that reach a thickness of 9 km. Minor inversion tectonics, related to strike-slip movement, took place during the Late Eocene, forming anticlinal structures. However, the expulsion of hydrocarbons from the source rocks took place between 110 and 95Ma and also between 80 and 60 Ma. Therefore, the timing of inversion post-dated the migration of hydrocarbons from the source rocks. No commercial amounts of hydrocarbons have been discovered in this basin (ElHassan and El Nadi, 2015).

The Heglig field, located in the south-eastern part of the Muglad basin, also underwent mild inversion tectonics during the Santonian (ElHassan *et al.*, 2017). The Lower Cretaceous lacustrine shales of the Abu Gabra Formation form the source rocks of this area. The inversion created anticlinal structures that trapped significant amounts of oil in an area that lacked a horizontal fault seal. It also created an angular unconformity. The mild inversion preserved the extensional geometry of the basin (Warren, 2009).

The Bogal area shows some similarities to the two basins described above. The Cretaceous sediments in the Sudan and Kenyan basins contain the main petroleum system elements. Similarly, inversion tectonics in the Anza basin took place during the Late Cretaceous to Early Tertiary, forming inversion anticlines. This study has shown that the inversion tectonics was mild, therefore the original distribution of the source rocks, reservoirs and seals were not significantly redistributed. TTI analysis as well as geochemical data have revealed that the major source rock interval of the Bogal area is the Lower Cretaceous mudstones that lie between 4275 and 5085m. The maturation and expulsion of hydrocarbons is estimated to have occurred during the Oligocene, approximately 27 Ma. Structural inversion may have occurred synchronously with hydrocarbon expulsion; therefore, the timing of hydrocarbon entrapment in the newly formed anticlinal traps may have been sufficient.

CHAPTER 5: CONCLUSIONS AND RECOMMENDATIONS

5.1 CONCLUSIONS

The petroleum system of the Bogal play is similar to the others developed in the Anza basin. The thick Cretaceous syn-rift strata contains the source rocks, reservoirs and sealing rocks of the Bogal play. The major source rock interval is related to the Lower Cretaceous mudstones while the primary reservoir rocks are the Upper and Lower Cretaceous sandstones. Thick Upper Cretaceous mudstones may have potentially formed the regional top lateral seal. An angular unconformity separates the syn-rift Paleogene sediments and Neogene post-rift sediments.

The Bogal structural zone experienced mode I type of inversion tectonics, where the post rift strata in thinner than the syn-rift. The Bogal area underwent mild inversion during the Cretaceous-Paloegene that may have been triggered by a combination of the stress that led to the opening of the Red Sea as well as the maturity of the Anza rift itself. Structural restoration gives a shortening factor of approximately 1,714m. Positive, negative and hybrid flower structures occur in the thick Cretaceous and Karoo sediments, forming inversion anticlines. The study suggests that two phases of inversion occurred. The extensional geometry of the basin is still evident, implying that the translational stress was more dominant than the compressional stress.

The inversion had the following implications on the petroleum system:

1. The mild inversion in the Bogal area did not cause any significant redistribution of the source rocks, reservoirs, or seal.
2. The uplift was not large enough to cause the erosion of seals and reservoirs. The structures remained fully buried.
3. Inversion created large anticlinal features that may act as potential hydrocarbon traps.
4. An angular unconformity between the Paleogene and Neogene sediments was also created. It may also be a possible stratigraphic trap for hydrocarbons.
5. The sandstones in the Bogal play have fair to low porosities and permeability. The inversion caused an extensive fracture network that may have enhanced the permeability of the reservoirs.

TTI analysis reveals that the source rocks are situated within the wet gas window that lies between depths of 4300 to 5085m. Maturation and expulsion has been estimated to have occurred in the Oligocene (~27Ma). Therefore, the timing of gas expulsion might have been sufficient to trap the hydrocarbons that may have migrated towards the new anticlinal traps formed during inversion.

5.2 RECOMMENDATIONS

Based on this study, the following recommendations have been tabled:

1. Bogal-1 well and the seismic lines were acquired on the flank of a larger anticlinal structure that lies in the Yamicha sag, as shown in the satellite gravity map in chapter 3 (figure 3.7). More seismic lines and wells should be drilled to examine the possibility of finding gas that may have migrated to the other inversion structures that may lie farther towards the south-east of the Anza basin.
2. The angular unconformity, that lies between the Paleogene and Neogene strata, may form a possible stratigraphic trap. More wells should be drilled in this area to examine the viability of this trap.
3. This study proposes other drilling targets in the Bogal area as indicated in figure 5.1 below.

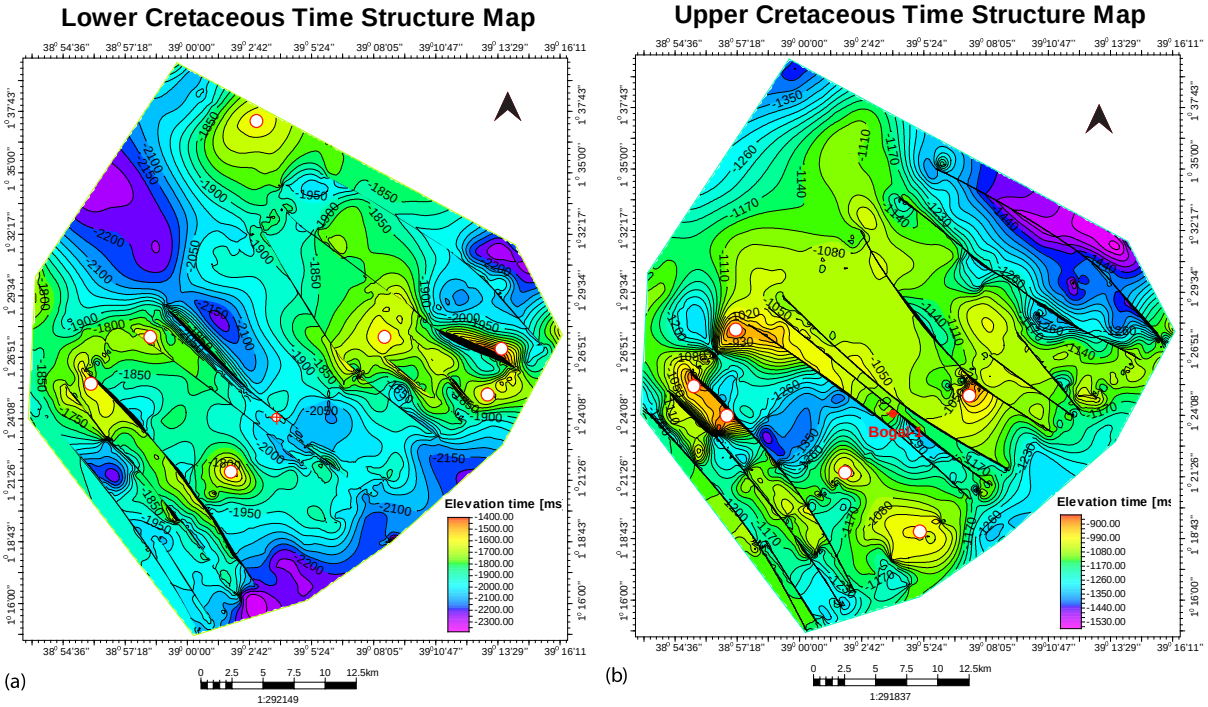

Figure 5.1: Recommended target areas (white circles) on the time structure maps in the Bogal area

REFERENCES

Africa Oil Corp (2008) *Evaluation of the Interests of Africa Oil Corp. in Two PSC Exploration Blocks in Kenya And Five Exploration Blocks in Ethiopia*.

Bally, A. W. (1984) 'Tectogenése et sismique réflexion', *Bulletin Société Géologique de France*, XXVI(7), pp. 279–285. doi: 10.2113/gssgfbull.S7-XXVI.2.279.

Barker, C. (1996) *Thermal Modeling of Petroleum Generation:Theory and Applications*. Elsevier.

Bjørlykke, K. (2010) *Petroleum Geoscience: From Sedimentary Environments to Rock Physycs*. Springer. doi: 10.1007/978-3-642-02332-3.

Bosworth, W. (1992) 'Mesozoic and Early Tertiary Rift Tectonics in East Africa', *Tectonophysics*, 209, pp. 115–137. doi: 10.1016/0040-1951(92)90014-W.

Bosworth, W. and Morley, C. K. (1994) 'Structural and Stratigraphic Evolution of the Anza Rift, Kenya', *Tectonophysics*, 236(1–4), pp. 93–115. doi: 10.1016/0040-1951(94)90171-6.

Breugel, P. Van, Kindt, R., Lillesø, J., Bingham, M., Demissew, S., Dudley, C., Friis, I., Gachathi, F., Kalema, J., Mbago, F., Moshi, H., Mulumba, J., Namaganda, M., Ndangalasi, H., Ruffo, C., Védaste, M., Jamnadass, R. and Graudal, L. (2015) *Potential Natural Vegetation Map of Eastern Africa (Burundi, Ethiopia, Kenya, Malawi, Rwanda, Tanzania, Uganda and Zambia)*, *The Vegetationmap4africa project*. Forest & Landscape Denmark and World Agroforestry Centre (ICRAF). Available at: http://vegetationmap4africa.org (Accessed: 2 September 2018).

British Geological Survey (BGS) (2019) *Hydrogeology of Kenya*, *Earthwise*. Available at: http://earthwise.bgs.ac.uk/index.php/Hydrogeology_of_Kenya (Accessed: 1 October 2019).

Buiter, S. J. H. and Pfiffner, A. O. (2003) 'Numerical Models of the Inversion of Half-Graben Basins', *Tectonics*, 22(5), pp. 11:1-16. doi: 10.1029/2002TC001417.

CNOOC (2010) *Final Well Report: Bogal-1-1*.

Cooper, M. A., Williams, G. D., de Graciansky, P. C., Murphy, R. W., Needham, T., de Paor, D., Stoneley, R., Todd, S. P., Turner, J. P. and Ziegler, P. A. (1989) 'Inversion tectonics — a discussion', *Geological Society, London, Special Publications*, 44(1), pp. 335–347. doi: 10.1144/GSL.SP.1989.044.01.18.

Cooper, M. and Warren, M. J. (2010) 'The Geometric Characteristics, Genesis and Petroleum Significance of Inversion Structures', *Geological Society, London, Special Publications*, 335(1), pp. 827–846. doi: 10.1144/SP335.33.

Cristallini, E. O., Giambiagi, L. and Allmendinger, R. W. (2004) 'True three-dimensional trishear : A kinematic model for strike-slip and oblique-slip deformation', *GSA Bulletin*, 116(7/8), pp. 938–952. doi: 10.1130/B25273.1.

DeGraciansky, P. C., Dardeau, G., Lemoine, M. and Tricart, P. (1989) 'The inverted margin of the French Alps and foreland basin inversion', *Geological Society Special Publication*, 44, pp. 87–104. doi: 10.1144/GSL.SP.1989.044.01.06.

Dindi, E. W. (1992) *Geophysical Studies of the Anza Graben, N.E. Kenya. PhD thesis.* University of Nairobi.

Dindi, E. W. (1994) 'Crustal Structure of the Anza Graben from Gravity and Magnetic Investigations', *Tectonophysics*, 236, pp. 359–371. doi: 10.1016/0040-1951(94)90184-8.

Ebinger, C. J. and Ibrahim, A. (1994) 'Multiple episodes of rifting in Central and East Africa : A re-evaluation of gravity data', *Geol Rundsch*, 83, pp. 689–702.

ElHassan, W. M., Farwa, A. G. and Awad, M. Z. (2017) 'Inversion tectonics in Central Africa Rift System: Evidence from the Heglig Field', *Marine and Petroleum Geology*. Elsevier Ltd, 80, pp. 293–306. doi: 10.1016/j.marpetgeo.2016.12.007.

ElHassan, W. M. and El Nadi, A. H. H. (2015) 'Impact of inversion tectonics on hydrocarbon entrapment in the Baggara Basin, western Sudan', *Marine and Petroleum Geology*. Elsevier Ltd, 68, pp. 492–497. doi: 10.1016/j.marpetgeo.2015.09.012.

Erslev, E. A. (1991) 'Trishear fault-propagation folding', *Geology*, 19, pp. 617–620. doi: 10.1130/0091-7613(1991)019<0617.

EWURA (2017) *Annual Report*. Available at: www.ewura.go.tz.

Fairhead, J. D. (1988) 'Mesozoic Plate Tectonic Reconstructions of the Central South Atlantic Ocean : The Role of the West and Central African Rift System', *Tectonophysics*, 155, pp. 181–191. doi: 10.1016/0040-1951(88)90265-X.

Foster, D. A. and Gleadow, J. W. (1996) ‘Structural framework and denudation history of the flanks of the Kenya and Anza Rifts , East Africa’, *Tectonics*, 15(2), pp. 258–271. Available at: http://dx.doi.org/10.1029/95TC02744; doi:10.1029/95TC02744.

Genik, G. J. (1992) ‘Regional framework, structural and petroleum aspects of rift basins in Niger, Chad and the Central African Republic (C.A.R.)’, *Tectonophysics*, 213(1–2), pp. 169–185. doi: 10.1016/0040-1951(92)90257-7.

Genik, G. J. (1993) ‘Petroleum Geology of Cretaceous-Tertiary Rift Basins in Niger, Chad and Central African Republic’, *The American Association of Petroleum Geologists Bulletin*, 8(77), pp. 1405–1434.

GEO ExPro (2014) *Oil and Gas Exploration in East Africa: A Brief History*, *GEO ExPro*. Available at: https://www.geoexpro.com/articles/2014/09/oil-and-gas-exploration-in-east-africa-a-brief-history (Accessed: 25 November 2019).

Gomes, C. J. S., Filho, A. D., Posada, A. M. A. and Da Silva, A. C. (2010) ‘The role of backstop shape during inversion tectonics physical models’, *Anais da Academia Brasileira de Ciencias*, 82(4), pp. 997–1012. doi: 10.1590/S0001-37652010000400021.

Greene, L. C., Richards, D. R. and Johnson, R. A. (1991) ‘Crustal Structure and Tectonic Evolution of the Anza rift , Northern Kenya’, *Tectonophysics*, 197, pp. 203–211. doi: 10.1016/0040-1951(91)90041-P.

Hayward, A. B. and Graham, R. H. (1989) ‘Some geometrical characteristics of inversion’, *Geological Society, London, Special Publications*, 44(1), pp. 17–39. doi: 10.1144/GSL.SP.1989.044.01.03.

Hinte, J. E. Van (1978) ‘Geohistory Analysis-Application of Micropaleontology in Exploration Geology’, *The American Association of Petroleum Geologists Bulletin*, 62(2), pp. 201–222.

Kearey, P., Brooks, M. and Hill, I. (1991) *An Introduction to Geophysical Exploration. 2nd edition*. Third Edit, *Blackwell Science*. Third Edit. Blackwell.

Krhoda, G. O. (1989) ‘Groundwater assessment in sedimentary basins of eastern Kenya , Africa’, *Regional Characterizationof Water Quality (Proceedings of the Baltimore Symposium, May 1989*, (182).

Mohamed, A. Y., Iliffe, J. E., Ashcroft, W. A. and Whiteman, A. J. (2000) ‘Burial and Maturation History

of the Heglig Field Area, Muglad Basin, Sudan', *Journal of Petroleum Geology*, 23(1), pp. 107–128. doi: 10.1111/j.1747-5457.2000.tb00486.x.

Morley, C. K., Bosworth, W., Day, R. A., Lauck, R., Bosher, R., Stone, D. M., Wigger, S. T., Wescott, W. A., Haunn, D. and Bassett, N. (1999) 'Geology and Geophysics of the Anza Graben', *Geoscience of Rift Systems-Evolution of East Africa: AAPG Studies in Geology*, 44, pp. 67–90.

Morley, C. K. and Wigger, S. T. (1999) 'Tectonic Inversion in East Africa', *Geoscience of Rift Systems-Evolution of East Africa: AAPG Studies in Geology*, 12(44), pp. 193–210.

Moulin, M., Aslanian, D. and Unternehr, P. (2010) 'A new starting point for the South and Equatorial Atlantic Ocean', *Earth Science Reviews*. Elsevier B.V., 98(1–2), pp. 1–37. doi: 10.1016/j.earscirev.2009.08.001.

Nanda, N. C. (2016) *Seismic Data Interpretation and Evaluation for Hydrocarbon Exploration and Production*. Springer International Publishing. doi: 10.1007/978-3-319-26491-2.

NOCK (2005) 'Petroleum Potential of Anza Graben System, 2nd conference on the petroleum potential & investment Kenya Sedimentary Basins', *Conference Presentation, Entebbe Uganda*.

NOCK (2019) *Upstream – National Oil Corporation of Kenya*. Available at: https://nationaloil.co.ke/upstream/ (Accessed: 17 June 2019).

Nyaberi, M. D. and Rop, B. K. (2014) 'Petroleum Prospects of Lamu Basin, South-Eastern Kenya', *Journal of the Geological Society of India*, 83(4), pp. 414–422. doi: 10.1007/s12594-014-0058-6.

Petters, S. W. and Ekweozor, C. M. (1982) 'Petroleum Geology of Benue Trough and Southeastern Chad Basin , Nigeria', *The American Association of Petroleum Geologists*, 66, pp. 1141–1149.

Phethean, J. J. J., Kalnins, L. M., van Hunen, J., Biffi, P. G., Davies, R. J. and McCaffrey, K. J. W. (2016) 'Madagascar's escape from Africa: A high-resolution plate reconstruction for the Western Somali Basin and implications for supercontinent dispersal', *Geochemistry, Geophysics, Geosystems*, 17(12), pp. 5036–5055. doi: 10.1002/2016GC006624.

Rabinowitz, P. D., Coffin, M. F. and Falvey, D. (1983) 'The separation of Madagascar and Africa', *Science*, 220(4592), pp. 67–69. doi: 10.1126/science.220.4592.67.

Reeves, C. V., Karanja, F. M. and MacLeod, I. N. (1987) 'Geophysical Evidence for a Failed Jurassic rift

and Triple Junction in Kenya', *Earth and Planetary Science Letters*, 81(1986/87), pp. 299–311. doi: https://doi.org/10.1016/0012-821X(87)90166-X.

Rowan, M. G. and Kligfield, R. (1989) 'Cross Section Restoration and Balancing as Aid to Seismic Interpretation in Extensional Terranes', *American Association of Petroleum Geologists Bulletin*, 73(8), pp. 955–966. doi: 10.1306/44b4a2bc-170a-11d7-8645000102c1865d.

Sandwell, D. T., Garcia, E., Soofi, K., Wessel, P., Chandler, M. and Smith, W. H. F. (2013) 'Toward 1-mGal accuracy in global marine gravity from CryoSat-2, Envisat, and Jason-1', *The Leading Edge*, 32(August), pp. 892–899. doi: 10.1190/tle32080892.1.

Sandwell, D. T., Müller, R. D., Smith, W. H. F., Garcia, E. and Francis, R. (2014) 'New global marine gravity model from CryoSat-2 and Jason-1 reveals buried tectonic structure', *Science*, 346(6205), pp. 65–67. doi: 10.1126/science.1258213.

Sandwell, D. T. and Smith, W. H. F. (2009) 'Global marine gravity from retracked Geosat and ERS-1 altimetry: Ridge segmentation versus spreading rate', *Journal of Geophysical Research: Solid Earth*, 114(1), pp. 1–18. doi: 10.1029/2008JB006008.

Schull, T. J. (1988) 'Rift Basins of Interior Sudan : Petroleum Exploration and Discovery', *The American Association of Petroleum Geologists Bulletin*, 72(10), pp. 1128–1142.

Sewe, C. (1995) *Optimization Analysis of Organic Carbon Concentration and Sedimentation Rate in the Anza Graben Kenya*. University of Nairobi.

Tari, G., Arbouille, D., Schléder, Z. and Tóth, T. (2020) 'Inversion tectonics : a brief petroleum industry perspective', (1989), pp. 1865–1889.

Tullow Oil (2019) *East Africa-Kenya, Tullow Oil Plc*. Available at: https://www.tullowoil.com/operations/east-africa/kenya (Accessed: 17 June 2019).

Waga, D. D. and Mwachoni, E. (2018) 'The Source Rock Evaluation and Hydrocarbon Potential of the Cretaceous Rocks from Chalbi Basin (Block 10a) of the Anza Rift based on Lopatin–Waples Method'[Manuscript submitted for publication], *African Journal of Physical Sciences*.

Waples, D. W. (1980) 'Time and Temperature in Petroleum Formation: Application of Lopatin's Method to Petroleum Exploration', *American Association of Petroleum Geologists Bulletin*, 64(6), pp.

916–926. doi: 10.1306/2f9193d2-16ce-11d7-8645000102c1865d.

Waples, D. W. (1985) ‘Predicting Thermal Maturity’, in *Geochemistry in Petroleum Exploration*, pp. 121–154.

Warren, M. J. (2009) ‘Tectonic Inversion and Petroleum System Implications in the Rifts of Central Africa’, *The American Association of Petroleum Geologists Search and Discovery*, pp. 461–464.

Winn, R. D., Steinmetz, J. C. and Kerekgyarto, W. L. (1993) ‘Stratigraphy and Rifting History of the Mesozoic-Cenozoic Anza Rift, Kenya’, *The American Association of Petroleum Geologists Bulletin*, 11, pp. 1989–2005.

World Oil Review (2019) ‘World Oil Review 2019 - ENI’, p. 74. Available at: https://www.eni.com/en_IT/investors/global-energy-scenarios/world-oil-gas-review-eng.page.

Ziegler, P. A., Cloetingh, S. and van Wees, J. D. (1995) ‘Dynamics of Intra-Plate Compressional Deformation: The Alpine Foreland and Other Examples’, *Tectonophysics*, 252(1–4), pp. 7–59. doi: 10.1016/0040-1951(95)00102-6.

APPENDIX 1: Vertical seismic profile (VSP) for Bogal-1 well

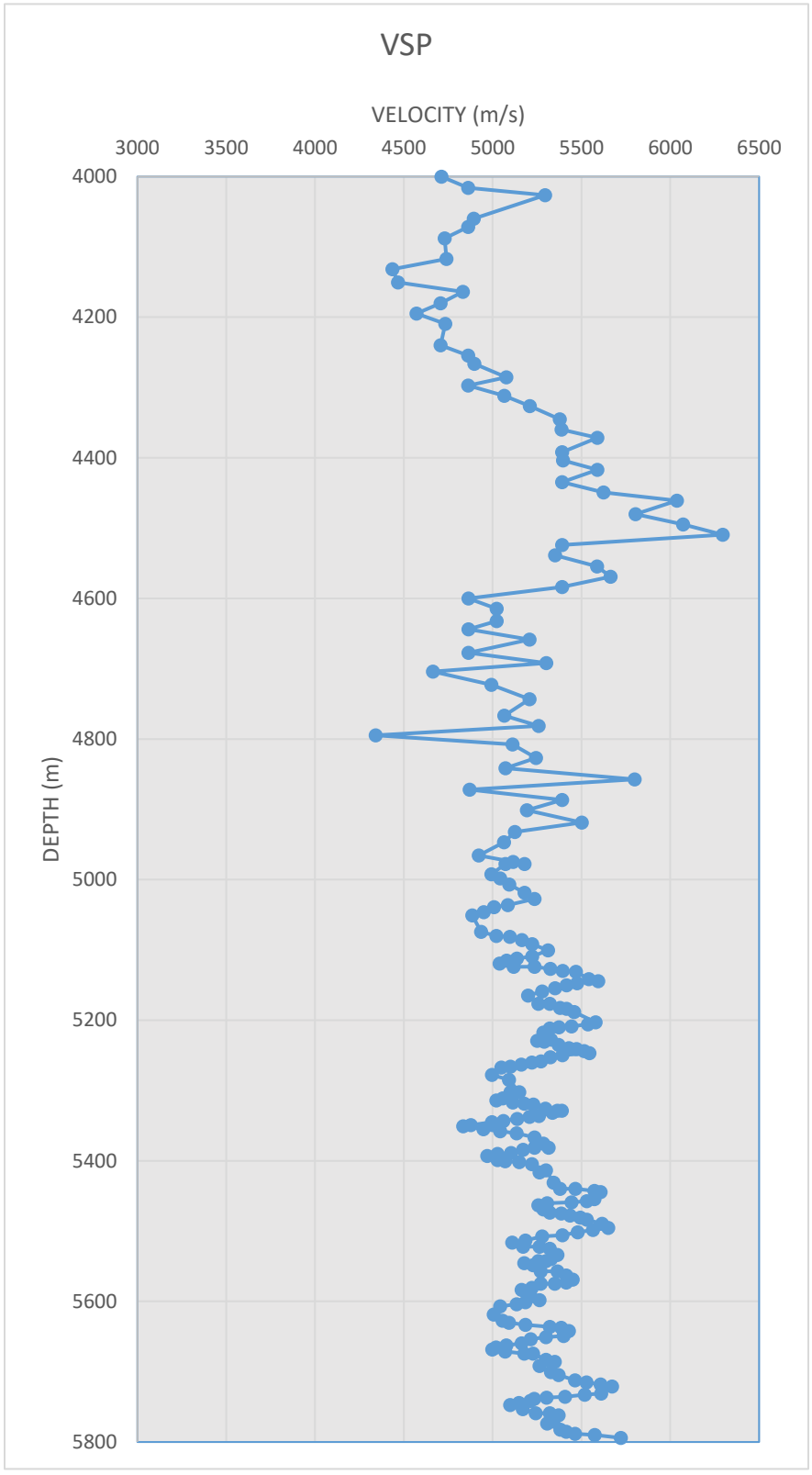

APPENDIX 2: Time-Depth chart for Bogal-1 well

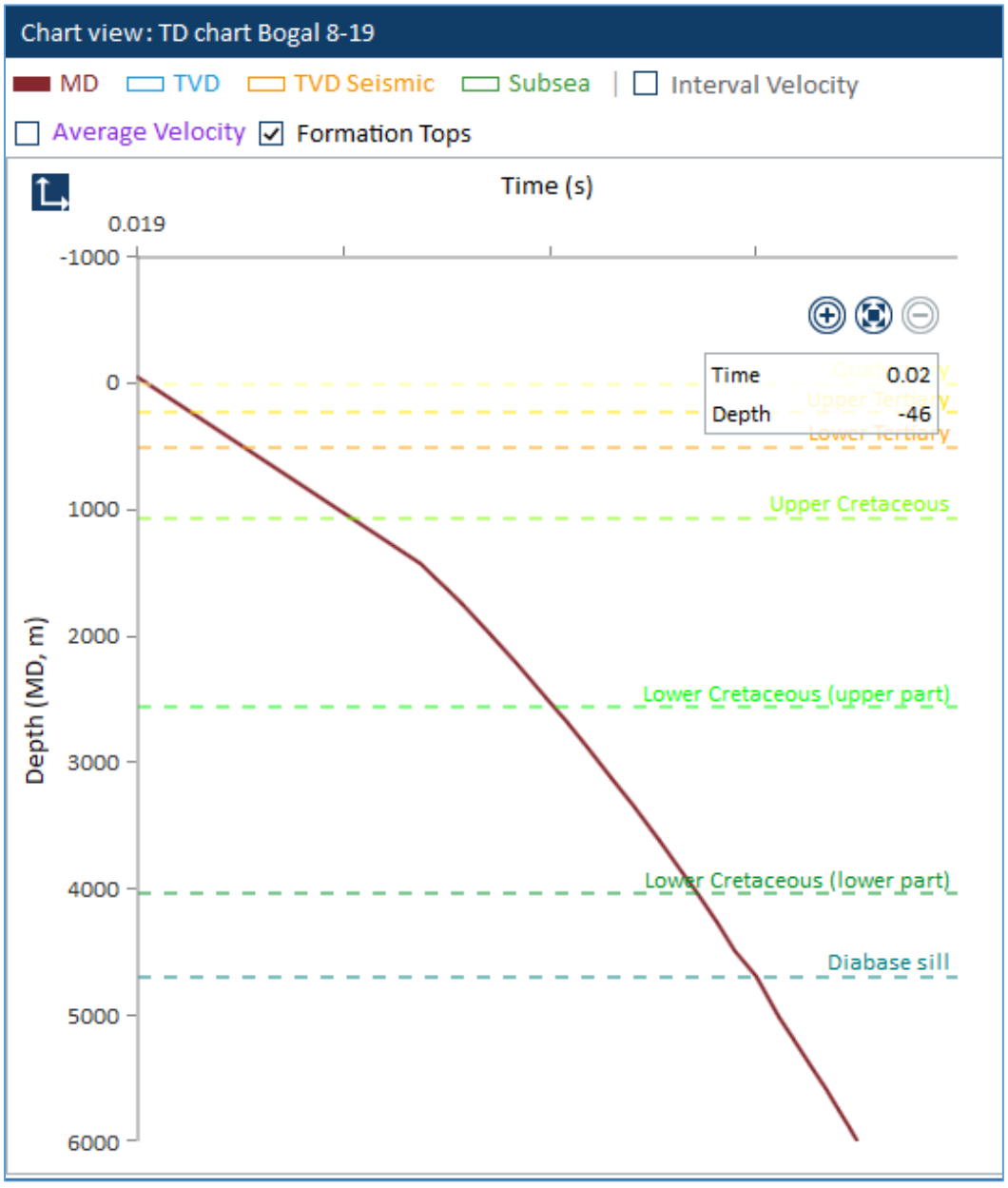

APPENDIX 3: Temperature gradient for Bogal-1 well

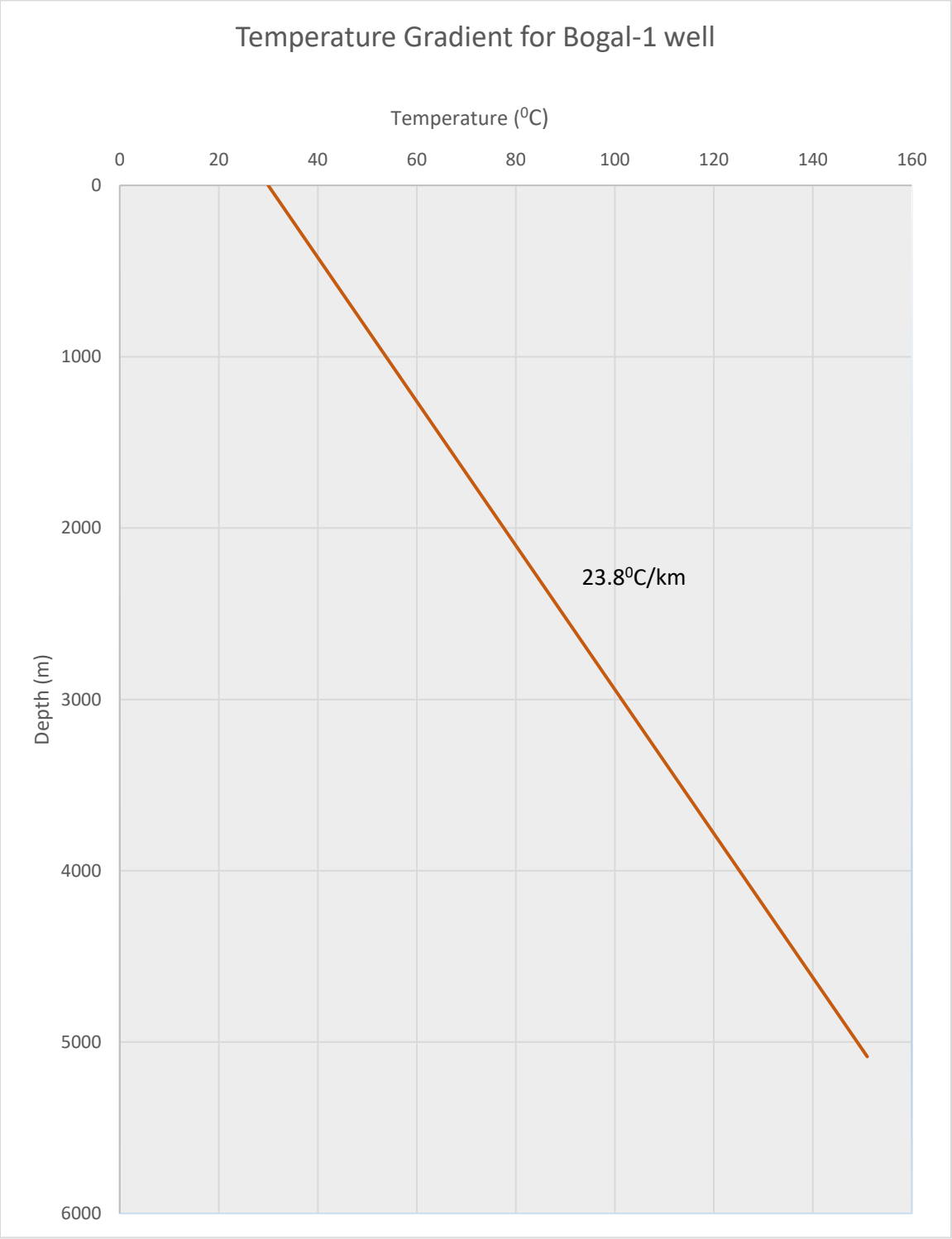

APPENDIX 4: Exploration blocks and wells in Kenya

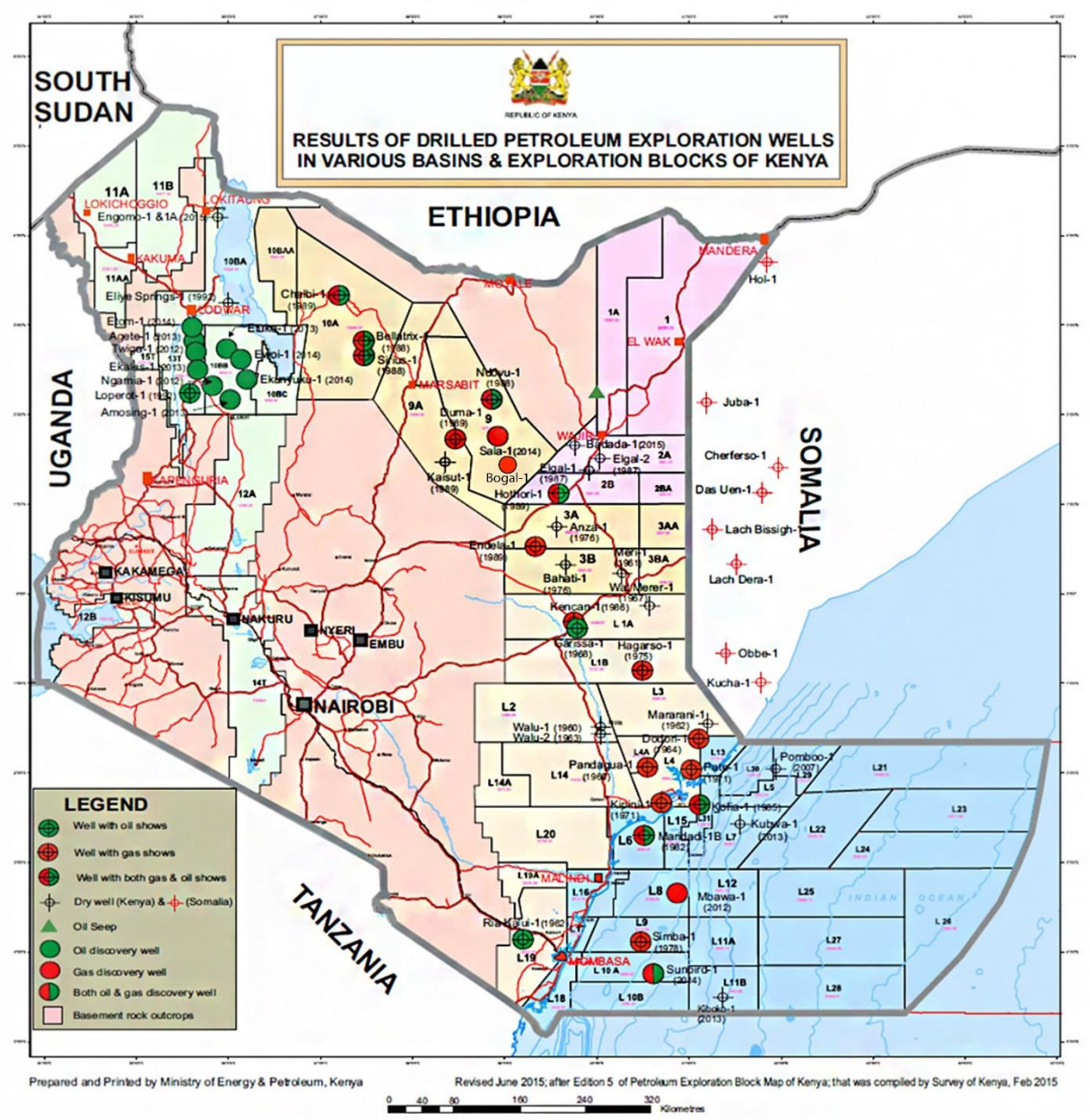

(Prepared by the Ministry of Energy and Petroleum, Kenya, 2015)